9th Workshop of
CODE_BRIGHT USERS

23th May 2017
Barcelona, Spain

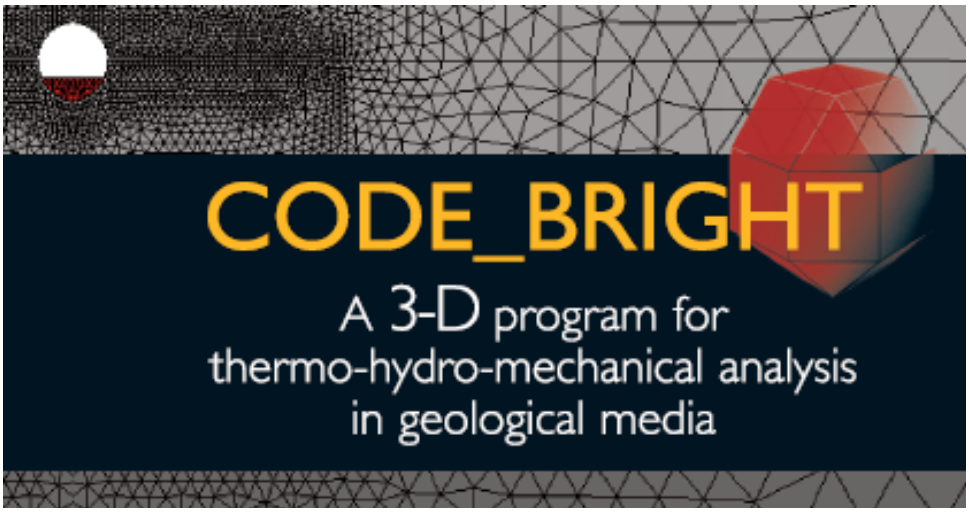

Department of Civil and Environmental Engineering
UPC-BarcelonaTech
Barcelona, Spain

CIMNE
International Center for Numerical Methods in Engineering
Barcelona, Spain

CODE_BRIGHT

A 3-D program for thermo-hydro-mechanical analysis in geological media

9th WORKSHOP OF CODE_BRIGHT USERS

Barcelona, 23th May 2017

Department of Civil and Environmental Engineering

(UPC-BarcelonaTech, Barcelona, Spain)

CIMNE

(International Center for Numerical Methods in Engineering, Barcelona, Spain)

CONTENTS

Sensitivity study for a scheme of the disposal of spent nuclear fuel isolation
E. Toprak, S. Olivella & X. Pintado

Influence of the geometry in KBS-3H spent nuclear fuel repository alternative simulation. 1-D, 2-D and 3-D simulations analyses
X. Pintado

Modelling tritium transport, matrix diffusion and multiphase flow in a concrete cell used for storing radioactive waste at El Cabril (Spain)
MC. Chaparro & MW. Saaltink

Towards a geotechnical model for Methane Hydrate Bearing Sediments
M. de la Fuente, H. Marín & J. Vaunat

Modelling gas permeability evolution in salt concrete
M. Middelhoff & O. Czaikowski

Modelling thermal induced damage in permeable rocks
C. Villarraga, J. Vaunat & M. Gasc

Modelling tunnel performance in chemically-induced swelling rocks
A. Ramon, E. Alonso, S. Olivella

Sensitivity analysis on the swelling effects of Bentonite in Code_Bright using different approaches
A. Rodriguez-Dono & S. Olivella

Modelling Gas Flow Experiments in MX80 Bentonite
IP. Damians, S. Olivella & A. Gens

3D Modelling of Reinforced Soil Walls
IP. Damians, RJ. Bathurst, S. Olivella, A. Lloret, A. Josa

Modelling the construction of an instrumented earth dam. The relevance of compaction conditions
NM. Pinyol & E. Alonso

Long-term deformation behaviour of crushed salt dump, subjected to atmospheric boundary conditions
MT. Yubero, S. Olivella, A. Gens

Parallel computing
S. Olivella & A. Rodriguez-Dono

SENSITIVITY STUDY FOR A SCHEME OF THE DISPOSAL OF SPENT NUCLEAR FUEL ISOLATION

Erdem Toprak[1], Sebastia Olivella[2] and Xavier Pintado[3]

[1] International Center for Numerical Methods in Engineering CIMNE
UPC Campus Norte, 08034 Barcelona, Spain
E-mail: erdem.toprak@upc.edu

[2]Department of Civil and Environmental Engineering
UPC Campus Norte, 08034 Barcelona, Spain
E-mail:sebastia.olivella@upc.edu

[3]B+TECH Oy, Laulukuja 4, 00420 Helsinki, Finland
E-mail:xavier.pintado@btech.fi

Abstract: This contribution describes the thermo-hydro-mechanical (THM) simulation of engineered barrier systems (EBS) for the final disposal of nuclear spent fuel in Finland. To represent the mechanical behavior of the bentonite barriers (MX80 and Friedland Clay) Barcelona Basic Model, BBM (Alonso et al., 1990), has been considered. The parameters of the mechanical and hydraulic model have been determined from the back-calculation of laboratory tests such as infiltration, water retention (Dueck, 2004) and oedometer tests. The Barcelona Expansive Model (Gens and Alonso, 1992) has been used to reproduce the mechanical response of pellets (pillow pellets between rock and buffer blocks, rod pellets between rock and backfill and granules between buffer blocks and backfill). Figure 1 shows used tests for material characterization and the materials.

2D (axisymmetric geometry) sensitivity analysis consist in doing simulations to investigate the effect, for instance, of: (1) thickness buffer-rock contact where pillow pellets are placed, (2) fracture position relative to canister and buffer, (3) type of buffer material to be used, (4) effect of water salinity, (5) initial water content of buffer, (6) permeability and (7) type of filling material between rock and buffer.

The results, shown in Figure 2, permit to estimate maximum temperatures (A) in the buffer material, hydration evolution (B), and stress (C) developed due to swelling, movement (D) at the contact between buffer material and drift backfill material.

KEY WORDS: BBM, BExM, macro and micro-porosity, KBS-3V alternative, coupled THM calculations, pellets, gap modelling, and salinity

Oedometer test devices

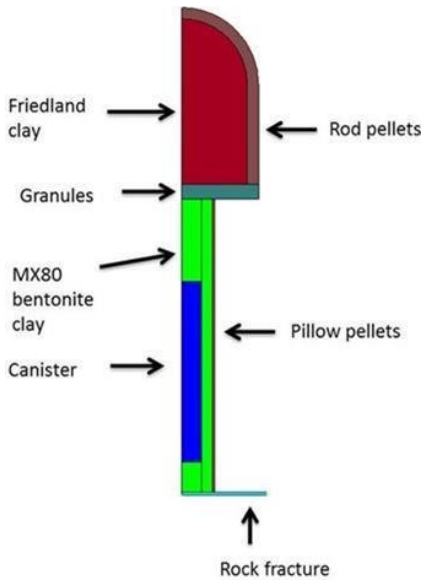

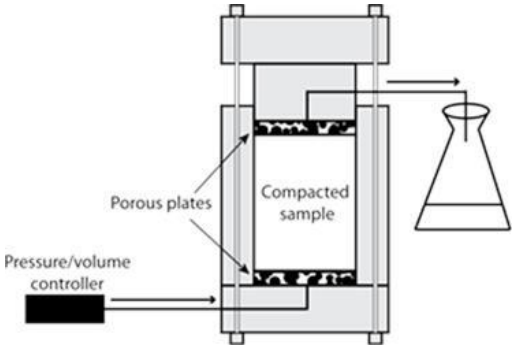

Infiltration test set up

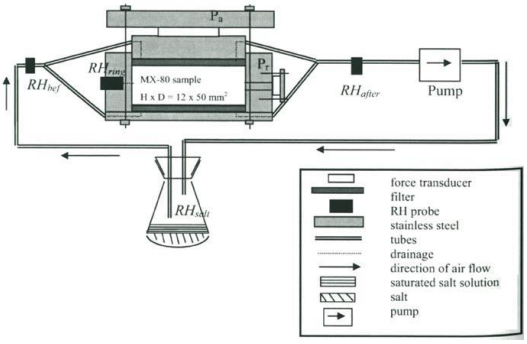

Duecks test set up for water retention curve

Figure 1. Used materials and performed test for material characterization

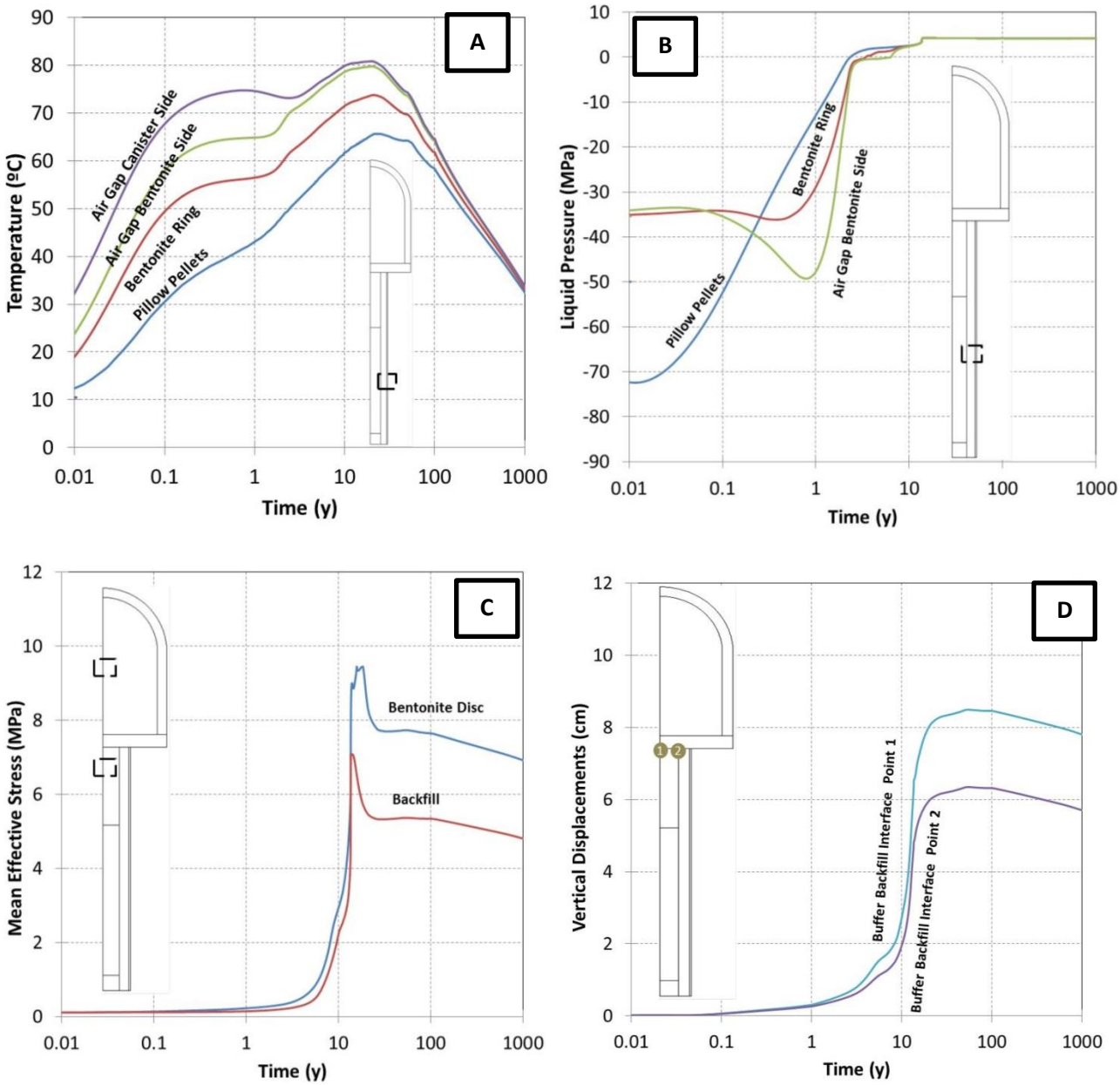

Figure 2. Evolution of tempreature (A), liquid pressure (B), mean effective stress (C) and vertical displacements (D) (model results).

INFLUENCE OF THE GEOMETRY IN KBS-3H SPENT NUCLEAR FUEL REPOSITORY ALTERNATIVE SIMULATION. 1-D, 2-D AND 3-D SIMULATION ANALYSES

X. Pintado*

* Saanio & Riekkola Oy; Laulukuja 4, 00420 Helsinki, Finland
Email: xavier.pintado@btech.fi

Key words: TH model, THM model, 1-D, 2-D, 3-D, KBS-3H alternative

Abstract. *Posiva Oy is implementing the disposal programme for spent nuclear fuel from the Loviisa and Olkiluoto nuclear power plants, and carrying out related research, technical design and development. The spent nuclear fuel will be disposed in a KBS-3 [1] repository at Olkiluoto site. Posiva is jointly with SKB developing a potential alternative design where multiple canisters containing the spent nuclear fuel are emplaced horizontally in deposition drifts (KBS-3H [2]). As part of these studies the thermo-hydro-mechanical (THM) behaviour of the deposition drifts has been studied. It is necessary to do some simplifications in the models, because it is not possible to simulate the entire repository with the coupled THM equations. The 1-D, 2-D and 3-D model geometries for analysing the thermo-hydraulic (TH) behaviour are compared. A 1-D thermo-hydro-mechanical (THM) analysis is also presented and discussed. The results indicate that simulations have similar evolution in thermal and saturation processes.*

1 INTRODUCTION

Spent nuclear fuel disposal is based on the use of multiple barriers, which ensures that the spent nuclear fuel cannot be released into the living environment or become accessible to humans in a way that constitutes a radiological hazard. In the KBS-3H design alternative. The spent nuclear fuel will be encapsulated in metal canisters emplaced in horizontal deposition drifts with tens of canisters in the same drift. This work presents different levels of geometry simplification of a KBS-3H deposition drift and compares the results from these simplifications.

2 DESCRIPTION OF THE GEOMETRIES

The canisters in the KBS-3H alternative are surrounded by buffer composed of ring blocks and end blocks. There is a gap of 5 mm thickness (nicknamed “inner gap” or “inner slot”) between the ring blocks and the canister. There is also a gap of 15 mm between the canister and the end block on one side. Both gaps are empty at the installation state. On the other side the end block is in contact with the canister. The canister, the ring blocks and the two end blocks on each side of the canister are installed inside a perforated metal shell[2](Figure 1c). The system is called a supercontainer and some tens of them are emplaced in each deposition drift. The supercontainers are separated by 3.6 m long blocks (in the reference design) referred to as distance blocks. The distance between supercontainers could be longer if there are fractures intersecting the drift. In this work, the gap between the supercontainers and the distance blocks to the host rock (outer slot) is considered to be 44.5

mm. The deposition drifts are separated by 25 m from each other [2]. More details of the simulations can be found in [3].

Figure 1 presents the geometries used for the analysis. The 1-D simplification simulating the supercontainer system and the separation between supercontainers is not possible due to the fact that there are two main sections: the section containing the canister inside the supercontainer and the sections without the canister (end blocks sections inside the supercontainer and distance blocks sections, see Figure 1c). Only the section containing the canister is presented in this work (see reference 3 for the entire simulations).

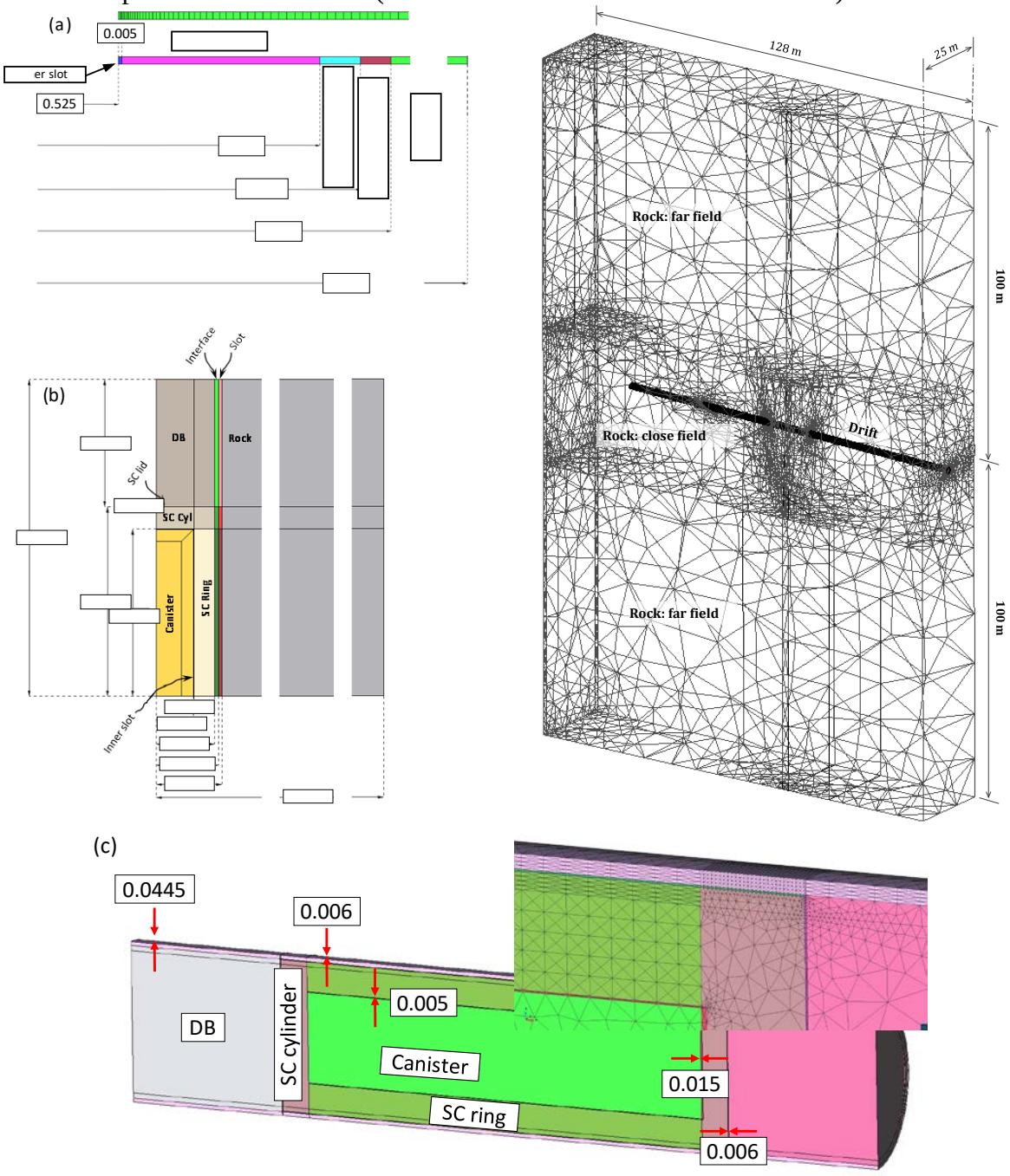

Figure 1: Geometries used in KBS-3H analysis. 1-D (a), 2-D with axisymmetry (b), 3-D with one supercontainer (c) and 3-D entire drift (d). Magnitudes in meters.

The 2-D approximation with axisymmetry simulates quite well the drift although it cannot take into account gravity effects and the fractures must be orthogonal to the axis drift. Axisymmetry and gravity are only compatible for vertical disposal schemes but not for horizontal assumptions. In this case, as most of the hydration process is driven by suction (negative pore pressures), gravity can be neglected. The 3-D approximation with one supercontainer can include the presence of any fracture and can also simulate an uneven process of hydration. An uneven process of hydration was observed in Prototype repository test [4]. It can also simulate a preference groundwater flow.

The entire drift geometry is presented in Figure 2. It includes 8 canisters and 3 fractures. The distances between canisters due to the presence of fractures follows the requirements presented in reference 2. Two extra volumes of rock were included on the top and bottom of the drift for more accurate thermal analysis (Figure 1-d). This geometry does not have the inner slot implemented but considers its presence modifying the buffer properties. More details about this simulation can be found in reference 3.

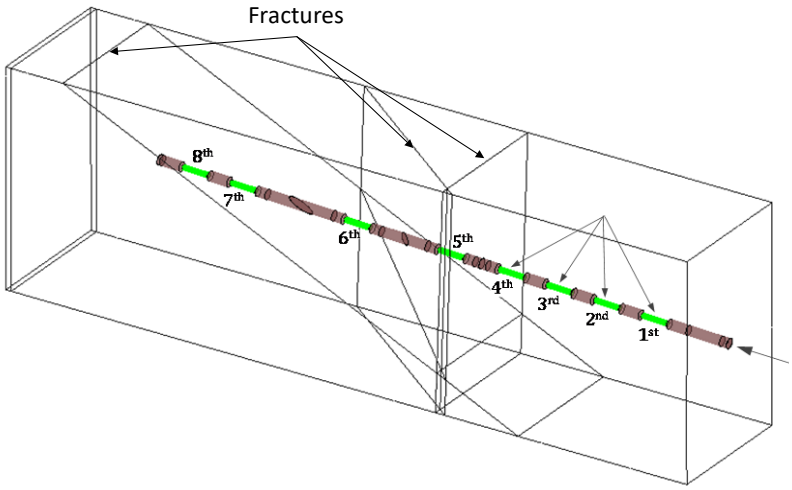

Figure 2: Detail of the 3-D entire drift model.

3 RESULTS

Figures 3, 4 and 5 display the results of the base case for the different model geometries. In the base case, the same parameter values as used for the KBS-3V in TURVA-2012 ([5]; [6], Base case in [3]) were applied.

The evolution of temperature (Figure 3) follows the same tendency in all cases under a qualitative point of view. The higher temperature calculated in the 1-D TH model is due to the fact that the sections without canisters are not considered in this simulation. As such, For in the 1D geometry case there is no heat dissipation in the axial direction. The effect of the inner gap (or inner slot) can be seen clearly in the THM simulations (decrease in temperature after the filling of the gap at around 1 year) and in the simulation where this inner gap is not considered (one supercontainer (SC), canister/buffer (no slot), Figure 3).

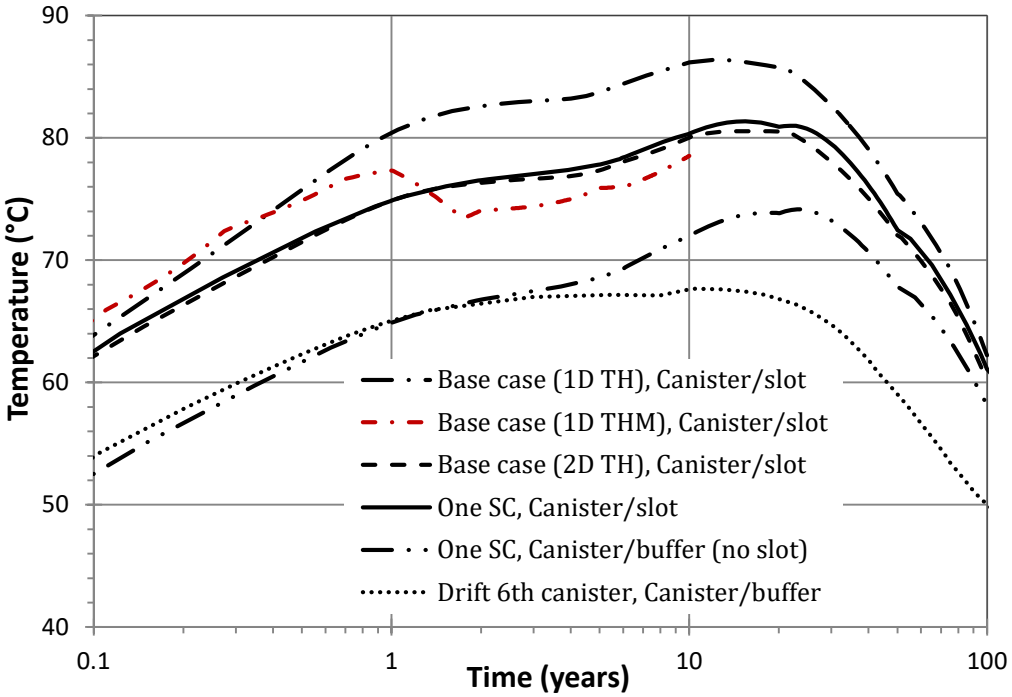

Figure 3: Maximum temperature in canister for different modelling assumptions.

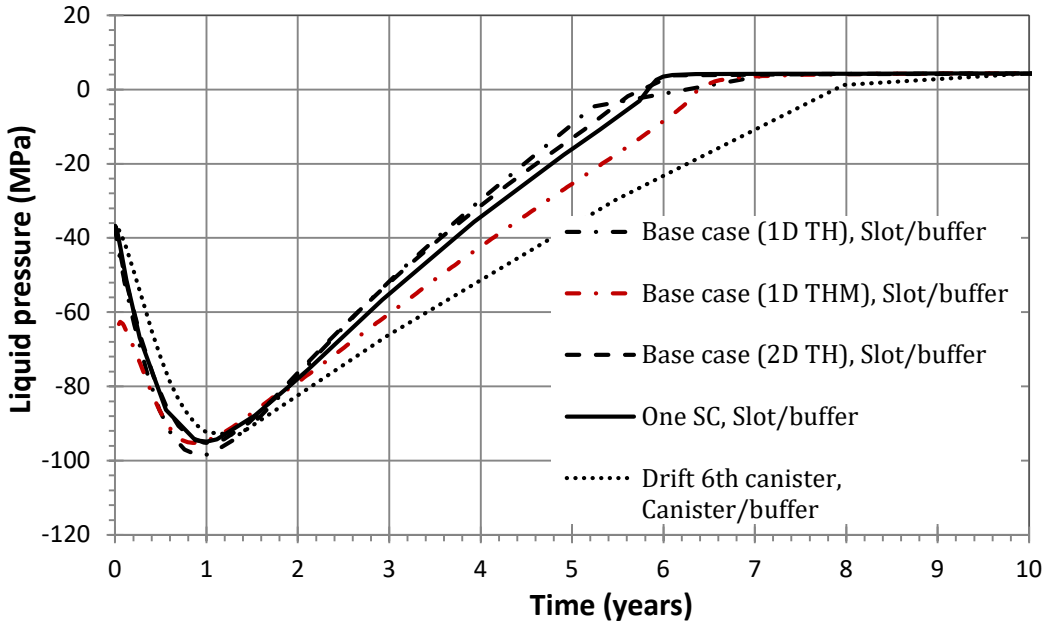

Figure 4: Liquid pressure evolution for different modelling assumptions in KBS-3H.

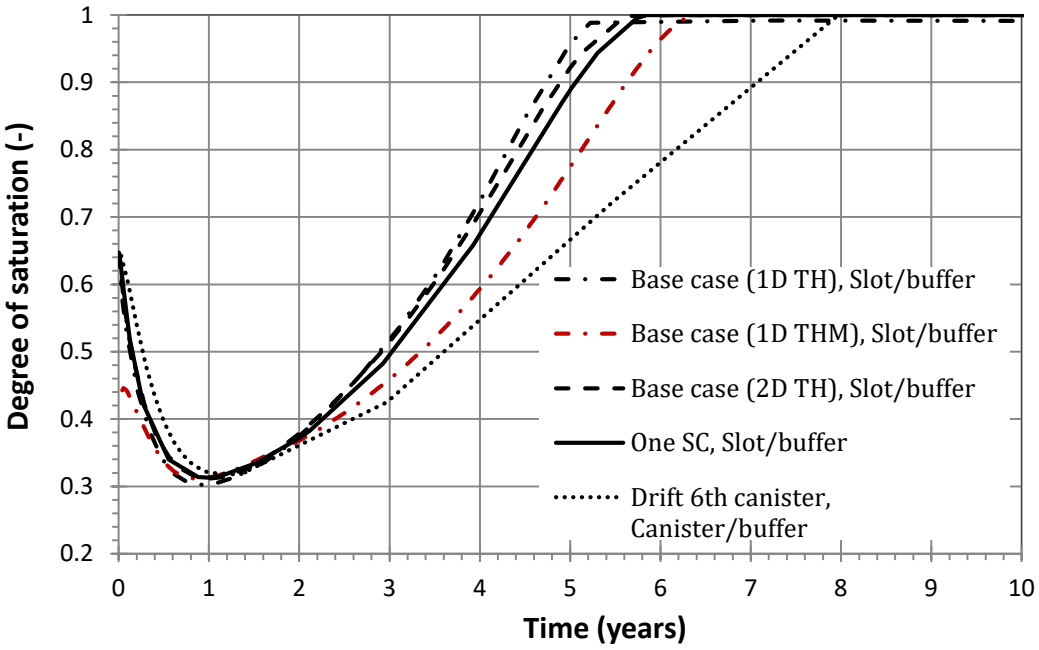

Figure 5: Degree of saturation evolution for different modelling assumptions in KBS-3H.

The evolution of the liquid pressure (Figure 4) and the degree of saturation (Figure 5) is quite similar in all cases and the difference could be due to the different water inflows from the rock. It is possible to see in Figure 1 the different volumes of rock considered in the analyses, which could have an influence on the total inflows to the drift. The differences in 1-D TH and THM simulations are due to the gap closure and the evolution of the hydraulic conductivity during the saturation process in the THM analysis. In the TH analyses, the porosity of the materials remains constant, so there are no changes of permeability.

4 CONCLUSIONS

- Gap closure affects the temperature evolution in the canister. After gap closure, the temperature drops due to the increased thermal conductivity of the gap as it closes and saturates (although the radiative heat flow was also considered when the gap was open and air filled).
- The maximum temperature when the entire drift is considered is lower. This is due to the longer distance between canisters which was assumed in the geometry as dictated by the presence of intersecting fractures. Homogeneous rock conditions are assumed for the 1D and 2D geometries, while for the entire drift in 3D, a particular zone including intersecting fractures has been assumed.
- The evolution of the liquid pressure in the inner slot/buffer contact is similar in all analyses. Drops in liquid pressure, corresponding to drying, is controlled by the early heating of the clay and, which is similar for all assumed geometries.

ACKNOWLEDGEMENTS

This work was supported by Posiva Oy. The author acknowledges Lasse Koskinen (Posiva Oy) and Margit Snellman (Saanio & Riekkola Oy) for their technical and administrative assistance. This work was performed in cooperation with Ola Kristensson, Daniel Malmberg and Mattias Åkesson from Clay Technology and Sebastià Olivella and Ivan Puig Damians from the Technical university of Catalonia.

REFERENCES

[1] M. Juvankoski, N. Marcos, *Design Basis for Buffer Components*, Posiva Working report 2009-132. Eurajoki, Finland, 2010.

[2] Posiva Oy, *KHS-3H Complementary Studies 2008-2010*, Posiva Report 2013-3, Eurajoki, Finland, 2013.

[3] X. Pintado, O. Kristensson, D. Malmberg, M. Åkesson, S. Olivella, I. Puig, TH and THM modelling of a KBS-3H deposition drift. Posiva Working report 2016-25, Eurajoki, Finland, 2017.

[4] Svemar, Ch., Johanesson, L-E, Grahm, P., Svensson, D. Prototype Repository. Opening and retrieval of outer section of Prototype repository at Äspö Hard Rock Laboratory. Summary report. SKB TR 13-22. Svensk Kärnbränslehantering AB, Stockholm. Sweden.

[5] X. Pintado, E. Rautioaho, Thermo-Hydraulic Modelling of Buffer and Backfill. Posiva Report 2012-48, Eurajoki, Finland, 2013.

[6] E. Toprak, N. Mokni, S. Olivella, X. Pintado, Thermo-Hydro-Mechanical Modelling of Buffer, Synthesis Report. Posiva Report 2012-47, Eurajoki, Findland, 2013.

MODELLING TRITIUM TRANSPORT, MATRIX DIFFUSION AND MULTIPHASE FLOW IN A CONCRETE CELL USED FOR STORING RADIOACTIVE WASTE AT 'EL CABRIL' (SPAIN)

M. Carme Chaparro[a,c] and Maarten W. Saaltink[b,c]

[a] Institute of Environmental Assessment and Water Research (IDAEA), CSIC, Jordi Girona 18, 08034, Barcelona, Spain, e-mail: mcarme.chaparro@gmail.com

[b] Department of Civil and Environmental Engineering, Universitat Politècnica de Catalunya (UPC), Jordi Girona 1-3, 08034 Barcelona, Spain, e-mail: maarten.saaltink@upc.edu

[c] Associated Unit: Hydrogeology Group (UPC-CSIC), Spain

Key words: Tritium transport, double porosity, matrix diffusion, multiphase flow.

Abstract *'El Cabril' is the low and intermediate level radioactive waste disposal facility of Spain. Water with high concentration of tritium is collected from a drain, which is situated at the centre of a concrete cell that stores radioactive waste, indicating flow of water within the cell. 2D numerical models have been made in order to develop a qualitative and partial quantitative understanding of the processes that causes this phenomenon. The conceptual model considers evaporation and condensation processes due to temperature gradients, matrix diffusion between a mobile zone (with advection, dispersion and diffusion) and an immobile zone (with only diffusion). Model results suggest that only the tritiated water used to prepare the mortar to refill the containers, which can be in liquid and gas phases, could leave the cell being collected in the drain.*

1 INTRODUCTION

Cementitious materials play an important role in the radioactive waste storage. Not only are they used to store low and intermediate radioactive waste, but also they are the final barrier in nuclear reactors that avoids tritium contact with the atmosphere[i]. Tritium is one of the isotopes of hydrogen, which can take part of the water molecules as tritiated water, both in liquid and gas phases. Often it is related with nuclear industry. It is for this reason that it is important to study the transport of tritium in cementitious materials. In the literature there are several studies related with tritium transport in non-saturated conditions in soils[ii, iii, iv, v]. Also, there are some studies related to the tritium diffusion in cementitious materials[i, vi, vii, viii]. Our work is focused on the concrete used for storing radioactive waste at 'El Cabril', which is the low- and intermediate- radioactive waste facility for Spain, where tritiated water is collected from the concrete cells storing the waste. A previous work studied the processes within the concrete that allow flow of water inside the cells by means of 2D numerical models. Results showed that this phenomenon was caused by capillary rise from the phreatic level, evaporation and condensation within the cell produced by temperature gradients caused by seasonal temperature fluctuations outside[ix]. However, the concentration of tritium of the collected water was not taken into account. In this work, we want to understand why the collected water contains tritium. To do so, we follow the same conceptual model used by Chaparro and Saaltink (2016), taking into account the temperature oscillations outside the cells and the capillary rise from the phreatic level. Moreover, we apply the same double porosity conceptual model used by Chaparro et al. (2015) in tracer test where the same concrete manufactured at 'El Cabril' was studied.

2 NUMERICAL MODEL

2.1 Conceptual model

Figure 1 displays the conceptual model and a scheme of a concrete cell where the low- and intermediate- radioactive waste is stored. The same conceptual model used by Chaparro and Saaltink (2016), is used, which considers that water (without tritium) could ascend from the phreatic level to the wall of the cell due to capillary rise through the unsaturated rock. In summer, the wall of the cell is hotter and the wall of the container is colder because the air gap acts as a thermal insulation. Thus, water can evaporate from the wall of the cell. Vapour diffuses through the air gap due to the temperature gradient between the wall of the cell and the wall of the container. Water condensates at the wall of the container because of its lower temperature. Then the condensed water could be mixed with the tritiated water in the container. Consequently, tritiated water runs off to the drain. In winter, the wall is colder and the container is hotter. Hence, tritiated water evaporates at the container and condenses at the wall. So, again tritiated water runs off to the drain. This occurs in summer and winter because the temperature difference across the air gap is large enough to produce this phenomenon. In addition, we also applied the double porosity conceptual model used by Chaparro et al, (2015), which considers a mobile zone with advection, dispersion and diffusion and an immobile zone with only diffusion. Moreover, the conceptual model considered isotopic fractionation and radioactive decay. The simulations were carried out using the code Code_Bright[xi]. Some changes had to be made in order to be able to simulate isotope fractionation and tritium existing in both liquid water and vapor.

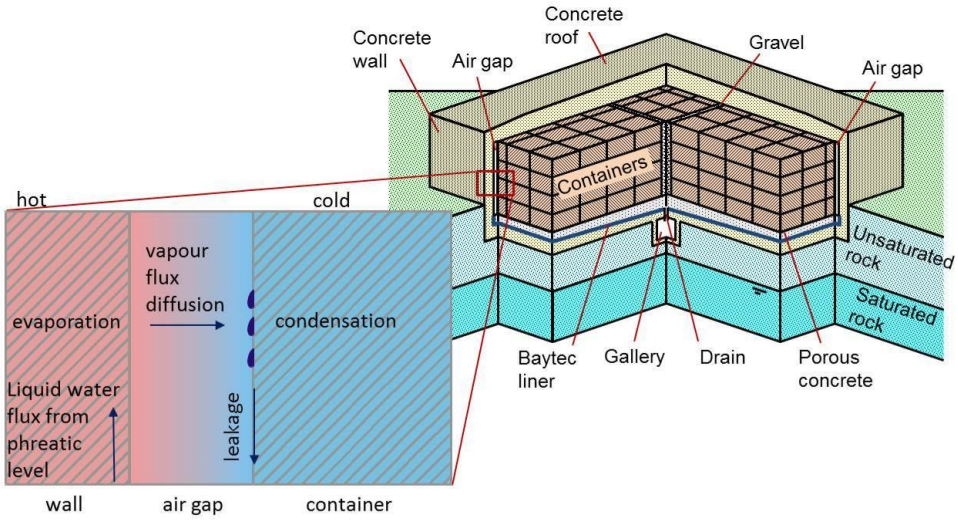

Figure 1: Conceptual model[ix]. Situation in summer: water ascends from the phreatic surface, evaporates at the hot side (wall of the cell), vapour diffuses through the air gap and water condensates at the cold side (wall of container).

2.2 Geometry, mesh and materials

First, we added the tritium transport to the same numerical model (single porosity model) that Chaparro and Saaltink, (2016), which had an axisymmetric geometry, considering the

geometry of the cell as a cylinder where the volume/surface ratio was the same as the real cell. However, that geometry was too complex to apply the double porosity conceptual model, in which the porosity is divided into a mobile and immobile part. Then, before applying the double porosity, an 1D numerical model with 105 nodes and 104 one-dimensional elements was made. The model considered the wall of the cell, the air gap and the container where the waste is stored. Finally, we distinguished a mobile zone and an immobile zone in a 2D domain, the second domain representing the immobile zone. The mobile zone was represented by the *x* axis (the same as the 1D model). From each of the nodes of the mobile zone, we added a series of 10 one-dimensional elements in the *y* axis representing the immobile zone. Therefore, the whole mesh had 625 nodes and 624 elements.

2.3 Initial and boundary conditions

The initial temperature of the entire cell was 19 ºC and the initial liquid pressure was -0.9 MPa. Containers had an initial tritium concentration of 1.45×10^{-4} GBq/L. As Chaparro and Saaltink (2016) did, temperature was prescribed and varies with time at the wall of the cell, using the daily average temperature measured by the sensors situated outside the cell. The water table was simulated by prescribing the liquid pressure at 0.1 MPa. A leakage boundary condition was applied to the gap of air between the wall and the container allowing water to leave the cell only when liquid pressure exceeds atmospheric pressure. This represents the leakage to the drain.

3 RESULTS AND DISCUSSION

Figure 2 displays the flow rate. Measured data, results from the axisymmetric model[ix] and the double porosity model are compared. The two periods (summer and winter) can be distinguished. Data are only available for the two last years, which the axisymmetric model reproduces well. However, the calculated flow rate for the double porosity model is lower than the measured one. Results from axisymmetric model show that water from the water table enters the cell; with a maximum of 5 l/d during the summer. Then the wall of the cell is dryer and a larger amount of water can ascend from the water table. Nonetheless, the double porosity model shows that water enters the cell with a maximum of 1 l/d. According to the axisymmetric model, condensed water leaves the cell in two periods with large fluxes in winter (around 10-15 l/d) and small fluxes in summer (less than 5 l/d). The double porosity model shows that water leaves the cell in the same periods but with lesser amounts (around 2 l/d in winter and 1 l/d in summer). These differences could be due to the simpler geometry deminishing the effect of the temperature in the entire cell. Nonetheless, our objective is to develop a qualitative and partially quantitative understanding of the processes that yield the tritiated water in the drain. Hence, we assume this differences not to be important.

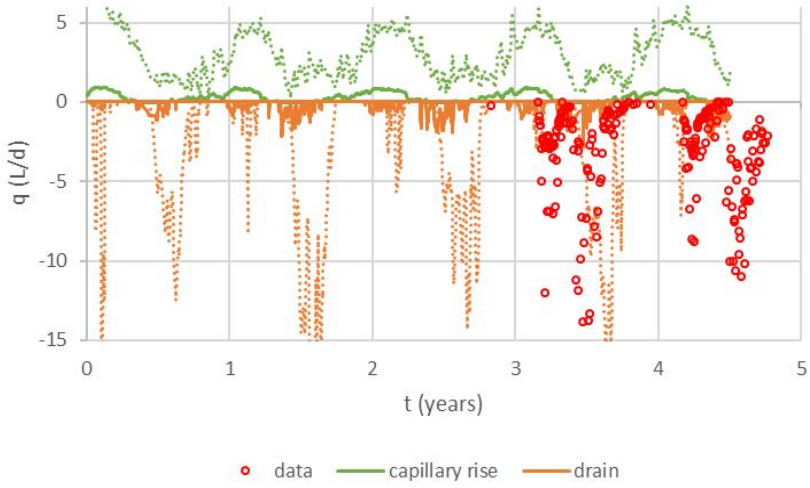

Figure 2: Flow rate of water. Positive values mean that water enters the cell, and negative values mean that water leaves the cell. Continuous lines are the double porosity model, dashed lines are the axisymmetric model and dots are the measured data.

Figure 3 compares the concentration of tritium measured in the collected water at the drain, calculated by the axisymmetric model and the double porosity model. Measured data corresponds to an average of the measured data in winter and summer respectively. The measured tritium concentrations are between 900 and 2500 Bq/l, being larger in winter because, then, the evaporation is produced in the containers. However, both model results show larger tritium concentrations in comparison to the measured data. The axisymmetric model gives concentrations between 15000 and 40000 Bq/l, and the double porosity model calculates tritium concentrations between 7000 and 30000 Bq/l. Both models show larger concentrations in winter as measured data. Applying the double porosity conceptual model, a maximum reduction of tritium concentration by a factor of 2 is obtained. This reduction of tritium concentration in the collected water in the drain could be due to matrix diffusion, but also due to the fact that the flow rate is lower. However, we think that the double porosity conceptual model is more realistic, because the concrete cell also contains iron (reinforced concrete), metals (drums) and solid waste, which is considered as immobile zone, where the transport mechanism is diffusion. The main point is the fact that both model overestimated the tritium concentration by an order of magnitude. The reason of that is because both models consider as initial tritium concentration the concentration that is in the whole cell. However, ENRESA stores tritium in the containers but also they use tritiated water for preparing the mortar used the refill the containers once all the drums are inside. Results obtained suggest that only the tritiated water used in the mortar, which can be in liquid or gas phases, could leave the cell through the drain. Moreover, only the containers near the wall can be affected by the evaporation and condensation processes, because inside the cell the temperature gradients are not high enough for causing this phenomenon.

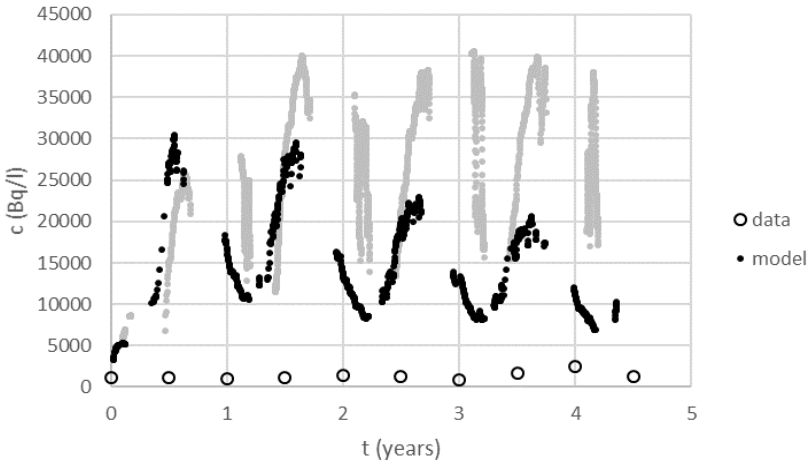

Figure 3: Concentration of tritium of the collected water. Filled black dots correspond to double porosity model, filled grey dots correspond to the axisymmetric model and empty dots are the measured data.

4 CONCLUSIONS

- Numerical models taking into account multiphase flow, matrix diffusion and tritium transport has been developed with Code_Bright in order to understand why tritiated water is collected at the drain of a concrete cell where radioactive waste is stored.
- Two numerical models have been compared, one with an axisymmetric geometry and single porosity, and another one with a simpler 2D geometry but with double porosity.
- Results suggest that only the tritiated water used to prepare the mortar used to refill the containers, which can be in liquid and gas phases, could leave the cell.

REFERENCES

[i] Nishikawa, M., K. Furuichi y H. Takata (2006), Study on permeation behaviour of gaseous tritium through concrete walls, Fusion Science and technology, 50:521-527.

[ii] Atarashi-Andoh, M., H. Yamazawa y H. Amano (2002), Numerical modelling and laboratory experiments of tritium transport in unsaturated soil, Fusion science and technology, 41:464-469.

[iii] Mayers, C.J., B.J. Andraski, C.A. Cooper, S.W. Wheatcraft, D.A. Stonestrom y R.L. Michel (2005), Vadose Zone Journal, 4:967-976.

[iv] Garcia, C.A., B.J. Andraski, D.A. Stonestrom, C.A. Cooper, M.J. Johnson, R.L. Michel y S.W. Wheatcraft (2009), Transport of tritium contamination to the atmosphere in an arid environment, Vadose Zone Journal, 8, 450-461.

[v] Furuichi, K; Katayama, K; Date, H; Takeishi, T; Fukada, S (2016), Tritium sorption behavior on the percolation of tritiated water into a soil packed bed, Fusion Engineering and Desing, 109-111:1371-1375.

[vi] Furuichi, K., H. Takata, T. Motoshima, S. Satake, M. Nishikawa (2006), Study on behavior of tritium in concrete wall, Journal of Nuclear Materials, 350, 246-253.

[vii] Furuichi, K., H. Takata, K. Katayama, T. Takeishi, M. Nishikawa, T. Hayashi, K. Kobayashi, H. Namba (2007), Evaluation of tritium behavior in concrete, Journal of Nuclear Materials, 367, 1243-1247.

[viii] Wattez, T; Duhart-Barone, A; Lorente, S (2015), Tritium through-diffusion test in non steady state: Can the effective diffusion coefficient be determined?, Construction and Building Materials, 93:121-129.

[ix] Chaparro, M. C. and Saaltink, M. W. (2016), Water, vapour and heat transport in the concrete cells for storing radioactive. Advances in Water Resources, 94:120-130.

[x] Chaparro, M. C., Saaltink M. W., Soler J. M., Slooten L. J., Mäder U. K. (2015), Modelling of matrix diffusion in a tracer test in concrete. Transport in Porous Media, 111:27-40.

[xi] Olivella, S., A. Gens, J. Carrera, E.E. Alonso (1996), Numerical formulation for a simulator (CODE_BRIGHT) for the coupled analysis of saline media, Eng. Comput.,13(7), 87-112.

TOWARDS A GEOTECHNICAL MODEL FOR METHANE HYDRATE BEARING SEDIMENT

M. De La Fuente*, †, J. Vaunat×, H. Marín-Moreno†

* National Oceanography Centre, University of Southampton, European Way, Southampton, SO14 3ZH, United Kingdom.
e-mail: mdlf1g15@soton.ac.uk,

× Department of Geotechnical Engineering and Geosciences. Technical University of Catalonia (UPC) Campus Norte UPC, 08034 Barcelona, Spain.
e-mail: jean.vaunat@upc.edu

† National Oceanography Centre, University of Southampton Waterfront Campus, European Way, Southampton SO14 3ZH, United Kingdom.
e-mail: hector.marin.moreno@noc.ac.uk

Key words: Methane hydrates; Geomechanical behaviour; Densification; Constitutive modelling; Hydrate-CASM; Hydrate dissociation.

Abstract. *Methane hydrates (MH) are metastable solid, ice-like substance formed at high pressure, low temperature conditions, and present beneath the seabed on many continental margins and permafrost regions. Its occurrence within the pores can alter profoundly the mechanical behaviour of the soil. The study of methane hydrate-bearing sediments (MHBS) geomechanical response is driven by the increasing interest in methane gas extraction from hydrates as an alternative clean fossil fuel energy. Here we present the Hydrate-CASM as a new constitutive model to investigate the impact of hydrate saturation on the stress-strain behaviour of hydrate-bearing sand formations, which are the most likely target of marine gas exploitation. Hydrate-CASM considers MHBS as a deformable elastoplastic continuum and changes in the stress-strain behaviour caused by hydrate are predicted through a densification mechanism. Our model was successfully validated against experimental literature data from triaxial tests performed at different confinement stress conditions and with various hydrate saturation values and morphologies. Particular attention was paid in adequately calibrating the mechanical behaviour of the host sediment, and considering secondary effects derived from the sample preparation procedure. Future work will explore the capability of Hydrate-CASM at modelling the evolution of MHBS mechanical properties during hydrate dissociation by applying a novel characteristic hydrate function. This new approach to predict changes in phase saturation during hydrate dissociation has been developed based on the thermodynamic equilibrium occurring in frozen soils. Future simulations of gas and water production and stability assessment of the seafloor and associated submarine infrastructures will be performed in a fully coupled THM framework using Code_Bright together with GiD.*

1 INTRODUCTION

Gas hydrates are ice-like crystalline compounds formed by gas molecules trapped in a solid cage-like water structure, known as a clathrate. Methane hydrates ($CH_4 \cdot nH_2O$) are the most common occurring gas hydrate in nature, and they may hold between 550-2680 GtC globally[1], from which about 150 GtC are estimated to may be technically recoverable[2]. This

vast amount of methane stored in hydrate's structure is consider as future alternative clean fossil fuel energy. The energy demand projected over the next decades, together with climate concerns, have motivated an increasing interest in a better understanding of basic physics and chemistry of gas hydrates, their impact on the physical properties of the sediment, and their role in global environmental processes, including natural geohazards, long-term carbon cycling and global climate.

From a soil mechanics perspective, it is generally accepted that the presence of hydrate in the pores has a major effect on the sediment geomechanical properties. Hydrate favours the sediment to behave as a denser, bonded or cemented soil, exhibiting greater stiffness, strength, and dilatancy with respect to those of the same sediment without hydrate[3] (Figure 1). However, once hydrate becomes unstable due to natural and/or anthropogenic perturbations in the thermodynamic parameters controlling its stability, its contribution to the host sediment mechanical properties disappear. The loss of shear resistance and the increase in the pore space caused by dissociation may trigger small to large scale deformations (i.e., ground settlement, submarine landslide or borehole collapse) affecting pipelines and other submarine infrastructures[4].

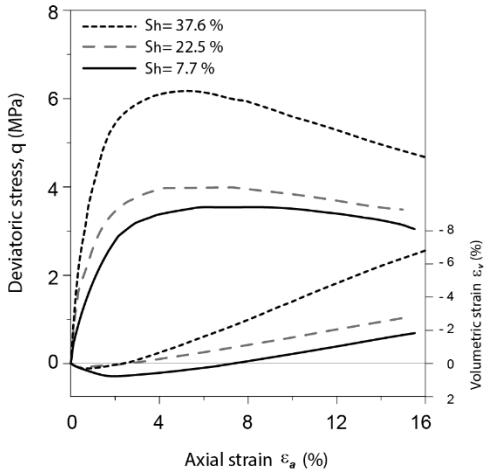

Figure 2*: Drained triaxial tests on natural samples from the Nankai Trough with different hydrate saturations. The experimental data is presented in terms of stress-strain behaviour and volumetric response. After*[5].

Here we present the Hydrate-CASM, a new constitutive model for MHBS, which is particularly suitable for sands. This constitutive model adds the subloading concept and a densification mechanism to the existing unified critical state model CASM (Clay and Sand Model)[6]. Densification is sufficient to explain the effect that hydrate saturation has on the composite sediment stress-strain behaviour. It accounts for the mechanical contribution of a solid phase formed within the pores through a reduction of the available void ratio, an increase in the sediment stiffness, and an increment of the volumetric yield stress. The Hydrate-CASM parameters have a clear physical meaning and can be derived from conventional geotechnical laboratory tests. Only one parametric adjustments is required to adjust the sediment stiffness and its applications is simple and proportional to hydrate saturation. Therefore our formulation only needs one empirical hydrate-dependent parameters, which extends its validity to a wide range of sediments with other solid phases growing in the pores. The model results capture well the enhancement in strength, stiffness and dilatant behaviour of the sediment, and particularly allows getting further insights on certain

experimental behaviours traditionally attributed to the mechanical effects of the hydrate morphology. To expand Hydrate-CASM capabilities to scenarios in which dissociation is induced, we also present a characteristic hydrate function, based on the thermodynamic equilibrium of freezing soils[7].

2. A NEW CONSTITUTIVE MODEL FOR MHBS

Hydrate-CASM is an enhancement of the existing unified critical state model CASM[6], a non-associated critical state model with volumetric hardening and formulated in terms of the state parameter concept[8]. This parameter (Eq 1) is defined in the $v - \ln(p')$ space (Figure 2a) as the vertical distance between the current state (v, p') and that at the critical state line (CSL), and plays a key role on the densification mechanism presented in the following section.

$$\xi_0 = v + \lambda\, ln(p') - \Gamma \quad (1)$$

Where v is the specific volume, λ is the slope of the NCL, p' is the mean effective stress in the current state and Γ is the specific volume at the critical state with p'=1Kpa. The state parameter value depends on the sample current state regarding the CSL, and is associated with a specific mechanical response of the sediment. Loose sand located in the right side of the CSL, are characterized by a positive ξ_0 and tend to show hardening on the $p' - q$ stress space, and contraction dominates the volumetric response. For dense sands, which are on the left side of the CSL, ξ_0 reaches negative values and the triaxial response show a distinctive peak in the deviatoric stress followed by softening before the critical state is achieved, and dilatancy dominates the volumetric response (Figure 2b).

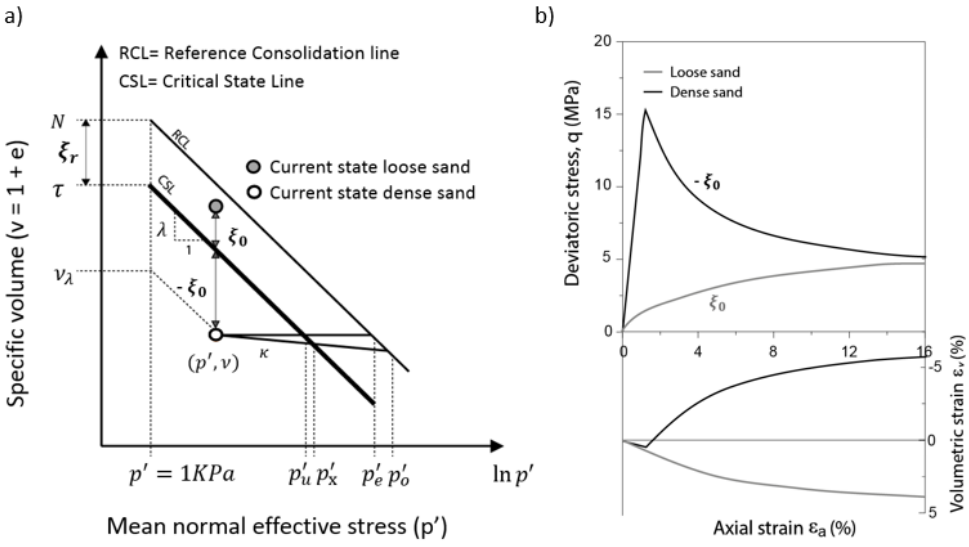

***Figure 2**: CASM framework. (a) Graphical description of model parameters and critical state constants, and (b) qualitative mechanical response for samples with positive and negative values of the state parameter. After*[6].

2.1. Hydrate saturation effect on stress-strain behaviour: Densification process

Densification is understood as a mechanism that naturally reduces the sediment porosity (Figure 3a) and increases the composite elastic bulk moduli proportionally to the hydrate

saturation. When considering a certain hydrate fraction the original state of the sample is shift to a new lower void ratio state according to the volume of voids occupied by the hydrate phase (Figure 3b):

$$e_{a_{hbs}} = e_p - e_h \quad (9)$$

This change decreases the state parameter by the same e_h amount ($\Delta\xi_0 = \Delta e_{available} = e_h$). By reducing the value of ξ_0 our model naturally tends to show peaks in the deviatoric stress and dilatant volumetric responses such as those observed in MHBS (Figure 2b). Additionally, an increase in the sediment stiffness is applied by decreasing the slope of the swelling line:

$$\kappa_{hbs} = \kappa_{hs} \cdot \kappa_{rf} \quad (10)$$

In all the analyses conducted in our work, a good agreement with the experimental data was obtained for:

$$\kappa_{rf} = 0.0003\, {S_h}^2 - 0.0268\, S_h + 0.9949 \quad (11)$$

The intersection of the corrected k_{hbs} slope with the NCL at the new current state explains an increase of the volumetric yield stress with respect to the original one, which strongly influences the hardening law (Figure 3b):

$$p_{0hbs} = \frac{\Gamma - e_{a_{hbs}}}{(\lambda - \kappa_{hbs})} \quad (12)$$

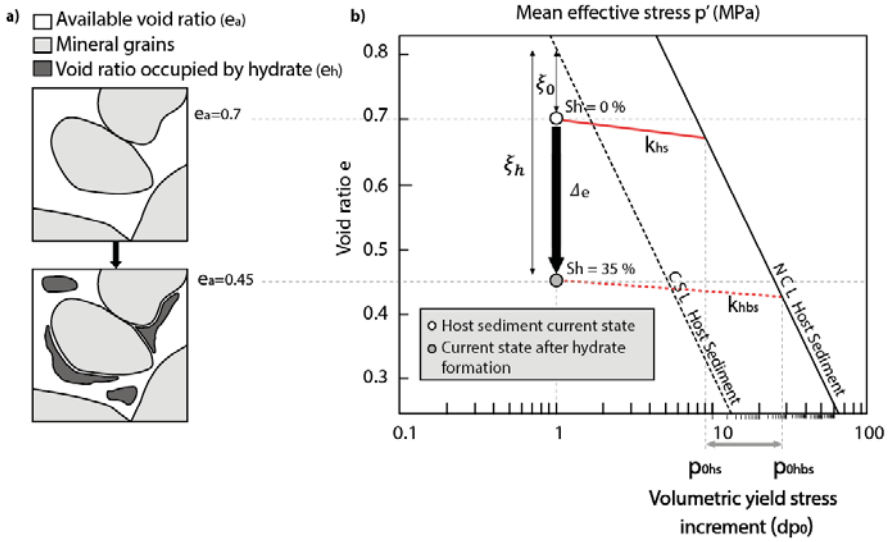

***Figure 3**: Densification process due to hydrate formation. (a) Reduction of the host sediment void ratio and (b) effect of hydrate saturation on Hydrate-CASM parameters.*

2.2. Model validation

The capability of Hydrate-CASM at reproducing the geomechanical behaviour of MHBS was examined with experimental literature data from several drained triaxial tests conducted on synthetic sand. Here we present the model performance for the drained triaxial test carried

out by[9] on synthetic MHBS samples with different hydrate saturations and growth morphologies.

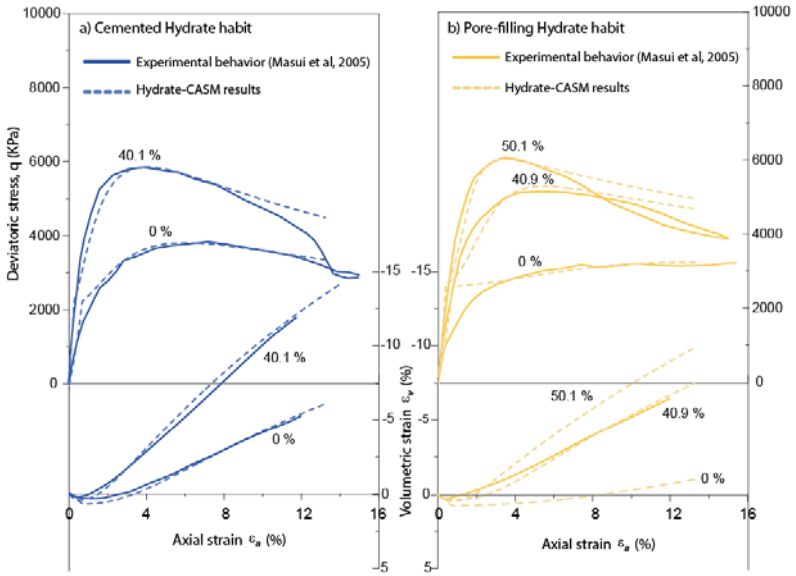

Figure 4: *Comparisons between Hydrate-CASM predictions and experimental results for synthetic Toyoura sand samples with different hydrate saturations and morphologies. Stress strain behaviour and volumetric response of (a) cementing hydrate samples, and (b) pore-filling hydrate samples. After*[9].

The main features of the mechanical response of the different samples are well captured by our model, although the softening response for axial deformations greater than 8% is slightly overestimated (Figure 4). Our results show that accurate calibration of the mechanical response of the host sediment is essential to reduce uncertainty in the causes (e.g., hydrate morphology), explaining different mechanical responses observed for a given hydrate saturation.

3. HYDRATE DISSOCIATION: ONGOING WORK

Dissociation of hydrates is one of the most challenging phenomena in the geomechanical study of MHBS. The experimental study of the mechanical characteristics of hydrate-bearing sediments during hydrate dissociation[10,11], together with the significant wellbore deformation encountered during different gas extraction field trials[12] prove the strong impact of hydrate phase change in the soil mechanical response. To expand the Hydrate-CASM capabilities to scenarios in which dissociation is induced, we developed a characteristic hydrate function, based on the thermodynamic equilibrium of freezing soils[7]. Hydrate formation and dissociation within the sediment porosity involves complex thermal, hydraulic and mechanical processes that have significant geotechnical interactions. For instance, phase changes modify the hydraulic regime of the soil, which in turn induces mechanical deformation. Simultaneously, any change in the hydraulic and mechanical conditions feeds back the thermal processes by way of advection and changes in hydrate, gas and water contents. The formulation suggested in this section intends to address changes in the saturation of the different phases that can coexist in the system (hydrate, liquid water and methane gas) when formation/dissociation is induced by changes in pressure and temperature conditions. Gas hydrates in natural reservoirs are generally not in thermodynamic

equilibrium, and there may be numerous competing phase transitions involving hydrate[13]. However, the present formulation treat the dissociation as an equilibrium reaction. Based on the Clausius–Clapeyron equation the equilibrium of chemical potentials in the three-phase system considered led as to the following hydrate characteristic function:

$$P^H = P^l - \rho^H \bar{l} \ln\left(\frac{T}{T(P^g)}\right) \quad (13)$$

This equation represents a thermodynamic requirement for equilibrium that needs to be satisfied by hydrate, liquid water and methane gas pressures (P^H,P^l and P^g) and the system temperature (T). This function will allow us to track the evolution of hydrate, water and gas saturations along formation or dissociation reaction and therefore asses the mechanical changes related.

4. CONCLUSIONS

We have presented the Hydrate-CASM, as a new constitutive model for MHBS, which is particularly suitable for sands. The proposed extension of the CASM model can satisfactorily capture key mechanical features of MHBS, such as an increase in stiffness, strength, and dilatancy and suggest some re-thinking on the hydrate contribution to the overall sediment mechanical response is needed. Forthcoming simulations will account for hydrate dissociation to introduce the interdependent physical phenomena that typically characterizes MHBS systems, such as phase changes, non-isothermal multi-phase, multi-component flow, geomechanical deformation, and changes in the hydraulic and mechanical properties of the sediment.

5. REFERENCES

1.Milkov, A. V. Global estimates of hydrate-bound gas in marine sediments: how much is really out there? *Earth-Sci. Rev., 66, 183– 197, doi10.1016/j.earscirev.2003.11.002* (2004).

2.Boswell, R. & Collett, T. S. Current perspectives on gas hydrate resources. *Energy Environ. Sci.* **4,** 1206 (2011).

3.Soga, K., S. L. Lee, M. Y. A. Ng, and A. K. Characterisation and engineering properties of methane hydrate soils, in Characterization and Engineering Properties of Natural Soils, vol. 4, edited by K. Soga et al., pp. 2591–2642, Taylor and Francis, London, U. K. (2006). doi:10.1201/NOE0415426916.ch26

4.Settari, A. Reservoir compaction, J. Pet. Technol., 54(8), 62–69. Sharma, S. S., and M. Fahey (2003), Degradation of stiffness of cemented calcareous soil in cyclic triaxial tests. *J. Geotech. Geoenviron. Eng., 129(7), 619–629.* (2002).

5.Masui, A., K. Miyazaki, H. Haneda, Y. Ogata, and K. A. Mechanical characteristics of natural and artificial gas hydrate-bearing sediments, in Proceedings of the 6th International Conference on Gas Hydrates, Vancouver. *Proc. 6th Int. Conf. gas hydrates, Vancouver, Canada ICGH. p. 6–10.* (2008).

6.Yu, H. S. CASM: a unified state parameter model for clay and sand. *Int. J. Numer. Anal. Methods Geomech.* 22, 621–653 (1998).

7.Nishimura, S., Gens, A., Jardine, R. J. & Olivella, S. THM-coupled finite element analysis of frozen soil: formulation and application. *Géotechnique* **59,** 159–171 (2009).

8.Jefferies, K. B. and M. G. A state parameter for sands', Geotechnique, 35(2), 99—112. (1985).

9.Masui, A., H. Haneda, Y. Ogata, and K. A. The effect of saturation degree of methane hydrate on the shear strength of syn- thetic methane hydrate sediments, Proceedings of the 5th International Conference on Gas Hydrates, Trondheim, Norway, vol. 2037, pp. 657–663. (2005).

10.Masui, A., H. Haneda, Y. Ogata, and K. A. Mechanical properties of sandy sediment containing marine gas hydrates in deep sea offshore Japan survey drilling in Nankai Trough. *Proc. Seventh ISOPE Ocean Min. Symp. pp. 53–56, Int. Soc. Offshore Polar Eng. Lisbon, Port.* (2007).

11.Lee, J. Y., Santamarina, J. C. & Ruppel, C. Volume change associated with formation and dissociation of

hydrate in sediment. *Geochemistry, Geophys. Geosystems* 11, (2010).
12.Dallimore, S. R., J. F. Wright, K. Yamamoto, and G. B. Proof of concept for gas hydrate production using the depressurization technique, as established by the JOGMEC/NRCan/Auroa Mallik 2007–2008 Gas Hydrate production research well program, Mackenzie Delta, Northwest Territories, Canada. *Bull. Geol. Surv. Can., 601, 1–15*,(2012).
13.Vafaei, M.T., Kvamme, B., Chejara, A., Jemai, K. Non-equilibrium modeling of hydrate dynamics in reservoir. *Energy Fuels, 26 (6), pp 3564–3576* (2012).

MODELLING GAS PERMEABILITY EVOLUTION IN SALT CONCRETE

M. Middelhoff [1], O. Czaikowski [2]

[1] Institute of Disposal Research (IELF)
Clausthal University of Technology
Adolph-Roemer-Straße 2a, 38678 Clausthal-Zellerfeld, Germany
E-Mail: Marvin.Middelhoff@tu-clausthal.de, Web Page: https://www.ielf.tu-clausthal.de/de/

[2] Gesellschaft für Anlagen- und Reaktorsicherheit (GRS) gGmbH
Theodor-Heuss-Straße 4, 38122 Braunschweig, Germany
E-Mail: Oliver.Czaikowski@grs.de, Web Page: http://www.grs.de/

Key words: Permeability evolution, Sealing materials, Rock salt, Salt concrete

Abstract: *In the former German concept, rock salt was the favorite host rock to dispose heat-generating radioactive waste. To assure the integrity of the complete repository system after closure, shafts and drifts have to be sealed. In the context of the DOPAS project GRS performed a laboratory test program and numerical simulations to investigate the properties of concrete based sealing materials. The test program and the numerical simulations mainly focused on salt concrete. This paper pursues the objective to describe an approach of a sequential simulation of the observed gas permeability evolution in salt concrete. The present approach involves a recently developed visco-plasticity model being employed for modelling the mechanical behavior on the one hand and a model basing on percolation theory for estimating the permeability evolution on the other.*

1 INTRODUCTION

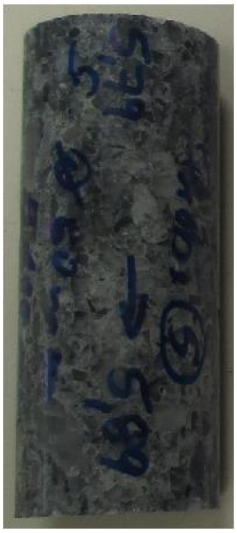

Fig. 1-1: Example of a salt concrete specimen used by GRS

Following an international broad agreement the former German repository concept envisaged the disposal of heat-generating radioactive waste in rock salt formations located several hundred meters below ground level. As the major part of a planned multiple barrier system, a containment-providing rock zone (CRZ) should inhibit, reduce and delay the migration of radionuclides from the waste to the biosphere and prevent a continuous advective transport of fluid phases from the overburden to the waste. By this means the long-term safety of people and the environment against the hazard of ionizing radiation should be ensured. Since the maximal sealing capacity of the natural barrier is not reached upon repository closure, the isolation of the waste should still be guaranteed by installing engineered barriers (EBS) as a further part of the multiple barrier system. In interaction with the CRZ, the EBS serve their purpose as long as the recovery of the natural barrier lasts [1].

On behalf of the Federal Ministry for Economic Affairs and Energy (BMWi), the national funding organisation for research and development work related to radioactive waste management in Germany, GRS has investigated sealing and backfilling materials potentially employed in rock salt formations.

All concepts of the construction of geotechnical barrier in rock salt envisaged the utilization of concrete based sealing materials. Among many, salt concrete has been suggested as one construction material prospectively employed. It is composed of salt grains, cement and brine.

In order to investigate the sealing capacity of salt concrete, GRS carried out a comprehensive laboratory test program accompanied by numerical simulations using Code_Bright. The precise description of the hydro-mechanical behavior is of great interest as fractures are likely to impair the integrity of geotechnical barriers. Curing processes inside the employed concrete-based materials account for the initialization of fracture development. Fluid phases driven by a pressure gradient could then intrude into the barrier system through the created fractures. Thus the laboratory test program predominately attempted to determine whether creep processes inhibit the mentioned intrusions by closing the fractures in time.

The laboratory test program comprised different experiments examining the short- and the long-term mechanical behavior of salt concrete. Gas permeability was recorded while loading the salt concrete specimen. On the one side the experiments revealed that the deformation behavior of salt concrete changes significantly when subjecting it to deviatoric stresses greater than σ_{Dev} = 20 MPa. On the other side the magnitude of gas permeability strongly depends on the evolution of fissures inside the sample, which was estimated by volumetric strain measurement [2].

This paper presents one approach dealing with the sequential simulation of the observed gas permeability evolution, which has been recorded while performing different triaxial compression tests.

2 CONSTITUTIVE MODELS

A recently developed visco-plasticity constitutive model has been selected in order to reproduce the deformation behavior. The gas permeability evolution has been simulated by employing a constitutive model basing upon percolation theory.

2.1 Mechanical constitutive model

Within the framework of the employed visco-plasticity model, the total strain increment tensor $d\boldsymbol{\varepsilon}^{tot}$ is decomposed into an elastic strain increment tensor $d\boldsymbol{\varepsilon}^{e}$, a plastic strain increment tensor $d\boldsymbol{\varepsilon}^{p}$ and a creep strain increment tensor $d\boldsymbol{\varepsilon}^{c}$. The elastic as well as the plastic increment are essential to describe the time-independent response of the material, whereas the latter increment considers creep deformations induced by constantly applied stresses. As the experiments presented in this text exclusively examine the short-term behavior, the explanation of the reproduction of the time-dependent behavior is skipped.

A modified Mohr-Coulomb yield criterion was employed defining a yield surface in the stress space. The yield surface separates the elastic and plastic parts of the mechanical response:

$$f = \left(\cos\theta + 1/\sqrt{3}\sin\theta\sin\varphi\right) J - \sin\varphi\,(c\cot\varphi + p) = 0 \qquad \text{Eq. (1)}$$

where φ is the friction angle, c is the cohesion and stress invariants are considered in the form of p, J and θ. The constitutive model enables the reproduction of observed strain-hardening prior peak, peak strength and strain-softening post peak by using isotropic hardening-softening laws governed by the evolution of the strength parameters φ_{mob} and c_{mob}. The evolution is controlled by the selected state variable of equivalent plastic strains ε^{p}_{eq} defined as:

$$\boldsymbol{\varepsilon}^{p}_{eq} = \sqrt{(2/3\ \boldsymbol{\varepsilon}^{p} : \boldsymbol{\varepsilon}^{p})} \qquad \text{Eq. (2)}$$

where $\boldsymbol{\varepsilon}^{p}$ is the plastic strain tensor. The evolving parameters φ_{mob} and c_{mob} are calculated stepwise from the equivalent plastic strains combined with hardening and softening parameters.

The *Fig. 2-1* depicts the friction angle evolution within the strain-hardening and -softening branch. Corresponding evolution laws are listed in *Tab. 2-1*.

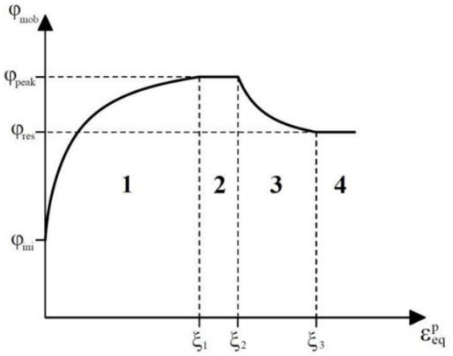

Fig. 2-1: Friction angle evolution including strain-hardening and –softening

Zone	Evolution law
Zone 1	$\varphi_{mob} = \varphi_{ini} + \frac{\varepsilon^p_{eq}}{a_{hard} + \frac{\varepsilon^p_{eq}}{\Delta\varphi_{hard}}}$; $\Delta\varphi_{hard} = \frac{\xi_1}{\frac{\xi_1}{\varphi_{peak} - \varphi_{ini}} - a_{hard}}$
Zone 2	$\varphi_{mob} = \varphi_{peak}$
Zone 3	$\varphi_{mob} = \varphi_{peak} - \frac{\varepsilon^p_{eq} - \xi_2}{a_{soft} + \frac{\varepsilon^p_{eq} - \xi_2}{\Delta\varphi_{soft}}}$; $\Delta\varphi_{soft} = \frac{\xi_3 - \xi_2}{\frac{\xi_3 - \xi_2}{\varphi_{peak} - \varphi_{res}} - a_{soft}}$
Zone 4	$\varphi_{mob} = \varphi_{res}$

Tab. 2-1: Corresponding evolution laws

Cohesion evolves as a function of the calculated friction angle. At any point it is derived from the following expression:

$$c_{mob} = c_{peak} \cot\varphi_{ini} \tan\varphi_{mob} \qquad \text{Eq. (3)}$$

where c_{peak} is the peak cohesion and φ_{ini} is the initial friction angle.

The implemented flow rule was directly derived from the previously defined yield-criterion:

$$\partial g/\partial \boldsymbol{\sigma} = \omega\,(\partial f/\partial p)\,(\partial p/\partial \boldsymbol{\sigma}) + (\partial f/\partial J)(\partial J/\partial \boldsymbol{\sigma}) + (\partial f/\partial \theta)(\partial \theta/\partial \boldsymbol{\sigma}) \qquad \text{Eq. (4)}$$

where g is the plastic potential, ω is a constant, which controls the amount of plastic volumetric strains. In case ω is set to 1, a completely associated flow rule is considered. In contrast, when ω is set to 0, no plastic volumetric strains occur [3].

2.2 Hydraulic constitutive model

The present constitutive model adopts the principles of percolation theory for permeability estimation. It postulates that micro fractures are induced inside the salt concrete sample by applied deviatoric stresses. Once reaching a particular deviatoric stress threshold, the permeability increases suddenly. This observation can be attributed to coalescing micro fractures within the cement matrix.

The selected model combines a cubic law, which is applied to a conventional semi-empirical estimation of micro fracture aperture, with a percolation model. Following the approach presented in [2] and [4], the process of coalescence is modeled with a probability density function as a function of the ratio of volume V to volume $V_{per.}$ when percolation is noticed for the first time. Since the measurement of porosity changes while performing the experiments represents a demanding task, the volumetric strains are taken as a substitute of porosity. The relationship is given by:

$$k = A\,k_f \left[1 - \exp\left(-\left(dV/dV_{per.}\right)\right) - 0.63\right]^2 \qquad \text{Eq. (5)}$$

Where k is the calculated permeability, A is a network parameter and k_f is the maximum expectable permeability. The ratio of both volumes is derived as follows:

$$dV/\,dV_{per.} = (\varepsilon_{vol.} + 1)/(\varepsilon_{vol.\,per.} + 1) \qquad \text{Eq. (5.1)}$$

where $\varepsilon_{vol.}$ is the simulated volumetric strain and $\varepsilon_{vol.\,per.}$ is the volumetric strain when percolation is detected within the experiment for the first time respectively.

2.3 Sequential calculation

The sequential calculation of the permeability has been carried out by making use of a previously developed program. It follows the scheme illustrated in *Fig. 2-2*.

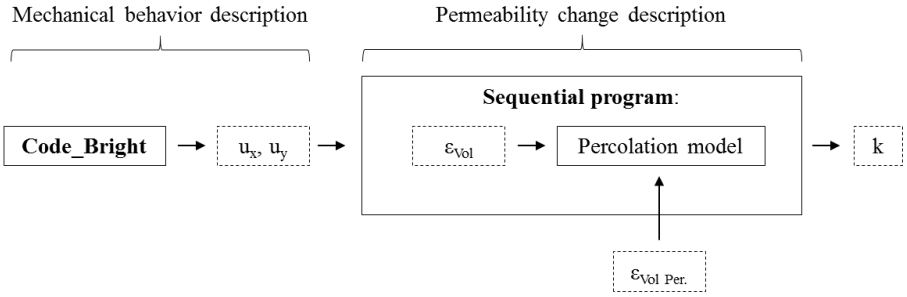

Fig. 2-2: Sequential calculation of permeability

The calculation of k is performed in two steps: The volumetric strains ε_{vol} are computed by the axial and radial displacements (u_x, u_y) previously obtained from the calculations of the mechanical part. Then the estimated volumetric strains ε_{vol} and the measured percolation threshold $\varepsilon_{vol.\ per}$ are inserted into Eq. (5.1), whereas the volumetric strains ε_{vol} is the control variable. The evolution of permeability is described by this means.

3 NUMERICAL SIMULATION

As it has been mentioned in the introduction, the numerical simulations focused on the reproduction of gas permeability changes recorded while performing triaxial compression tests (TC-tests).

3.1 Main features

The salt concrete is considered to be dry, intact, isotropic, homogenized (disregard of salt concrete as a multi-component material) and isothermal. The laboratory temperature is neglected for simplification purpose as well. The sample is exclusively simulated, whereas the rest of the testing apparatus is ignored. In order to remain as close to the real condition as necessary, the model geometry is equal to the sample geometry. The sample is considered to be l = 0.14 m high and r = 0.035 m in radius. Due to the symmetry with respect to the center line, the sample is simulated axial symmetrically (compare left side of *Fig. 3-1*). The initial stresses are set to $\sigma_{0\ x,y,z}$ = - 0.1 MPa and the initial porosity of the salt concrete is considered to be ϕ_0 = 0.06.

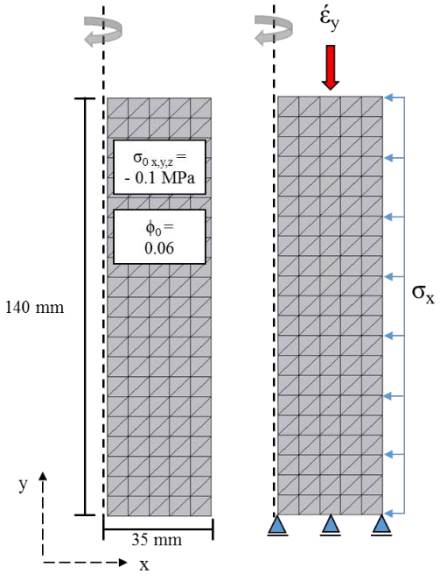

Fig. 3-1: Model geometry, initial and boundary conditions

The right side of *Fig. 3-1* shows the applied boundary conditions. Horizontal displacements are allowed on the top as well as the bottom part of the sample. Different stresses confine the sample laterally (depicted by σ_x). By this means a homogenous stress distribution in horizontal direction is created thereupon.

The simulation comprises one time interval only, in which the sample is compressed by a constant displacement rate of $\dot{\varepsilon}_y$ = - 3.1e-5 s^{-1}, and is stopped when failure is identified. In this case it is not possible to reach converging values within the simulation.

In order to reproduce the deformation behavior as well as the permeability evolution, both constitutive models had to be calibrated. The results of the parameter calibration are listed in *Tab. 3-1*.

	Mechanical part (1)							
	E [MPa]	ν [-]	Φ [°]	ω [-]	φ peak [°]	c peak [MPa]	φ ini [°]	φ res [°]
Sample P5	10 000	0.18	25	0.30	23.50	12.30	9.40	2.35
Sample P13	10 000	0.18	25	0.30	23.50	12.30	9.40	2.35

	Mechanical part (2)					Hydraulic part		
	a hard [-]	a soft [-]	ξ_1 [-]	ξ_2 [-]	ξ_3 [-]	k_f [m²]	ε vol. per. [-]	A [-]
Sample P5	0.005	1.0	0.02	0.04	0.04	3.e-17	0.0008	2
Sample P13	0.005	1.0	0.009	0.01	0.01	2.e-17	0.001	12

Tab. 3-1: Calibrated sets of material parameters

Triangular elements are selected for mesh generation. In whole the generated mesh consists of 210 elements and 132 nodes. The elements are equally distributed.

4 RESULTS

The *Fig. 4-1* and *Fig. 4-3* show the finally obtained results of parameter calibration. The employed visco-plasticity model enables the description of the deformation behavior including a sufficient estimation of strain-hardening prior peak and peak strength. By employing a non-associated flow rule, the volumetric strain development has been simulated satisfactorily as well.

Even though the present percolation model has not been implemented in Code_Bright yet and it has not been possible to perform a hydraulic-mechanically coupled simulation of the TC-tests thus, the sequential reproduction has yielded satisfying results as it can be seen in *Fig. 4-2* and *Fig. 4-4*. Likewise the results published in [2], the obtained results depict a trend, which is in accordance with the experiment values. The present percolation model has proved to be beneficial in order to reproduce the observed permeability evolution in salt concrete.

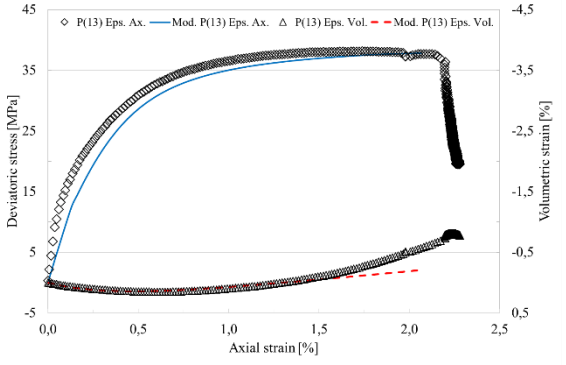

Fig. 4-1: Mechanical behavior simulation of P13 (σ_3 = 1 MPa)

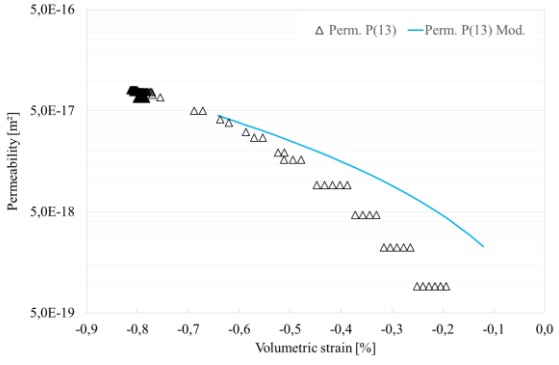

Fig. 4-2: Permeability evolution simulation of P13

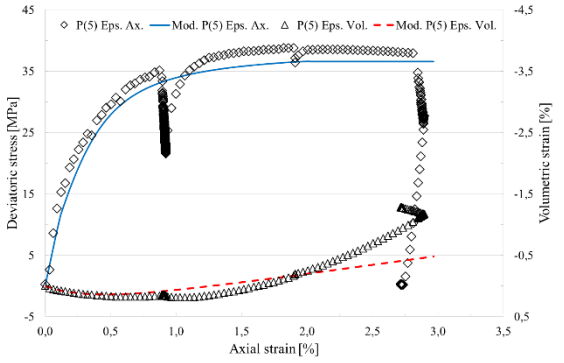

Fig. 4-3: Mechanical behavior simulation of P5 (σ_3 = 2 MPa)

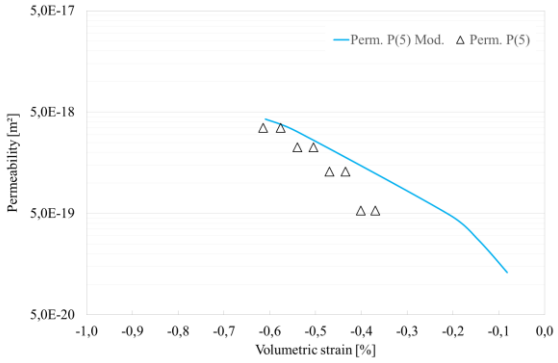

Fig. 4-4: Permeability evolution simulation of P5

5 CONCLUSION

The observed increase of gas permeability has sufficiently been reproduced by employing a constitutive model basing upon percolation theory, even though the volumetric strain has been used as a substitute of porosity.

Focusing on salt concrete, the percolation model involves some drawbacks identified while experiment simulation, for instance the disregard of retention processes inside the cement matrix. Further the percolation model does not only require information about the threshold of volumetric strain, at which a stable gas flux is expectable for the first time, but also about the maximum expectable permeability. The determination of proper values of these parameters represents a demanding task. Beside the confining stress, both values strongly depend on the material homogeneity and isotropy.

One suggestion for improving the employed form of the percolation model is to make use of a threshold parameter, which is not dependent from the volumetric strains but rather from the deviatoric stress. Thus the great variation of percolation threshold values can be counteracted efficiently.

6 REFERENCES

[1] Bundesministerium für Umwelt, Naturschutz and Reaktorsicherheit (BMUB). Sicherheitsanforderungen an die Endlagerung wärmeentwickelnder radioaktiver Abfälle; 2010.

[2] Czaikowski O. Full scale demonstration of plugs and seals (DOPAS) Deliverable D3.28 &D5.5: Status report on LASA related laboratory tests and on process modelling activities. Braunschweig: GRS; 2016.

[3] Mánica M, Gens A, Vaunat J, Ruiz DF. A time-dependent anisotropic model for argillaceous rocks. Application to an underground excavation in Callovo-Oxfordian claystone. Computers and Geotechnics 2016.

[4] Wieczorek K. THERESA: Coupled thermal-hydrological-mechanical-chemical processes for application in repository assessment. Köln, Hannover: Ges. für Anlagen- und Reaktorsicherheit (GRS); 2009.

MODELLING THERMAL INDUCED DAMAGE IN PERMEABLE ROCKS

C.J. Villarraga[*], J. Vaunat[*] and M. Gasc-Barbier[†]

[*] Department of Civil and Environmental Engineering
Technical University of Catalonia (UPC)
Campus Nord UPC, 08034 Barcelona, Spain
E-mail : claudia.juliana.villarraga@estudiant.upc.edu, jean.vaunat@upc.edu

[†] Centre for studies and expertise on risks, environment mobility and urban and country planning (CEREMA)
Rue Albert Einstein, 13290 Aix-en-Provence, France
E-mail : muriel.gasc@cerema.fr

Key words: GiD interface, THM coupled analysis, Geological media

Abstract. *The environmental conditions play an important role in the stability of rock cliffs. In fact, in several cases the weather-induced mechanisms have been considered as the triggering factor of instabilities. Daily and seasonal temperature fluctuations can generate internal stress; high enough to create and propagate cracks in the most superficial zone of rock cliffs. An experimental program has been developed to evaluate the damage induce in a limestone, due to natural thermal cycles. A numerical constitutive model is proposed and implemented in Code_Bright in order to be able to reproduce the phenomena observed.*

1 INTRODUCTION

Rock degradation due to weather conditions can be a triggering factor for rockfalls, generally, those weathering process are related to freeze-thaw phenomena [1,2]. Nevertheless, thermal cycling whit temperatures far from extreme values may lead to the generation and propagation of existent fissures, inducing damage in the rock mass and eventually producing rockfalls, that may occurred without any evident triggering factor, like earthquakes or rains periods. [3,4]

The thermal degradation of rocks is mostly influenced by the different thermal properties of the minerals that compose the rock. Differences in thermal expansion, thermal conductivity and principal mineral axis direction, controls the mineral to mineral thermal stress induced by the thermal gradients. Hence, additional stress can be generated leading to failure across the minerals boundaries, and lines of weakness, producing some intergranular disintegration and propagation of existent fissures. [5,6]

This environmental thermal induce damage can be analysed under laboratory conditions by the evolution of different physical and mechanical properties, under prescribed thermal cycles. The elastic wave propagation velocity is a common parameter used for this purpose, since, it is extremely sensitive to the presence of defects in the sample, (like the internal fissures) due to the considerable difference of this parameter between the air and the solid materials [7,8].

Additionally, the elastic wave propagation velocity can easily be related to the dynamic Young and Poisson modulus, allowing the comparison with the results obtained with mechanical test[9]

The response of this phenomena is commonly represented with microscopic models, were

the mineralogical interaction is analysed[10,11]. For this reason, a numerical model is proposed with the aim of reproducing the macroscale phenomena observed whit an experimental program focused in the thermal fatigue of a Limestone coming from a rock cliff prone to rockfalls.

2 PROBLEM DESCRIPTION.

La Roque Gageac is a small town located at the south-west of France. It is placed in the border of La Dordogne river at the toe of an 80m high limestone cliff. As presented in Figure 1. This cliff has a troglodyte cavern that is an important tourist attraction to the region..

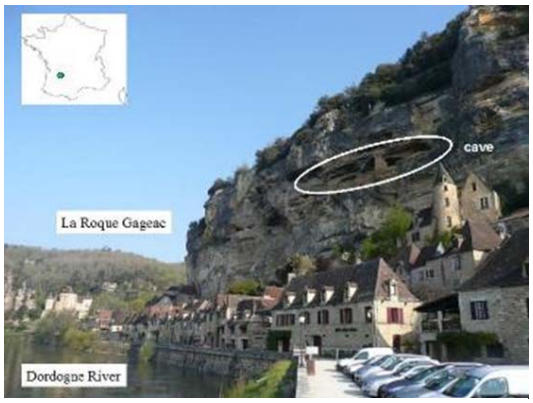

Figure 1 La Roque Gageac localization

This cliff is mainly composed by limestones conformed under marine conditions from the intermediate and the upper coniacian. Due to its calcareous nature, the most permeable layer placed in the upper coniacian formation is affected by the karst phenomena. Nevertheless, this cliff is composed by layer of different ages: the upper coniacian and the lower coniacian (an impermeable layer) in the inferior zone. As consequence, the karst phenomena cannot be completely developed in vertical direction.

The town of La Roque Gageac has suffered several rock falls, with a periodicity of more or less 50 years. The last event occurred in January 2010 when a part of the roof of the troglodyte caver collapsed. After this event, several instrumentation systems were installed within and around the troglodyte cavern. Description and first results of this instrumentation program are presented in Ruiz (2013)[12] and Gasc-Barbier (2015)[13]. The response observed with the devices installed show an important relation between deformations in the cliff and natural thermal cycles. As result, a laboratory program has been developed to evaluate the thermal-mechanical rock properties.

3 EXPERIMENTAL PROGRAM

An experimental program is developed to evaluate the possible damage induced natural thermal variations. For this, samples from La Roque Gageac limestone were submitted to thermal cycles. Since, the aim of this laboratory study is to evaluate the effect of natural thermal variations, the thermal gradient considered is close to the one observed in the cliff, 40ºC. Each cycle last 3 hours and temperature varies from 10ºC to 50ºC.

The degradation of the samples was evaluated through different mechanical parameters, like the elastic wave propagation velocity. The reduction in this parameter can be related to the rock damage, even if, the sample don't show any superficial crack [14]. Moreover, this parameter is obtained whit a non-destructive test, hence, is possible to evaluate its evolution in the same sample through the complete laboratory study.

3.1 Samples description

For this experimental program two types of samples were considered: samples drilled from rock blocks dropped within the cavern during the 2010 event and samples drilled directly from the cliff face, nearby the troglodyte cavern.

Even if, both groups of samples were obtained from the same cliff, they show some mineralogical differences associated to the heterogeneity of this geological formation. From mineralogical analysis, it is observed that samples obtained from the blocks are mainly composed by calcite (90% calcite) but, samples form the cliff face are composed by quartz (50%) and calcite (45%)

This mineralogical composition difference may be the responsible of differences observed in the initial elastic wave propagation velocity value. Samples from the rock blocks have a mean compression elastic wave propagation velocity (VP) of 4400 m/s while samples from the cliff face 2900m/s

3.2 Elastic wave propagation velocities results.

The elastic compression (Vp) and shear (Vs) wave propagation velocities are obtained by the ultrasonic pulse technique following the French Standard NF P 94-411. From the results of elastic compression (Vp) and shear (Vs) wave propagation velocities, the dynamic Young (E) and Poisson (υ) modulus can be calculated[9], following the next equation:

$$K = \left(\frac{E}{3(1+2\nu)} \right) \quad \text{Where,} \quad E = \left(\rho \frac{V_p^2 (1+\nu)(1-2\nu)}{(1+\nu)} \right) \quad \text{and} \quad \nu = \left(\frac{-0.5\left(\frac{V_s}{V_p}\right)^2}{1-\left(\frac{V_s}{V_p}\right)^2} \right) \quad (1)$$

After 500 cycles of temperature a reduction in Vp and Vs values is observed. This reduction represents a stiffness reduction around 6% for the calcite mainly composed samples and 18% for quartz-calcite composed samples, as example Figure 2 shows the evolution of Vp and Stiffness (K) for sample the 5 obtained from the rock blocks and the sample 27 taken from the face cliff.

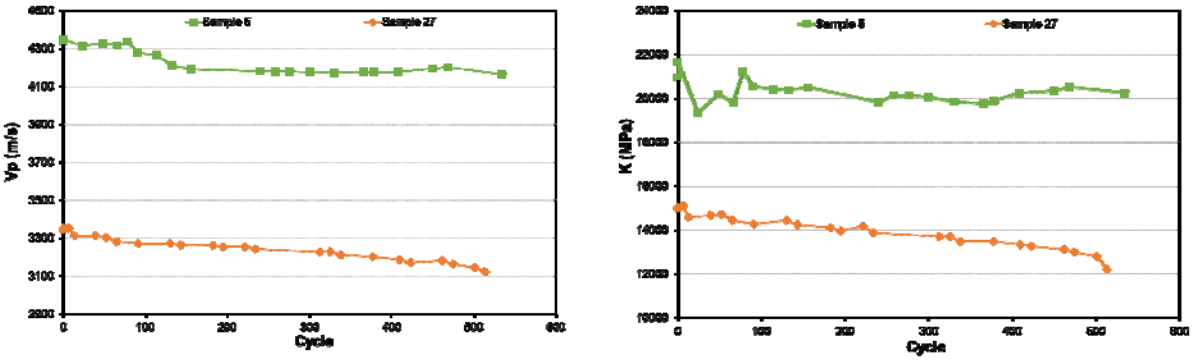

A) B)

Figure 2 Laboratory results for samples 5 and 27 A) Vp evolution B) Stiffness evolution

4 NUMERICAL MODELLING

4.1 Composite material model.

From de mineralogical point of view the thermal induce damage in rocks can be considered as a microstructural re-accommodation associated to the different thermo-mechanical response of the minerals that compose the rock. Nevertheless, the aim of this study is to be available of modelling this phenomenon at a macroscopic scale, not at mineral scale.

For this, the composite material model purposed by Vaunat and Gens (2003)[15] for argillaceous rocks is considered, this original model was modify in order to fulfilled the characteristics of the phenomena under study.

The model considers that the rock is composed by two different components: a strong matrix and bonds. As illustrated in Figure 3. For the case of La Roque Gageac, the matrix represents the sandy minerals, and the bonds, the calcite minerals. The mechanical response of the matrix may be defined by different failure criteria. In the other hand, the bond behavior is defined by the scalar damage model proposed by Carol et al (2001)[16], Its response is elastic, but with moduli that progressively decrease during loading as micro-cracks developed inside the material.

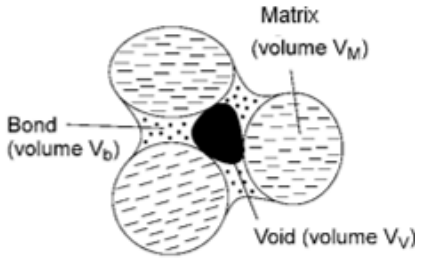

Figure 3 Schematic rock composition

From the original composite model, the principal difference introduced is that the two components of the material are considered to work in parallel; therefore, the new strain partition is defined as:

$$d\varepsilon_v^{ext} = -\frac{dV}{V} = -\frac{dV_V}{V} - c_b\frac{dV_b}{V_b} - c_M\frac{dV_M}{V_M} = d\varepsilon_v^{int} + c_b d\varepsilon_v^b + c_N d\varepsilon_v^M \tag{2}$$

Where $d\varepsilon_v^{ext}$ is the volumetric strain increment applied to the medium, $d\varepsilon_v^{int}$ the volumetric strain used to update soil porosity $d\varepsilon_v^b$ the volumetric strain inside bonds and $d\varepsilon_v^m$ the volumetric strain inside the matrix, C_b is the bond content and C_M the matrix content. Two proportional coefficients between $d\varepsilon_v^{int}$, $d\varepsilon_v^b$ and $d\varepsilon_v^m$ are defined, these coefficients are model parameters:

$$X_b = \frac{c_b d\varepsilon_v^b}{d\varepsilon_v^{int}}$$
$$X_M = \frac{c_M d\varepsilon_v^M}{d\varepsilon_v^{int}} \tag{3}$$

The stress partition is obtained by stating that the work input into the medium under any compatible external strain increment is equal to sum of the work input into the matrix and the bonds. Finally, the stress partition is defined by the equation 4.

$$\sigma^{ext} = \underbrace{\frac{X_M}{1 + X_b + X_M}}_{\delta_\sigma} \sigma^M + \underbrace{\frac{X_b}{1 + X_b + X_M}}_{\delta_\sigma} \sigma^b \quad (4)$$

4.2 Experimental results modelling.

The composite material model previously described was implemented in the finite element code CODE_BRIGHT[17]. This model is used to reproduce the experimental results obtained with samples from La Roque Gageac subjected to thermal cycles between 10ºC to 50ºC. For instance, the responses of samples 5 and 27 (presented in section 3), are modelled at Gauss-point level. Table 1 presents the damage parameter considered, the mechanical behavior of the matrix is defined by a Mohr-Coulomb failure criteria.

Parameter	Sample 5	Sample 27
Matrix stiffness K_u (Mpa)	15900	15900
Initial bonding stiffness K_{B0} (MPa)	18000	15200
Porosity (n)	0.15	0.12
Matrix thermal expansion α_M (1/ºC)	6e-6	6e-6
Bond thermal expansion α_b (1/ºC)	6e-6	6e-6
Bond damage locus r_{b0} (MPa)	1e-5	1e-5
Damage evolution rate r_1 (MPa)	0.005	0.005
C_B	0.7	0.5
X_M	3.5	2.5
X_B	5.5	5.5

Table 1 Damage model parameters

Note that the bonding content (C_b) consider for the modelling is different for each sample, this is related to the different mineralogical composition of the samples considered. Sample 5 is mainly composed by calcite. Therefore, the predominant component is the bond, nevertheless, sample 27 is composed in a 50-50 relation by quartz and calcite, then its bonding content is lower that for the 90% calcite sample.

Figure 4 presents the results obtained in the numerical modelling. In both cases the model is capable of reproducing the stiffness reduction observed whit the laboratory tests. Note also, that sample 5 has a slower damage rate that the one observed in sample 27, as is experienced whit the laboratory analysis.

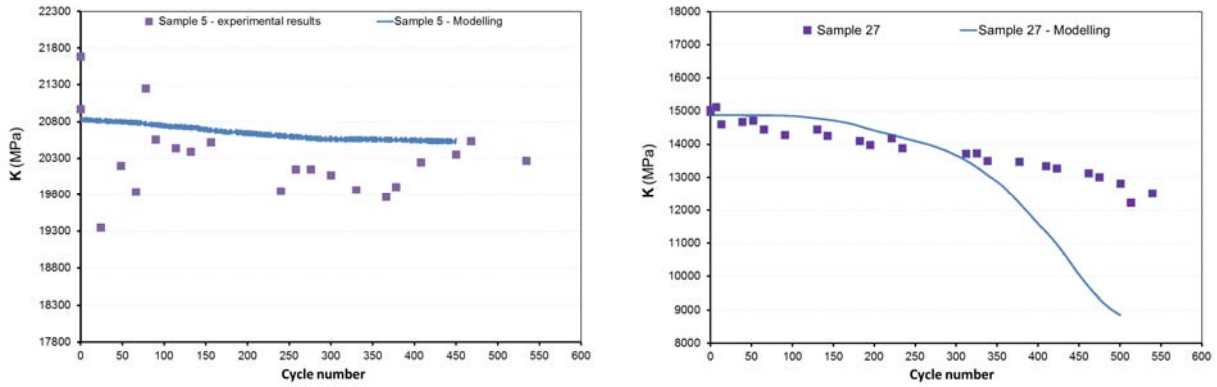

A) B)

Figure 4 Numerical model results A) sample 5 B) sample 27

5 CONCLUSIONS

- The results of the experimental program show a reduction in the sample stiffness with the augmentation of natural thermal cycles imposed. This phenomenon is associated to a damage induced in the rock
- A constitutive model is proposed with the aim of reproducing the damage process observed in the experimental program. This phenomenological approach is based in the hypothesis that the rock behaviour can be analysed as the interaction between two different materials whit different behaviours.
- The constitutive model presented and implemented in **CODE_BRIGHT** has the capability to reproduce the stiffness reduction observed with the experimental programs, for two samples whit different mineralogical composition.
- The thermal degradation of the rocks, induce the generation of micro-fissures but also the propagation of existent ones. This last phenomenon could be evaluated whit the numerical model presented. If we consider that the pre-existing fissure is a weaker zone whit lower bond damage locus stress. The response of this zone may increment the stress of the surrounding material inducing more damage.

REFERENCES

1. Hall K. Evidence for freeze-thaw events and their implications for rock weathering in northern Canada: II. The temperature at which water freezes in rock. *Earth Surf Process Landforms*. 2007;32(2):249-259. doi:10.1002/esp.1389.
2. Matsuoka N, Sakai H. Rockfall activity from an alpine cliff during thawing periods. *Geomorphology*. 1999;28(3-4):309-328. doi:10.1016/S0169-555X(98)00116-0.
3. Do Amaral Vargas E, Velloso RQ, Chávez LE, Gusmão L, Do Amaral CP. On the effect of thermally induced stresses in failures of some rock slopes in Rio de Janeiro, Brazil. *Rock Mech Rock Eng*. 2013;46(1):123-134. doi:10.1007/s00603-012-0247-9.
4. Vlcko J, Greif V, Grof V, Jezny M, Petro L, Brcek M. Rock displacement and thermal expansion study at historic heritage sites in Slovakia. *Environ Geol*. 2009;58(8):1727-1740. doi:10.1007/s00254-008-1672-7.
5. Hall K, Thorn CE. Thermal fatigue and thermal shock in bedrock: An attempt to unravel the geomorphic processes and products. *Geomorphology*. 2014;206:1-13. doi:10.1016/j.geomorph.2013.09.022.
6. Walsh SDC, Lomov IN. Micromechanical modeling of thermal spallation in granitic rock. *Int J Heat Mass Transf*. 2013;65:366-373. doi:10.1016/j.ijheatmasstransfer.2013.05.043.
7. Brotóns V, Tomás R, Ivorra S, Alarcón JC. Temperature influence on the physical and mechanical properties of a porous rock: San Julian's calcarenite. *Eng Geol*. 2013;167:117-127. doi:10.1016/j.enggeo.2013.10.012.
8. Martínez-Martínez J, Benavente D, García-del-Cura MA. Spatial attenuation: The most sensitive ultrasonic parameter for detecting petrographic features and decay processes in carbonate rocks. *Eng Geol*. 2011;119(3-4):84-95. doi:10.1016/j.enggeo.2011.02.002.
9. Kendrick JE, Smith R, Sammonds P, Meredith PG, Dainty M, Pallister JS. The influence of thermal and cyclic stressing on the strength of rocks from Mount St. Helens, Washington. *Bull Volcanol*. 2013;75(7):1-12. doi:10.1007/s00445-013-0728-z.
10. Wanne TS, Young RP. Bonded-particle modeling of thermally fractured granite. *Int J Rock Mech Min Sci*. 2008;45(5):789-799. doi:10.1016/j.ijrmms.2007.09.004.

11. Shushakova V, Fuller ER, Siegesmund S. Microcracking in calcite and dolomite marble: Microstructural influences and effects on properties. *Environ Earth Sci*. 2013;69(4):1263-1279. doi:10.1007/s12665-012-1995-2.
12. Ruiz D. Thermo-mechanical analysis of the stability of a rock-cliff under climatic actions. *upcommons.upc.edu*. 2013;(January).
13. Gasc-Babier M, Virely D, Guittard J. Termal fatigue in rocks- La Roque-Gageac's case study. *ISRM Congr 2015 Proc - Int Symp Rock Mech*. 2015.
14. Yavuz H, Altindag R, Sarac S, Ugur I, Sengun N. Estimating the index properties of deteriorated carbonate rocks due to freeze-thaw and thermal shock weathering. *Int J Rock Mech Min Sci*. 2006;43(5):767-775. doi:10.1016/j.ijrmms.2005.12.004.
15. Vaunat J, Gens A. Bond degradation and irreversible strains in soft argillaceous rock Degradación y deformación irreversible de una roca blanda arcillosa. *Symp Geotech Eng Hard Soils – Soft Rocks*. 2001:1-6.
16. Carol I, Rizzi E, Willam K. On the formulation of anisotropic elastic degradation. I. Theory based on a pseudo-logarithmic damage tensor rate. *Int J Solids Struct*. 2001;38:491-518. doi:10.1016/S0020-7683(00)00030-5.
17. Olivella S, Gens A, Carrera J, Alonso EE. Numerical formulation for a simulator (CODE_BRIGHT) for the coupled analysis of saline media. *Eng Comput*. 1996;13(7):87-112. doi:10.1108/02644409610151575.

MODELLING TUNNEL PERFORMANCE IN CHEMICALLY-INDUCED SWELLING ROCKS

Ramon, A., Alonso, E.E. and Olivella, S.

Department of Civil and Environmental Engineering, Division of Geotechnical Engineering and Geosciences
Technical University of Catalonia (UPC)
Campus Nord UPC, 08034 Barcelona, Spain
e-mail: anna.ramon@upc.edu

Key words: Tunnel, expansion, anhydrite, chemical, joints, gypsum

ABSTRACT

Severe sulphate-related damage has been described in tunnels in Central Europe [i,ii,iii]. One well known case is Lilla tunnel, which suffered the strongest damage observed in tunnels crossing sulphated formations in Spain. Damage and displacements were concentrated at tunnel floor. Topographic levelling of the original flat slab recorded mean values of floor heave rate ranging from 1.2 to 2 mm/day. A vertical displacement of the slab close to one meter was measured in a critical section 13 months after the beginning of swelling. Pressure cells installed at the rock/concrete contact at the invert of test sections measured maximum values of swelling pressures close to 5 MPa. The extreme damage induced by heave motivated the excavation of the entire tunnel and the construction of a circular, highly reinforced cross-section. The monitoring of Lilla tunnel during construction and operation has shown that the recorded intensity of heave and swelling pressure varies along the tunnel length. Figure 1 shows also one example of the large variation of vertical pressure in a cross section. Swelling pressures recorded during tunnel operation reach values up to 6-7 MPa against the reinforced circular concrete lining in some pressure cells. However, the maximum recorded swelling pressures during operation are close to 5 - 6 MPa in the majority of the sections.

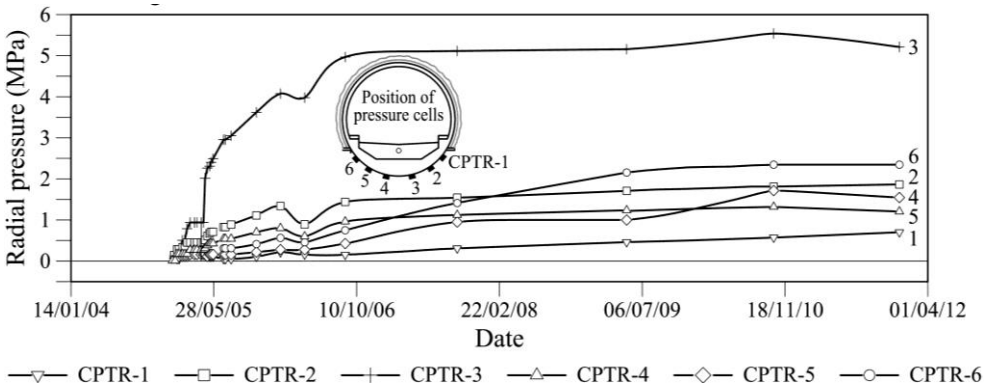

Figure 1. Recorded maximum radial pressures during tunnel operation in one section

Current understanding on sulphate-related damage in tunnels suggests that damage is induced by strong swelling strains and swelling pressures in the presence of saturated anhydritic-clayey formations. An additional condition for the triggering of swelling is the presence of soil or rock discontinuities, natural or induced by the tunnel excavation. Sustained

heave and swelling deformations are the result of the precipitation of gypsum crystals in discontinuities. The process of crystal growth in discontinuities enhances the opening of the fractures inducing expansions in the rock mass and generating swelling pressures when swelling strains are prevented. Gypsum crystals precipitate from sulphated water supersaturated with respect to gypsum. Since solubility of anhydrite is higher than the solubility of gypsum at the existing temperatures in the rock mass, supersaturation conditions in groundwater are achieved when anhydrite is present in the rock.

These phenomena are demonstrated in Lilla tunnel case. An active expanding layer 4-5 m thick, where swelling strains accumulated over time, was found below the floor of Lilla tunnel in the anhydritic claystone. Gypsum crystal growth was observed in rock discontinuities recovered from the active expanding layer.

The presentation describes a model capable of reproducing the observed fundamental swelling mechanisms at the real scale. A singular feature of the model is the simulation of the opening of discontinuities induced by tunnel excavation[iv]. A joint element embedded in a continuum formulation, where precipitation occurs, has been formulated to reproduce the generation of joints in tensile strain fields. Current strains, spacing and aperture of the fractures in the rock mass provide the opening of the fractures. The model describes that the opening of discontinuities increases the initial permeability of the rock and the presence of discontinuities triggers the precipitation of gypsum and associated swelling. A hydro-chemo-mechanical formulation consistent with dissolution and precipitation of sulphated minerals[v] was incorporated into a general coupled hydro-mechanical formulation. The mineralogical composition of the rock and groundwater as well as the chemical processes involved in the dissolution and precipitation of sulphated minerals are taken into account in the formulation.

The model helped to analyse the swelling phenomena and the lining response of a well-documented case history (Lilla tunnel) characterized by an extensive instrumentation and a long term monitoring record (ten years of data).

REFERENCES

[i] Wittke, M. (2006). Design, construction, supervision and long-term behaviour of tunnels in swelling rocks. Proc EUROCK 2006: Multiphysics Coupling and Long Term Behaviour in Rock Mechanics, Liège, 211-216.

[ii] Anagnostou, G., Pimentel, E. & Serafeimidis, K. (2010). Swelling of sulphatic claystones –some fundamental questions and their practical relevance. Geomechanics and Tunnelling, 3, No. 5, 567-573.

[iii] Alonso, E.E., Berdugo, I.R. and Ramon, A. (2013). Extreme expansive phenomena in anhydritic-gypsiferous claystone: the case of Lilla tunnel. Géotechnique 63 No. 7, 584 – 612, [http://dx.doi.org/10.1680/geot.12.P.143].

[iv] Ramon, A., Alonso, E.E and Olivella, S. (2017). Hydro-chemo-mechanical modelling of tunnels in sulphate rocks. Géotechnique SiP 2017, sent for publication.

[v] Ramon, A. and Alonso, E.E. 2013. Heave of a railway bridge: modelling gypsum crystal growth. Géotechnique, 63(9): 720–732. doi:10.1680/geot.12.P.035.

SENSITIVITY ANALYSIS ON THE SWELLING EFFECTS OF BENTONITE IN CODE_BRIGHT USING DIFFERENT APPROACHES

A. Rodriguez-Dono[*] and S. Olivella[*]

[*] Department of Civil and Environmental Engineering
Technical University of Catalonia (UPC)
Campus Nord UPC, 08034 Barcelona, Spain
e-mail: code.bright@upc.edu
web page: www.etcg.upc.edu/recerca/webs/code_bright/

Key words: Sensitivity analysis, coupled analysis, swelling, bentonite, nuclear waste.

Abstract. *Previous studies on the THM modelling of engineered barrier systems (EBS) for underground nuclear waste disposal showed strong sensitivities of the output quantities to changes in the input parameters and to the different approaches used in different numerical codes. To investigate the effects of value uncertainties on the modelling results, to improve the understanding of the coupled processes active in the repository near field and to increase confidence in the predictive capabilities of different numerical codes, a sensitivity analysis and code comparison of EBS simulations was perform. From this code comparison, some quantitative deviations have been found for coupled THM processes, although the overall qualitative agreement is good. For these deviations, explanations have been identified; among these are differences in process couplings and definition of the mechanical material behaviour of the bentonite, especially when including swelling, which are analysed in this paper.*

1 INTRODUCTION

Deep geological storage or disposal remains the preferred option for waste management of heat-emitting, high-level radioactive nuclear waste (HLW) in several countries.

The required degree of waste isolation needed for HLW is provided by a combination of engineered and natural barriers placed between the potentially harmful radionuclides and the biosphere. The natural barrier is fundamentally the host rock, and the artificial barriers are the solid matrix of the waste itself, the metallic canister enclosing the waste, and the backfill −the sealing material placed around the canisters. This backfill, also called an 'engineered barrier', is often constructed using compacted expansive clay. Bentonite has generally been chosen because of its high swelling capacity, low permeability and favorable retardation properties (Gens et al., 2009).

The bentonite barrier fulfills several important functions. In the first instance, a very low hydraulic conductivity restricts water penetration and retards significantly solute transport due to its low diffusion coefficient and to additional sorption effects. It should also provide a favorable chemical environment and be able to self-heal if subjected to physical perturbation such as cracking and fissuring events (Gens, 2003). The engineered clay barrier and adjacent host rock (usually called the 'near field') will be subjected to the heating effect of the nuclear waste, and to various associated hydraulic and mechanical phenomena that interact in a complex way.

In addition, compacted bentonite is initially unsaturated, and will therefore be subjected to

hydration from the surrounding rock, triggering further coupled thermo-hydro-mechanical (THM) phenomena. In order to achieve a safe and robust repository design, it is necessary to have a good understanding of the processes that occur in the near field and of their evolution over time (Gens et al., 2009).

Given the importance of the problem, it has proved useful to perform large-scale and medium-scale heating tests simulating repository conditions in underground laboratories around the world (Dixon et al., 2002; Pusch et al., 1985; Selvadurai, 1997; Volckaert et al., 1996). Because of the low permeability of the materials involved, such experiments usually require long testing times, measured in years, in order to obtain meaningful results. The complexity of the phenomena involved, and of their interactions, implies that process understanding and interpretation of results are limited unless supported by suitable numerical models able to reproduce the main features of the test. Owing to the coupled nature of the THM interactions, coupled THM formulations are inevitably required.

Previous studies on the THM modelling of engineered barrier systems (EBS) for underground nuclear waste disposal showed strong sensitivities of the output quantities to changes in the input parameters and to the different approaches used in different numerical codes. A sensitivity analysis and code comparison of EBS simulations has been chosen as one of the tasks within the project Task Force on Engineered Barrier Systems. The aim of this task is to investigate the effects of value uncertainties on the modelling results, improve the understanding of the coupled processes active in the repository near field and increase confidence in the predictive capabilities of different numerical codes.

Based on the Swedish disposal concept for spent nuclear fuel, the base case model of the sensitivity analysis and the code comparison is a simplified representation of a single KBS-3V deposition hole in a two-dimensional axisymmetric model. The broad sensitivity analysis included variations of material parameter values, boundary and initial conditions, considered physical processes and alternative model geometries amounting to about 60 different modelling cases. A sub-task of the sensitivity analysis was a code comparison, using the base case model as a benchmark example for coupled thermo-hydro-mechanical simulations of the near field. The code comparison has been divided into different stages with increasing complexity, from TH- to THM-calculations using a simplified swelling law for the bentonite. Six teams participated in the sub-task, providing results of six different numerical codes (Amec Foster Wheeler using Tough2-FLAC3D, BGR using OpenGeoSys, Clay Technology using Comsol, CRIEPI using LOSTUF, EPFL using Lagamine and UPC using Code_Bright). The results have been compared in terms of the evolution of temperature, liquid pore pressure, liquid saturation degree and stress components.

2 SENSITIVITY ANALYSIS

In the context of the sensitivity analysis task and given that the larger differences produced among all the codes happened when including swelling, this paper has been mainly focused on the different existing formulations for modelling swelling in Code_Bright and the different results obtain with each of it. In addition, we have compared the different results with the results from OGS, given by Annika Schäfers. To do that, we have selected a HM model, not considering this time the effects of the temperature for the sake of simplicity and easier analysis of the results.

The different formulations showed were: Linear elastic (1); Linear elastic + *f*(suction) (2); BBM (3); and Linear elastic + *f*(saturation) (4). The first three formulations are included in Code_Bright, meanwhile the last one (4) is not included in Code_Bright, but is the one used by OGS, and has been included for the sake of comparison (Figure 1).

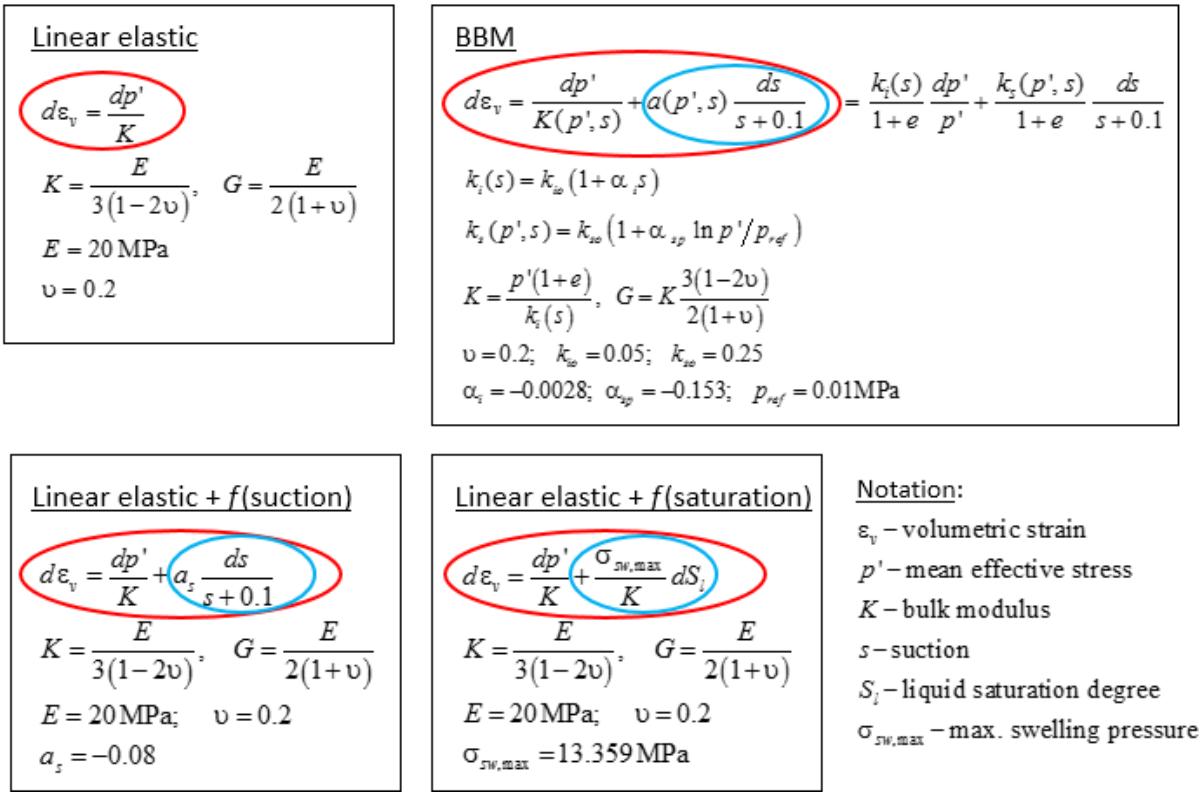

Figure 1. Different existing formulations for modelling swelling in Code_Bright and OGS.

We have observed that if we chose –in Code_Bright– formulation (1), that doesn't include swelling, we obtain the most similar results compared with the ones given by OGS (formulation 4) in terms of both liquid saturation degree and liquid pressure (Figure 2). However, the stress results obtained are of course very different, since this model does not include swelling. In addition, we have taken a close look to the changes in porosity, since we though it could be a key aspect regarding the explanation of the differences in the results. Thus, in this model, the porosity changes mainly occur once we reach saturation conditions, when some swelling will be produced due to positive water pore pressure and, because of this swelling, some contraction in the non-saturated elements.

If, instead, we select formulations (2) or (3), then some differences arise between Code_Bright and OGS results in terms of both liquid saturation degree and liquid pressure, being the stress results obtained, however, much closer now (Figures 3 and 4). We believe the differences are produced because the swelling of bentonite leads to changes in the porosity (coupling effects) when using these swelling models, meanwhile in OGS the porosity remains constant, as far as we understood from Annika Schäfers. Therefore, when porosity diminishes, both liquid saturation degree and liquid pressure tend to increase.

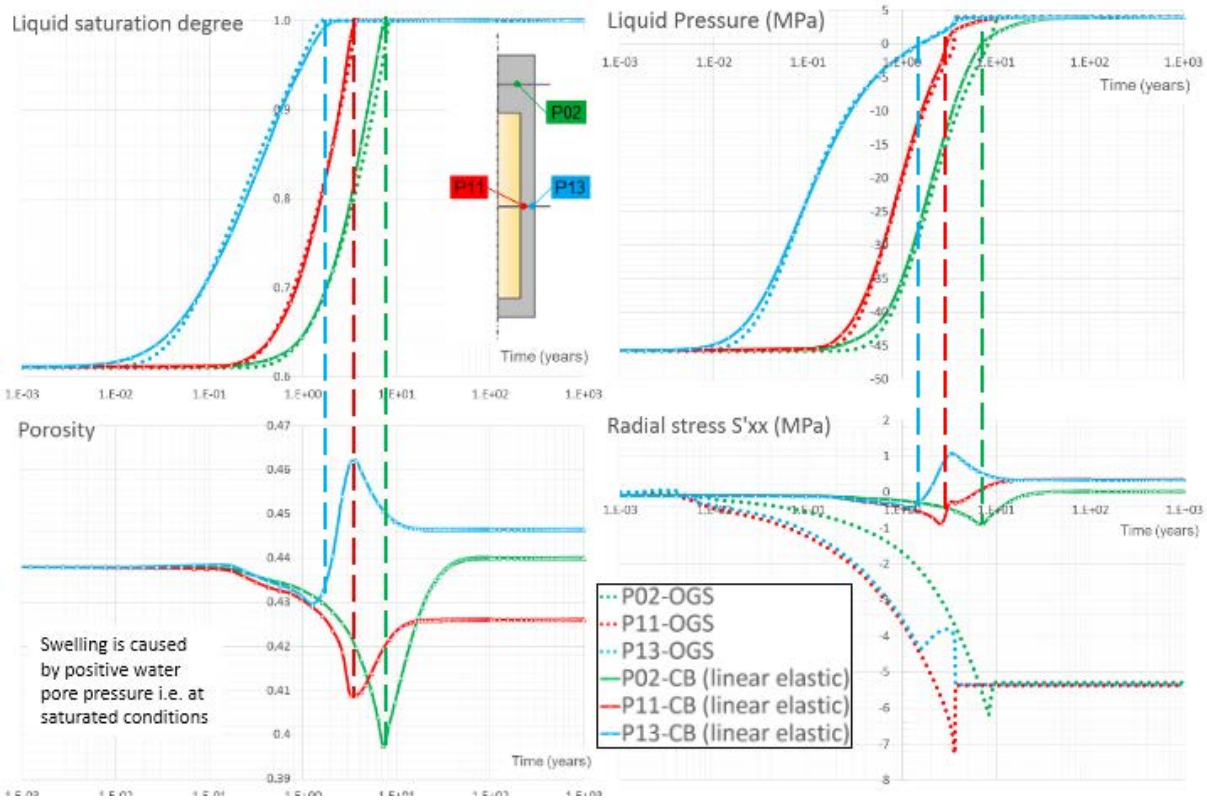

Figure 2. Code_Bright [linear elastic] vs OGS.

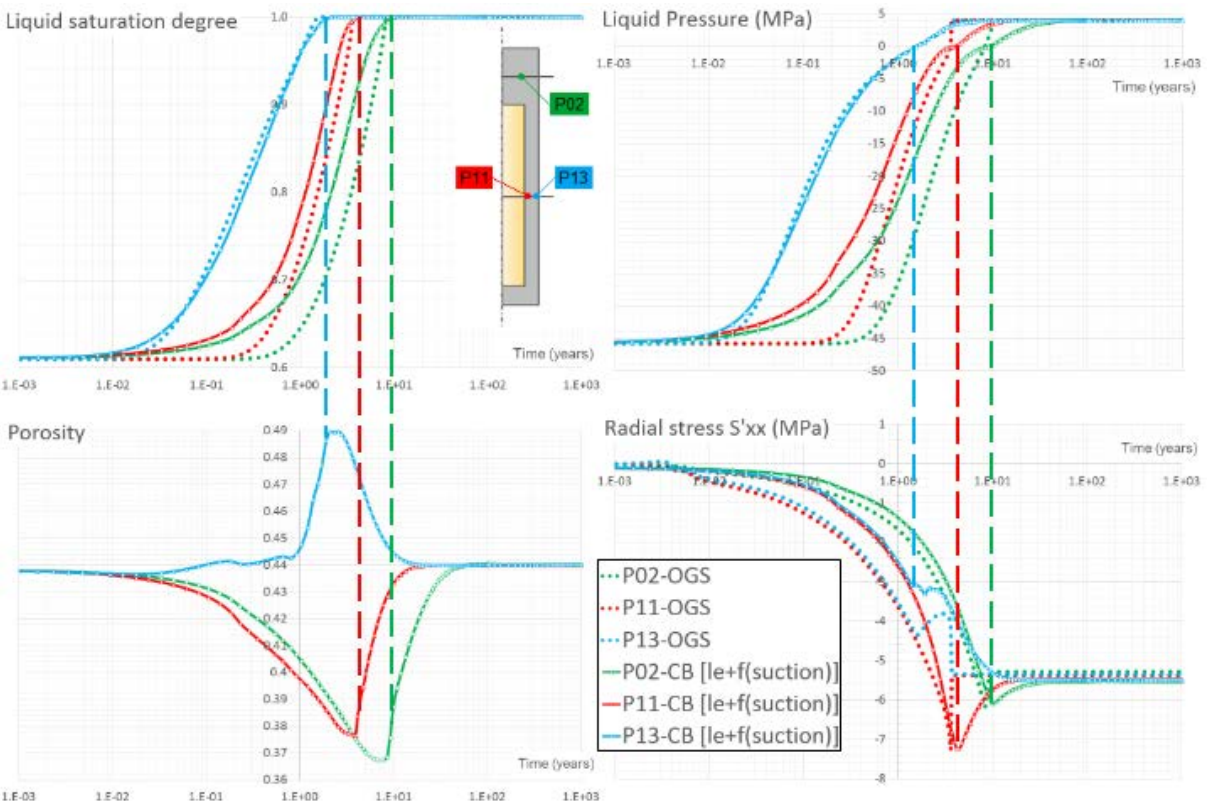

Figure 3. CB [linear elastic + f (suction)] vs OGS.

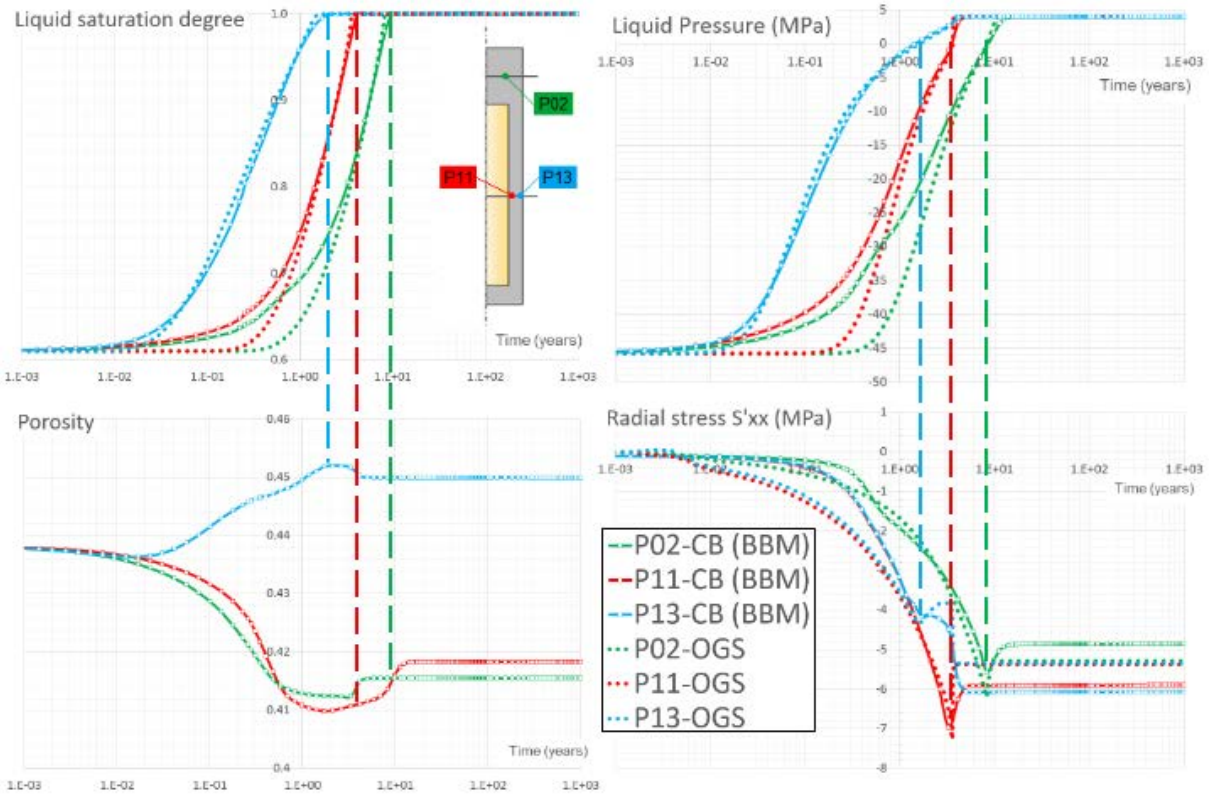

Figure 4. Code_Bright [BBM] vs OGS.

Finally, we wanted to compare the different formulations in terms of how suction and liquid saturation degree change with the change of the mean effective stress, showing the differences between using (2), (3) and (4), which do not seem dramatic, anyway (Figure 5). So the main conclusion is that it seems that we understand the reason for these differences.

3 CONCLUSIONS

In general, it can be concluded from the code comparison that very good agreement between the results of the different codes has been achieved for the TH-coupled processes. For the coupled THM processes some quantitative deviations remain, while the overall qualitative agreement is good. For these remaining differences some explanations were identified, among these are differences in process couplings and definition of the mechanical material behavior of the bentonite, which we will be trying to explain in this paper.

The cross code comparison encouraged a fruitful exchange between modelling teams. In particular, the step-wise increase of complexity of the coupled simulation helped to provide in-depth insights into the individual behavior of the codes when modelling the THM-coupled behavior of EBS. Serving as a benchmark example for THM-coupled simulations of bentonite based EBS, the code comparison task helped to increase the confidence in the modelling capabilities of several codes used for safety evaluations of repositories for spent fuel and high-level radioactive waste.

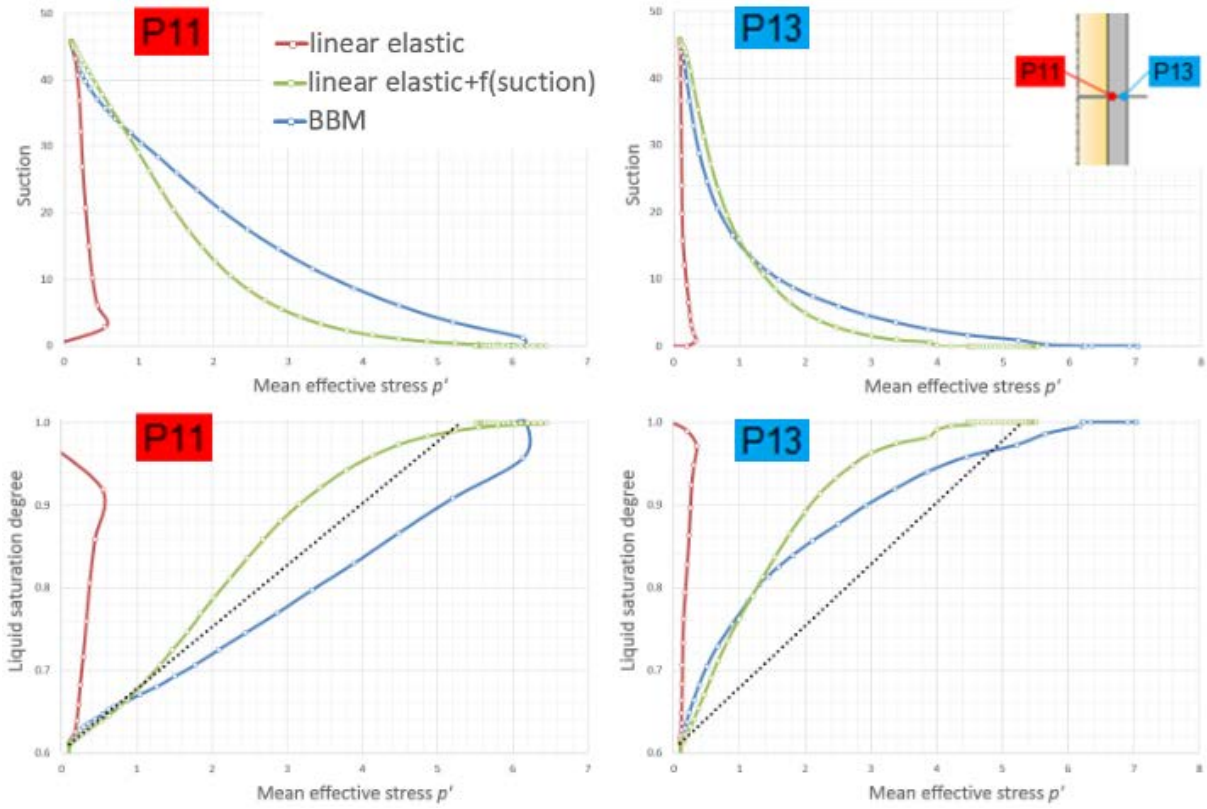

Figure 5. CB different formulations comparison.

REFERENCES

Dixon D, Chandler N, Graham J, Gray MN. Two large-scale sealing tests conducted at Atomic Energy of Canada's underground research laboratory: the buffer-container experiment and the isothermal test. Can Geotech J. 2002;39(3):503-18.

Gens A. The role of geotechnical engineering in nuclear energy utilisation: special lecture. In: Proc 13th Eur Conf Soil Mech Geotech Eng, Prague; 2003;3:25-67.

Gens A, Sanchez M, Guimaraes LDN, Alonso E, Lloret A, Olivella S et al. A full-scale in situ heating test for high-level nuclear waste disposal: observations, analysis and interpretation. Geotech. 2009;59(4):377-99. doi: 10.1680/geot.2009.59.4.377

Pusch R, Borgesson L, Ramqvist G. Final report of the mass buffer test -volume II: Test results, Stripa Project 85/12. Stockholm: SKB; 1985.

Selvadurai APS. Hydro-thermo-mechanics of engineered clay barriers and geological barriers. Eng Geol. 1997;47(4):311-2. doi: 10.1016/S0013-7952(97)00036-7

Volckaert G, Bernier F, Alonso E, Gens A, Samper J, Villar MV, Martin PL, Cuevas J, Campos R, Thomas HR, Imbert C, Zingarelli V. Thermal-hydraulic-mechanical and geochemical behaviour of the clay barrier in radioactive waste repositories (model development and validation), Nuclear Science and Technology, EUR 16744. Luxembourg: Commission of the European Communities; 1996.

MODELLING GAS FLOW EXPERIMENTS IN MX80 BENTONITE

I.P. Damians[*], S. Olivella[*], and A. Gens[*]

[*] Department of Civil and Environmental Engineering
Universitat Politècnica de Catalunya – BarcelonaTech (UPC)
Campus Nord UPC, 08034 Barcelona, Spain
Email: ivan.puig@upc.edu

Key words: Hydraulic 3D model, Gas flow, Mx80 bentonite

Abstract. *A gas injection test, performed on compact bentonite, was carried out at the British Geological Survey. The test is composed by two stages (i.e. hydration followed by gas injection testing). After gas breakthrough and a period of gas flow through the sample, the injection pump was stopped whilst the stresses and porewater pressures were continuously monitored. A 3D numerical model has been developed to simulate the gas injection test and to achieve similar gas pressure responses. After sensitivity analysis of the model, a satisfactory first-calibration approach was possible with only hydraulic model assumptions.*

1 INTRODUCTION: MX80-D TEST

A gas injection test performed on compacted Mx80 bentonite was carried out at the British Geological Survey. This experiment, designated as Mx80-D, represents the first test dataset for a series of tests analyzed by DECOVALEX Task A [1]. These tests are useful to increase the understanding of gas flow potential trough this low permeability materials. With these tests it is possible to improve bentonite functionality (e.g., in nuclear waste repositories) and confirm its suitability to isolate spent fuel.

Figure 1 presents the testing cell apparatus with the related main details of the instrumentation on the bentonite sample (dimensions: 12 cm-length × 6 cm-diameter).

The Mx80-D test is composed by two main stages: hydration stage followed by helium gas injection. The injected gas pressure was fixed to 1 MPa from 7.3 to 39.3 days and 3 MPa from 39.4 to 46 days according to test duration. After that, gas flow rate was continuously increased at the injection up to a constant flow rate value until a breakthrough point occurred (at 71.5 days). After breakthrough and a period of gas flow through the sample, the injection pump was stopped whilst the stresses and porewater pressures were continuously monitored at several sample control point locations (see Figure 1) up to the end of the test at day 121.

2 MATERIAL PROPERTIES, NUMERICAL MODEL, BOUNDARY CONDITIONS

Table 1 presents the material properties and Figure 2 presents the random porosity strategy assumed at each model sample layer.

The liquid pressure was imposed to 0.1 MPa from 0 to 7.3 days, 0.5 MPa at day 7.3, and 1 MPa from 7.3 to 7.5 days at the radial control point locations (see Figure 1b) according to the monitored radial fluid sensors data.

Two alternative treatment strategies of gas injection test were performed:

a) Gas pressure (P_g) prescribed according to measured gas pressure (from 46 to 71.5 days).
b) Gas flow rate (q_g) prescribed ramp from 0 to 8.0×10^{-7} kg/s/m^2 (from 46 to 67 days) and 8.0×10^{-7} kg/s/m^2 (from 67 to 71.5 days).

Gas flow rate (q_g) prescribed (option b) corresponds to the real conditions in the test. Gas pressure prescribed is only considered to help the calibration of the model. The numerical solution of the two options should converge as the parameters are correctly calibrated.

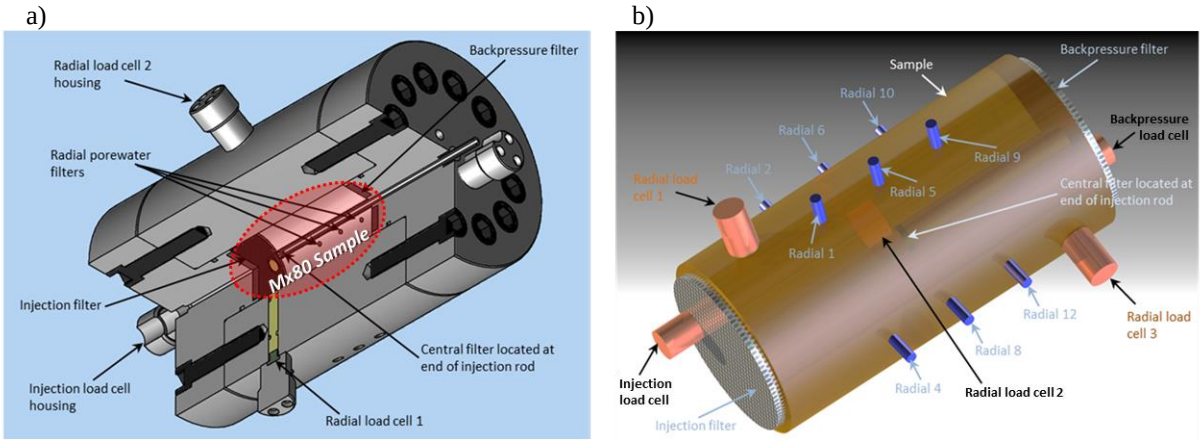

Figure 1: Mx80-D test: pressure vessel (a) and Mx80 sample (b) main details.

Table 1: Material properties.

	Parameters:						
Materials:	Porosity	Intrinsic permeability (a)	Water retention curve (b) P_0	Water retention curve (b) λ	Relative permeability (c)	Gas phase density – Molecular mass	Initial liquid and gas pressures
Soil (Mx80 bentonite)	from 0.36 to 0.38 (d)	5.6×10^{-18} and 5.6×10^{-19}	27	0.45	3	0.004	0.1
Porous stone filter	0.5 (e)	10^{-17}	0.1	0.25	3	0.004	0.1
Units:	-	m^2	MPa	-	n-power	kg/mol	MPa

Notes: (a) Intrinsic permeability defined as per the exponential law as follows: $k_{ii} = k_0 \exp\{b(\phi - \phi_0)\}$, with $b = 60$ and $\phi_0 = 0.37$;
(b) Water retention curve according to Van Genuchten model (λ: shape function);
(c) Relative permeability $k_{rl} = (S_l)^n$, where S_l is the degree of saturation;
(d) Random porosity between 0.36, 0.37, and 0.38 with 1/3 weighting each (see Figure 2);
(e) Despite the specified value was used at initial calculations, the porous stone porosity was fictitiously increased 40 times (i.e., $\phi_{porous\_stone} = 20$) featuring the equivalent larger volume of the actual injection system (interface vessel) of the test.

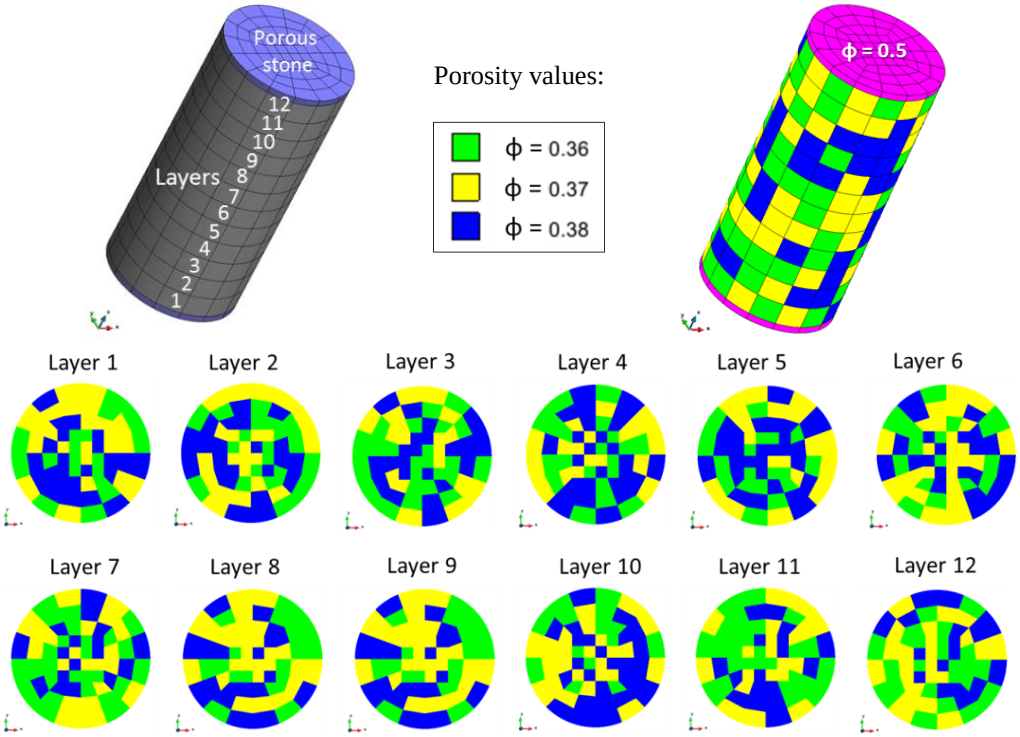

Figure 2: Layer-by-layer randomly porosity distribution assumed (1/3 weighting each).

3 RESULTS

Figure 3 presents the gas pressure evolution results for helium gas pressure (P_g) and gas flux (q_g) prescribed case conditions during injection phase (i.e., up to 71.5 days). Two cases of intrinsic permeability are analysed. Results are obtained at both injection filter and at radial porewater array 2 locations. As it can be observed, injection trends assuming q_g-prescribed returns different curvature in comparison with the test data. Not surprisingly, better agreement is obtained assuming P_g-prescribed cases and $k_0 = 5.6\times10^{-18}$ m^2 case at both control locations due to the different path shape of the q_g-prescribed case (different curvature with clearly too higher peak values).

Figure 4 shows the advective gas flux ($m^3/m^2/s$) vectors for prescribed gas pressure case with $k_0 = 5.6\times10^{-18}$ m^2 case during injection at day 65 and after the breakthrough (during dissipation) at day 75. The same scale (vectors size factor) is maintained to ease the comparison. As expected, different location of the larger flow-vector magnitudes take place before and after the breakthrough point at day 71.5.

In order to feature the actual larger volume of the injection filter and interface vessel, about 40 times higher-equivalent porosity was assumed to the porous stone. This allows to perform a more feasible gas compression during the helium injection at that zone of the test devices (i.e., from the pump up to the filter through the interface vessel). Figure 5 presents the results assuming this new porous stone porosity for both pressure and flow prescribed conditions cases P_g and q_g for the higher intrinsic permeability case (i.e., $k_0 = 5.6\times10^{-18}$ m^2). As it can be observed, gas pressure trending results have been improved in a significant manner, with a clearly better fit with regards to the given test data. And the assumptions for the boundary condition at the injection side produce much closer response.

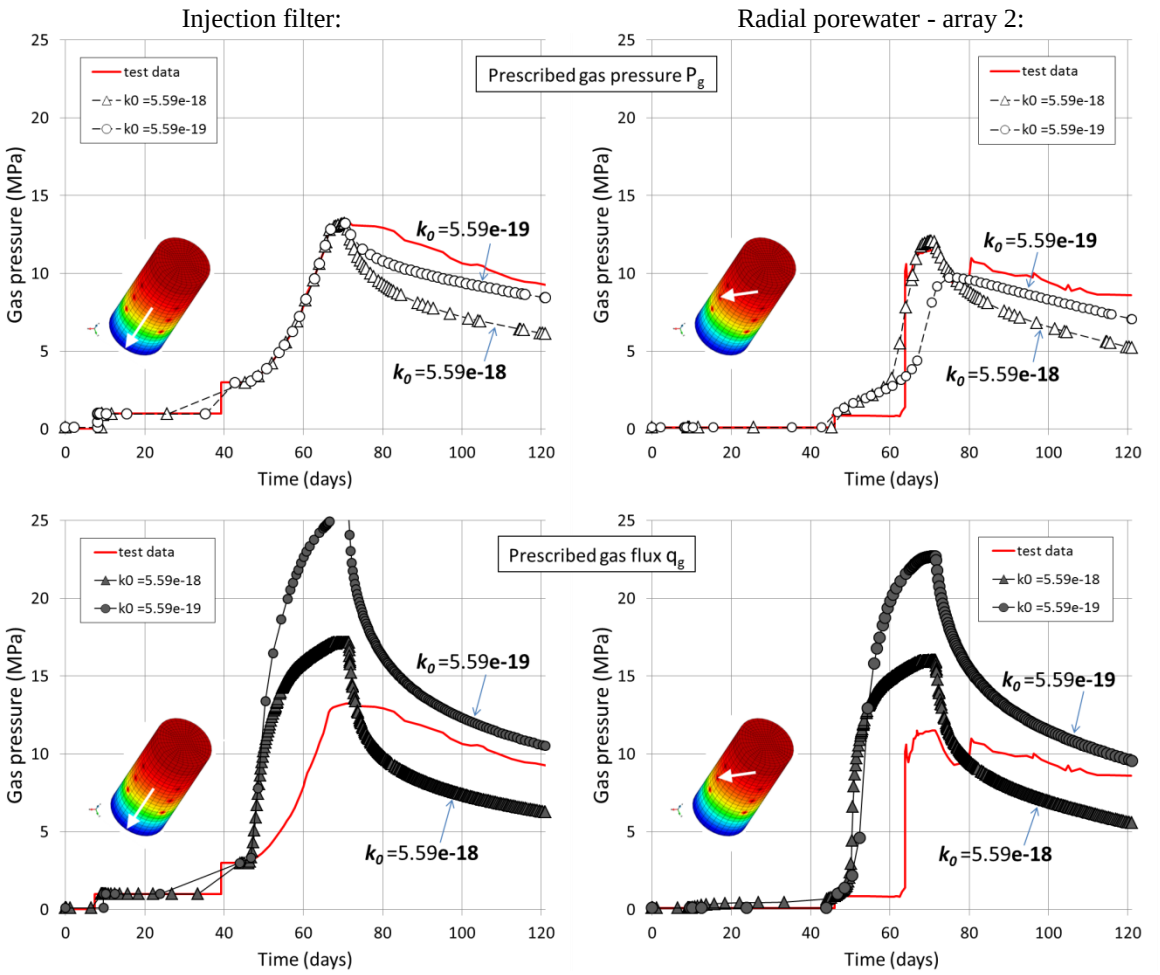

Figure 3: Gas pressure evolution evolution.

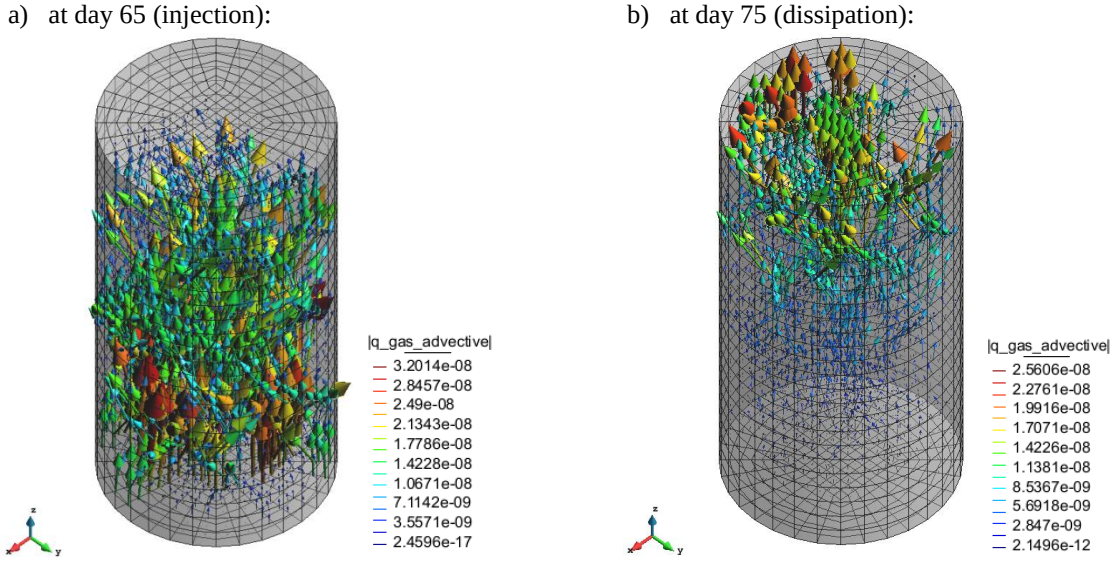

Figure 4: Advective gas flux at day 65 (a) and day 75 (b). Prescribed gas pressure case with $k_0 = 5.6\times10^{-18}$ m^2.

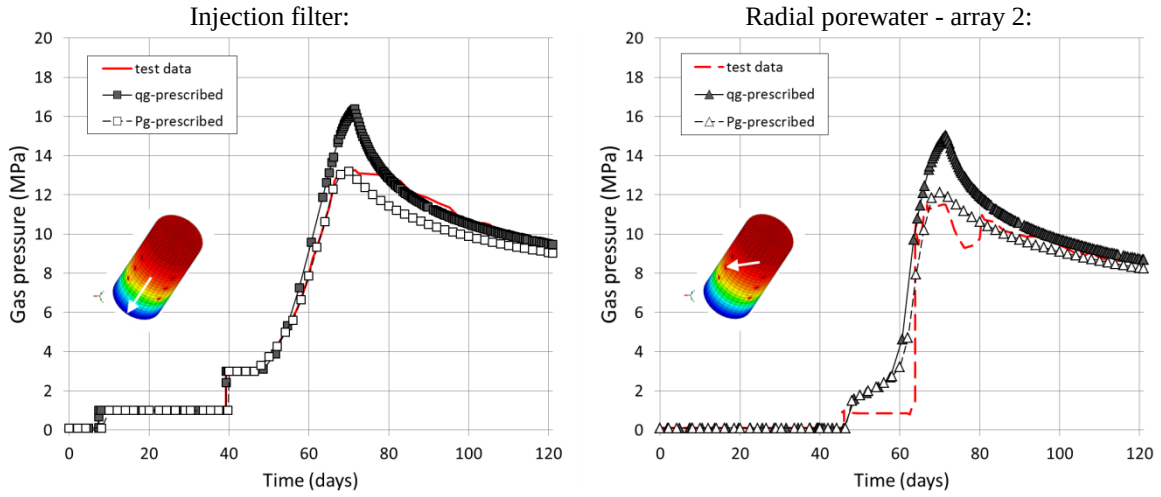

Figure 5: Gas pressure evolution evolution for larger volume of porous stone (ϕ_{porous_stone} = 20)

4 CONCLUSIONS

- The proposed methodology provides results reasonably satisfactory, according to the two phase flow in a rigid porous material assumption.
- Modelling gas injection tests using two phase flow in a rigid porous material is an on purpose and required previous step to a further couple with mechanical.
- It has been possible to find a combination of k_0 (and n_g) which leads to pressure evolution similar to measurements to be used as reference parameters for mechanical coupling calculations.

5 FUTURE WORKS

- The incorporation of the mechanical effect is planned assuming both elastic and elastoplastic models.
- It is also planned to include soil permeability based on embedded discontinuities (i.e, permeability depending on aperture which in turn depends on deformation).
- Recalibration of properties is also expected, so initial permeability would be lower and then would increase with deformations as gas pressures builds up.

ACKNOWLEDGEMENTS

Support by the National Radioactive Waste Management Agency (ANDRA) is greatly acknowledged.

REFERENCES

[1] Harrington, J, R Cuss, C Graham, S, British Geological Survey, Radioactive Waste Management Limited, ENGINEER (modElliNg Gas INjection ExpERiments), DECOVALEX 2019, Specifications for Task A.

3D MODELLING OF REINFORCED SOIL WALLS

I.P. Damians[*], R.J. Bathurst[†], S. Olivella[*], A. Lloret[*], and A. Josa[*]

[*] Department of Civil and Environmental Engineering
Universitat Politècnica de Catalunya – BarcelonaTech (UPC)
Campus Nord UPC, 08034 Barcelona, Spain
Email: ivan.puig@upc.edu

† GeoEngineering Centre at Queen's-RMC, Civil Engineering Department
Royal Military College of Canada (RMC)
K7K 7B4 Kingston, Ontario, Canada

Key words: MSE walls, Mechanical 3D modelling, Discontinuous soil reinforcement

Abstract. *This report summarizes the scope and conclusions of a 3D numerical modelling analysis of mechanically stabilized earth (MSE) walls constructed with concrete panels and strip reinforcement. These systems pose numerical challenges as a result of the discontinuous reinforcement arrangement which suggest the necessity on the 3D strategies instead of 2D modelling to determine and to fit its actual intrinsic behaviour.*

1 INTRODUCTION

This extended abstract summarizes the scope and conclusions of a 3D numerical modelling analysis of mechanically stabilized earth (MSE) walls constructed with concrete panels and strip reinforcement [1]. Numerical 2D models to perform mechanically stabilized earth (MSE) retaining wall full-height structures have been extendedly used and demonstrated that a proper calibration is possible even for non-planar reinforcement cases (i.e., strips, bars, ladders, etc.). The simplification from real 3D to 2D plane strain is possible by the transformation of the structural components width dimensions and the actual amount per width of any discrete component to equivalent 1 m-width component (which derives to an equivalent sheet in case of linear/discontinuous reinforcements). As the main (or weak) stress-strain directions of these kind of structures is well localized due to the slice symmetry assumed along the running direction of the wall, the transformation to a plane-strain continuum-slice is assumed to be, in general, faithfully representative.

However, in cases where linear reinforcement (e.g., strips and ladders) are used, it could be interesting to have a more complete understanding of the system behaviour. Under this scenario, it may be necessary to identify divergences on results which can appear between locations through the less representative plane space direction (i.e., running wall direction). These variations have been already identified many times in the context of the soil-reinforcement pullout tests performance. In those cases, relevant variability is typically obtained on vertical pressures through the width direction of the pullout box (i.e., on the horizontal and opposite to the reinforcement displacement direction) due to the real soil-soil vertical transfer of the shear stresses.

A simplified 3D finite element model with CODE_BRIGHT software program has been developed to analyze a 6 m-high mechanically stabilized earth strip-reinforcement retaining wall structure. The purpose of this model is to be capable to achieve more accurate and

faithfully behaviour results beyond the scope of the two-dimensional models. As known, the most relevant behaviour contribution of this type of structures is the soil-structure interfaces definition. After the followed methodology, results achieved, and learnings obtained from soil-facing (precast concrete panels) shear analysis, and soil-reinforcement (steel ladders and polymeric strips) pullout tests, proper interface features could be possible to be implemented in the developed and presented full-scale 3D model.

2 NUMERICAL MODEL

Figure 1 presents the mechanical 3D model mesh generated with its geometry, and main components and dimensions.

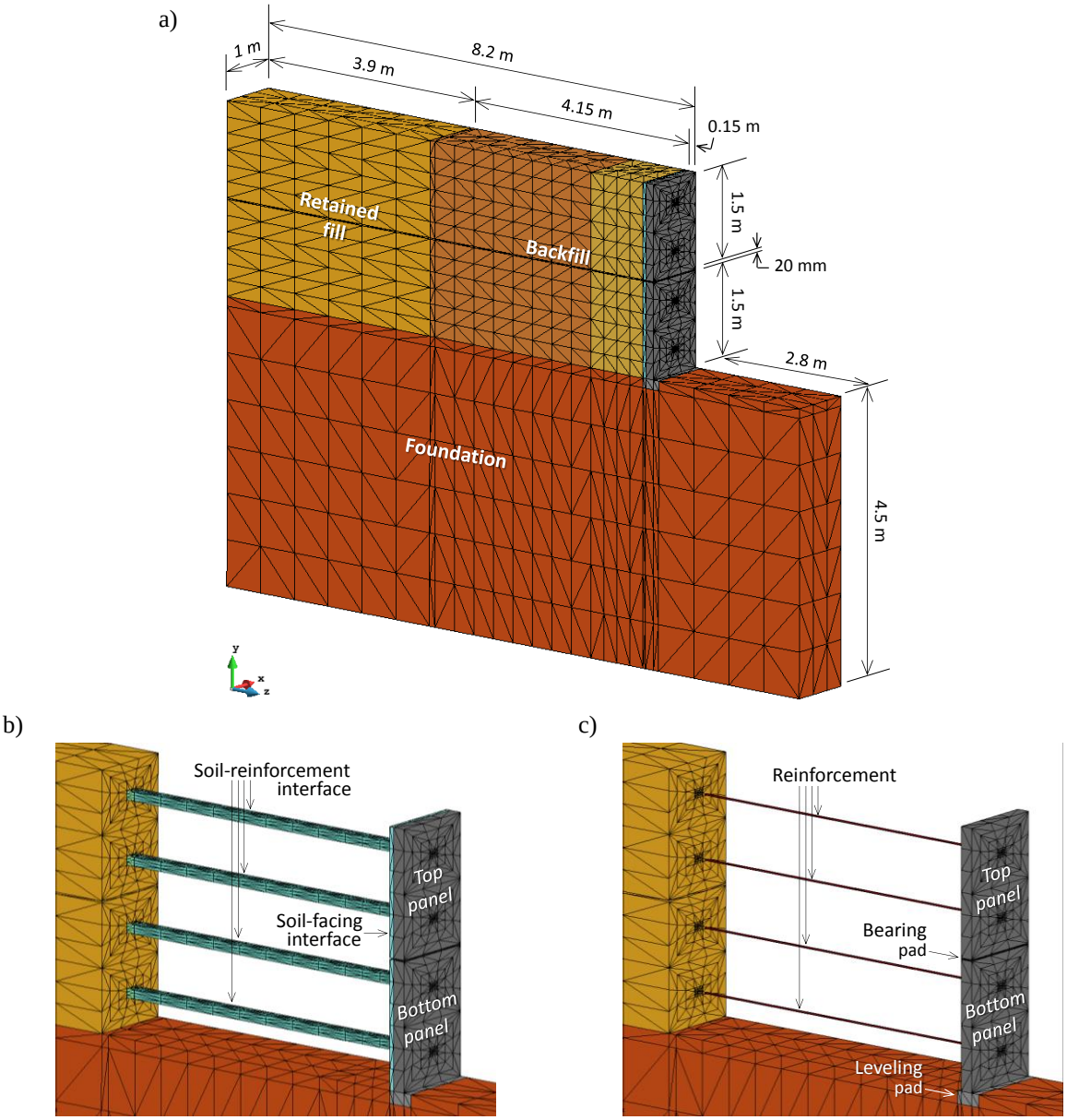

Figure 1: 3D model mesh, geometry, components and main dimensions: whole geometry (a), interfaces (b), and structural components detail (c).

3 RESULTS

Figure 2 presents general results from vertical and horizontal displacements after wall construction. Figure 3 presents results of the vertical displacements detailed at soil-facing interface rear view. Figure 4 presents the vertical pressures obtained at several locations above and below the reinforcement layers at a cross-section vertical plane 2 meters away from facing.

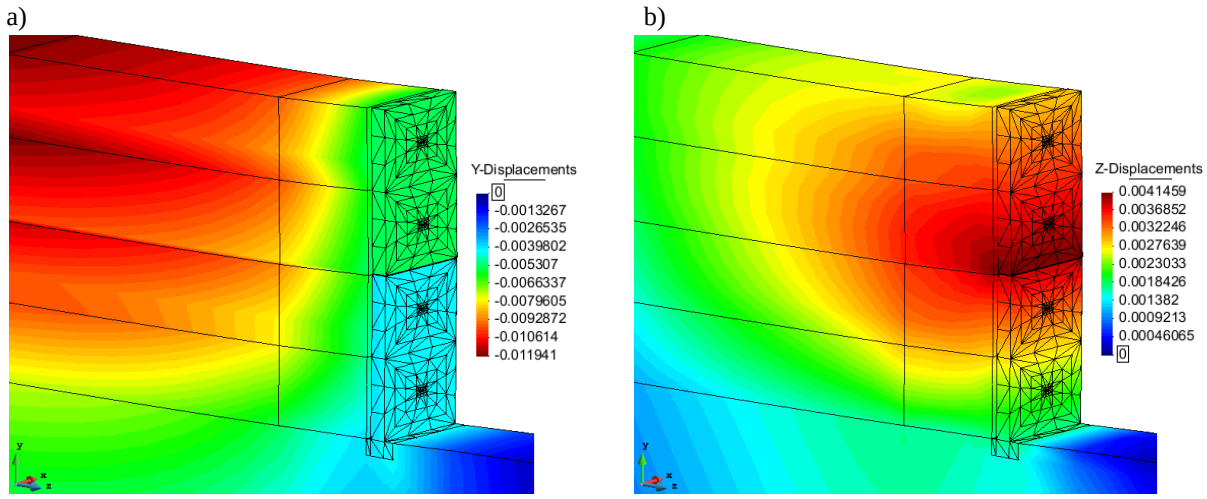

Figure 2: Vertical (a) and horizontal (b) displacements (mm) at H = 6 m-equivalent wall height construction..

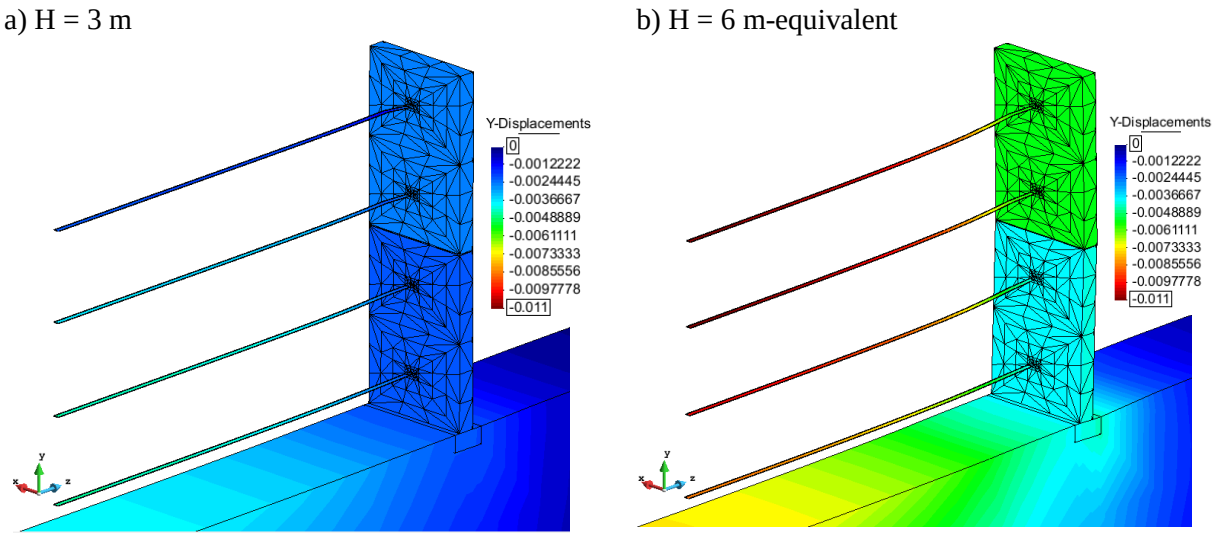

Figure 3: Vertical displacements (mm) detailed at soil-facing interface rear view: 3 m (a), and 6 m-equivalent (b) wall height construction. Deformed mesh amplified 20 times.

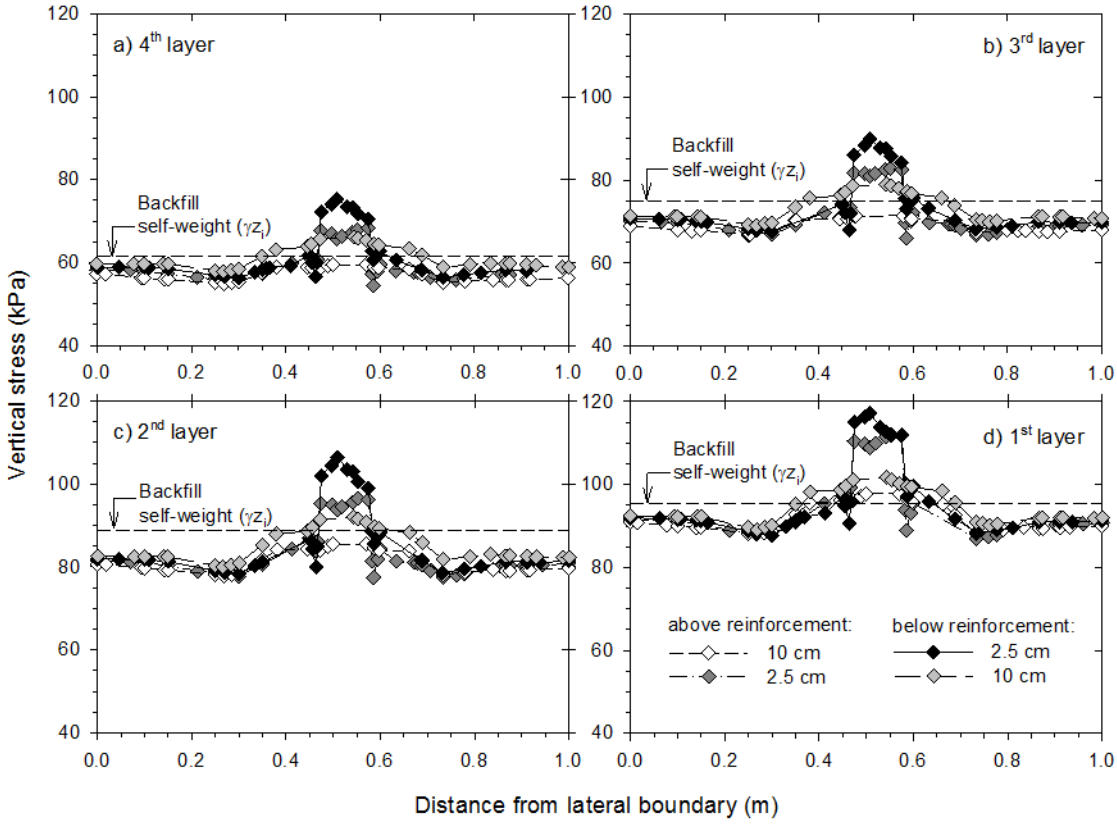

Figure 4: Vertical pressure at reinforcement layers location at 2.0 m from facing.

4 CONCLUSIONS

- A 3D numerical finite element modelling was generated to analyse a 6 m-high mechanically stabilized earth reinforced soil wall structure.
- The results obtained demonstrated that there is an actual 3D-effect in this kind of structures, not possible to be detected with 2D models analysis.
- Despite in many cases these 3D effects may not be such relevant to justify the use of these complex models (in addition to the related computational issues), the current study showed that this effects could be detected, if required, in particular cases of interest.
- The methodology presented looks promising to achieve further results to other geometries, structural material data, and even under different boundary conditions.

REFERENCES

[1] Damians, I.P., 2016. Mechanical performance and sustainability assessment of reinforced soil walls (Ph.D. Thesis). https://upcommons.upc.edu/handle/2117/98914/es?range=all.

MODELLING THE CONSTRUCTION OF AN INSTRUMENTED EARTH DAM. THE RELEVANCE OF COMPACTION CONDITIONS

Núria M. Pinyol[*†] and Eduardo E. Alonso [†]

[*] Department of Civil and Environmental Engineering. Technical University of Catalonia (UPC)
Building D2. Campus Nord UPC. Jordi Girona, 1-3.08034 Barcelona, Spain
e-mail: nuria.pinyol@upc.edu

[†] Centre de Metodes Numerics en Enginyeria (CIMNE)
Edificio C1, Campus Norte UPC
Gran Capitán s/n, 08034 Barcelona, Spain

Key words: earth dam, compaction conditions, real case

Abstract. *Albagés Dam is a zoned earth dam of compacted soils 85 m high built in Catalonia, Spain, which is in construction since 2015. Dam materials were extensively analysed during the design stage by means of laboratory tests. Also, a trial embankment was built during design activities to determine the proper compaction conditions of the core and shoulders materials. Afterwards, insitu tests were carried out on the embankment as well as laboratory tests on block samples taken insitu. The dam and the foundation were instrumented with the aim of registering displacements, total stresses and pore water pressures. In addition, nuclear probes were carried out at each construction layer throughout the whole dam to control compaction conditions.*

Code_Bright was used to perform a Class A analysis to predict the behaviour of the dam during construction and reservoir impoundment. The dam materials were characterized from the data available during the design stage. The prediction of the dam behaviour during construction up to the middle height was compared with the real response. A detailed analysis was performed to understand the causes of discrepancies observed between measurements and "Class A" calculations.

It was concluded that the constitutive model and the constitutive parameters selected were accurate enough and the causes of the discrepancies were due to the assumed initial conditions specified in the model. The initial density and humidity of the materials of the core and main shoulders were significantly different than the values introduced in the model. Based on the results of the nuclear probes, the initial conditions of the model were calibrated. This calibration lead to a satisfactory simulation of the observed settlements during construction.

1 INTRODUCTION

Code_Bright is a powerful tool for the modelling earth dams. The code has been successfully used to model the construction and subsequent reservoir impoundment of Beliche dam, Portugal [i], Lechago dam, Spain [ii] and SM-3, Canada [iii]. In order to be able to model properly the real behavior of dams, it is necessary (a) to select proper constitutive models which should be able to reproduce the main features of the soils under saturated and

non-saturated conditions; and (b) to have enough data to be able to calibrate the model parameters. In the case of compacted soils, it is required to know the compaction conditions which determine the soil response in terms of strength, stiffness and potential collapse upon wetting [iv,v]. The compaction process is, in general, not simulated and the initial conditions describe the state of the soils after compaction. Therefore, the constitutive model selected should be able to take into account the effect of this variables on the soil response.

In practice compaction conditions are defined in Proctor plane [iv] which relates dry density and water content. With the aim of modelling, these variables are interpreted in terms of two stress-like variables. Taking into account the normal consolidation line associated with each soil, the dry density, void ratio or porosity can be directly related with the applied stress. Once compacted, the soil is unloaded and the attained void ratio (leaving apart the elastic rebound) is related to the maximum (preconsolidation) stress. Therefore, the dry density of the soil can be associated with preconsolidation stress. Several contributions [vii-xi] focus on determining the relationship between preconsolidation stress and dry density based on experimental data of loading tests on compacted soils.

The water content is directly associated with suction through the water retention curve. The water retention curve depends also on the current void ratio, on the previous history of wetting/drying and on the "direction" of water content change (either wetting or drying).

Compaction conditions determining the behaviour of compacted soils is a key point in the construction of earth dams. This paper presents the modelling of an earth dam, Albagés dam, which nowadays is under construction. The dam was modelled in Code Bright in the design stage, a Class A modelling, with the aim of predicting the dam behaviour during construction and during future reservoir operations. During construction, the dam was instrumented and the results could be compared with measurements. The discrepancies observed are analysed with the aim of understanding the causes.

2 ALBAGÉS DAM. "CLASS A" MODELLING

The representative section of Albagés dam is shown in Figure 1. Foundation is constituted by layers of argillaceous rock and sandstone. In the model, the foundation was simplified to the layers shown in the figure. A vertical silty core is located at the central part of the dam (LL = 23-30%, LP = 14-19% e IP = 6-12%). There are two shoulder of well-graded soil which, after compaction, may reach high values of density (2.2 Mg/m^3 at Modified Proctor). The higher the value of density, the higher the strength and the stiffness and the lower the permeability. An outer shoulder is defined upstream by means of a pervious rockfill. The same material is placed at the toe of the downstream shoulder. This material helps to stabilize the dam and avoids the accumulation of pore water pressures.

The construction of the dam was simulated by means of 12 layers. All the materials were characterized by means of the BBM model [xi]. During the design stage, trial embankments made of the coarse soils for the shoulders and the silty clay for the core were built in order to evaluate compaction conditions and the properties of the soils after compaction. Laboratory tests (saturated and non-saturated oedometer tests, shear tests and permeability test) on samples compacted in the laboratory, as well as on block samples taken from the trial embankments, were carried out. Water retention curves were also measured for the silty clay of the core. Taking into account the features of the materials and the conclusions drawn from the construction of the trial embankments, the project specified the initial compacted conditions of the materials for the dam construction.

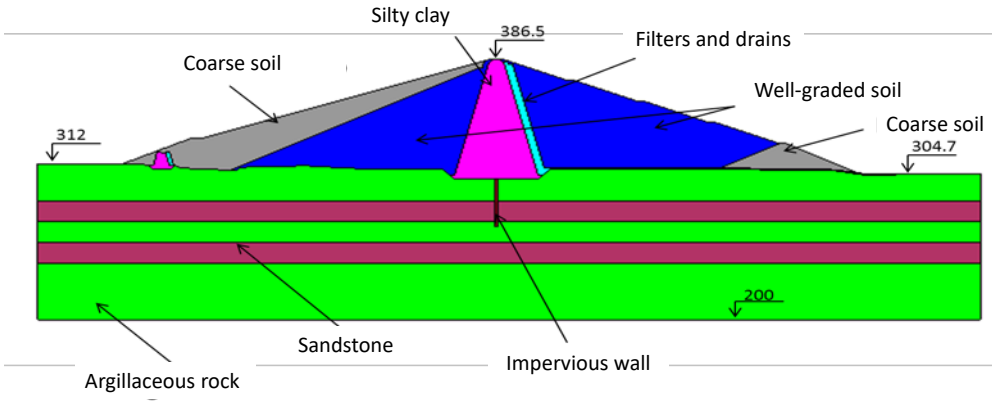

Figure 1: Modelling section of Albagés Dam.

Model parameters and initial conditions were calibrated taking into account this data. Figure 2 shows the results of the modelling of dam construction in terms of settlements for two vertical profiles shown in the figure. Only the curves corresponding to a dam level lower than 340 m are plotted and compared with measurements currently available. Significant discrepancies can be observed. The model predicted settlements higher than the observed values in the foundation. Only 2 cm of settlements were observed against 15 cm computed. In the calculation, the foundation was characterized as an elastic material having Young's modulus of 500 MPa and Poisson's coefficient of 0.3. The stiffness should be assumed higher to fit better the real behavior.

Regarding dam settlements, the calculated values in the central profile crossing the core are significantly lower than the measured values, even taking into account the settlements of the layered foundation rock. On the contrary, the model overestimates the settlements registered on the downstream shoulder.

3 CALIBRATED MODEL FROM COMPATION CONDITIONS

The differences observed between the predicted and the observed behavior of the dam in terms of displacements (Figure 2) could be due to a wrong estimation of the compressibility, the initial water content or the introduced initial preconsolidation stress. Regarding the compressibility of the materials, an elastic compressibility and a plastic compressibility for saturated states should be included in the model. Under drier conditions, the material exhibits higher stiffness. On the other hand, the initial apparent preconsolidation stress, which is an initial condition, determines the magnitude of elastic and plastic strains. This value varies as a function of suction (according to the LC referring to the BBM). The drier the soils, the higher the preconsolidation stress and the higher the elastic domain.

The comparison between pore water pressure measurements in the core and calculated values indicated that the pore pressure was not correctly estimated in the model. Positive pore water pressures were registered in the lower part of the silty clay core while de model predicted values lightly lower than 0.5 MPa of suction. This value, 0.5 MPa, corresponds to the initial value introduced according to the compaction water content specifications.

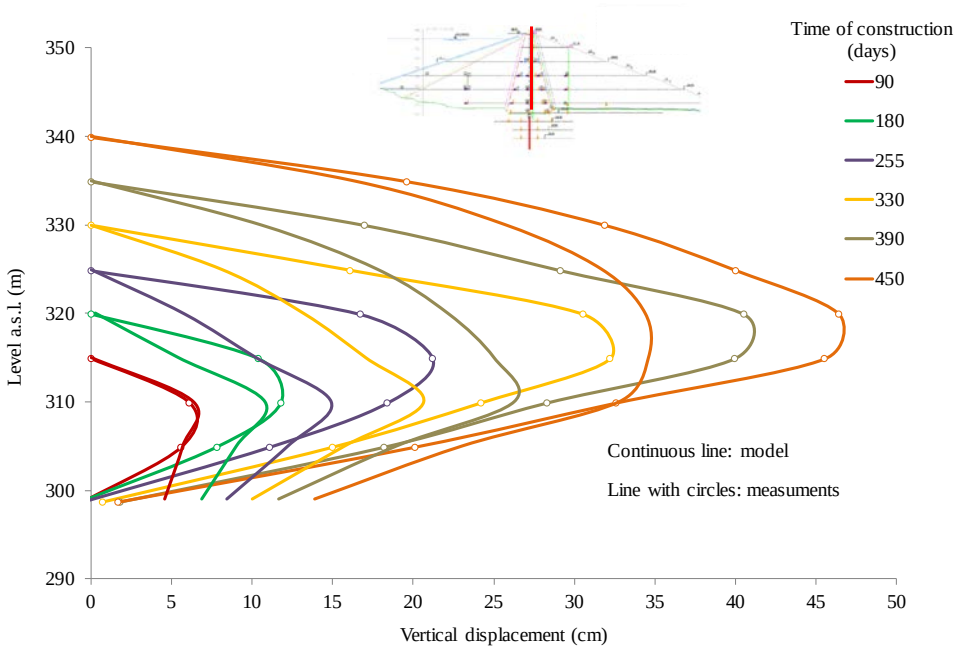

(a)

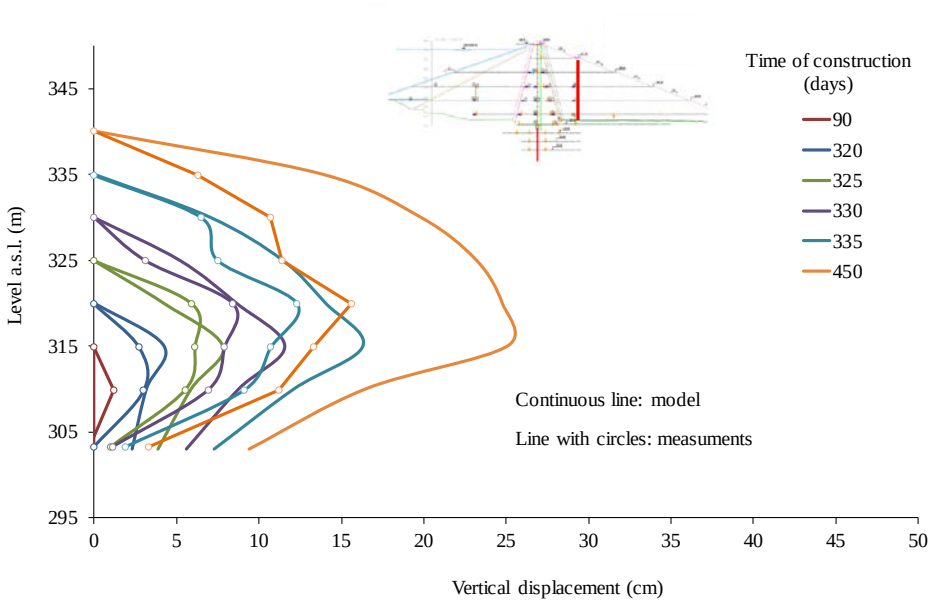

(b)

Figure 2: Computed (class A model) and measured vertical displacements along (a) a central profile and (b) a downstream profile indicated in the figures.

A detailed analysis of the compaction conditions from the nuclear probes carried out during dam construction at each compaction layer leads to observe important discrepancies between the actual initial conditions and the values estimated in the prediction. A calibrated model of the dam was defined taking into account the available data on the compaction conditions. Figure 3 shows the calculated settlements introducing the calibrated initial conditions, the rest of parameters being constant. Calculated settlements are compared with

measurements. The calibrated model is able to capture significantly well the settlements of the dam during the first stage of the construction.

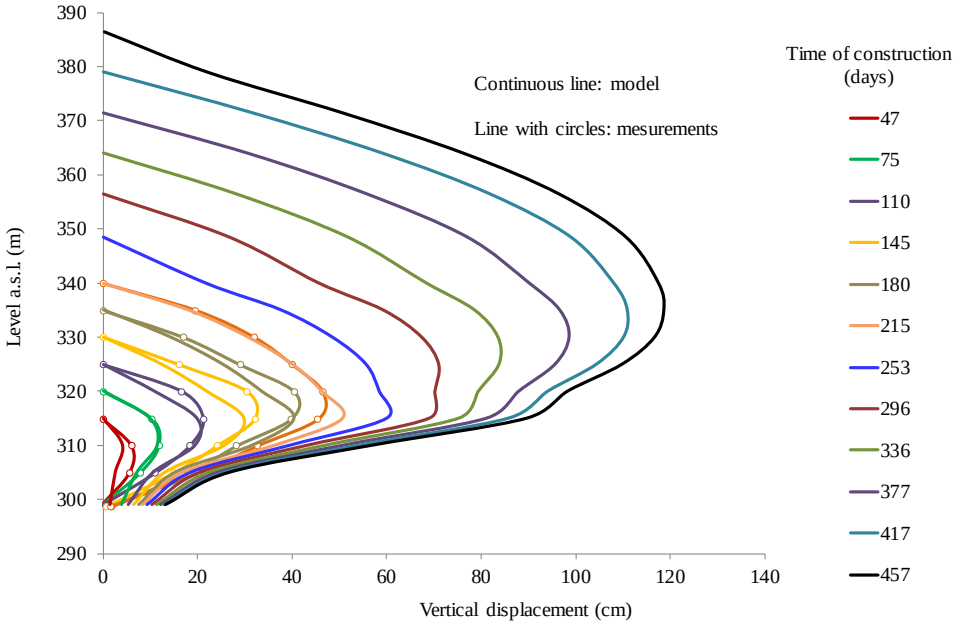

(a)

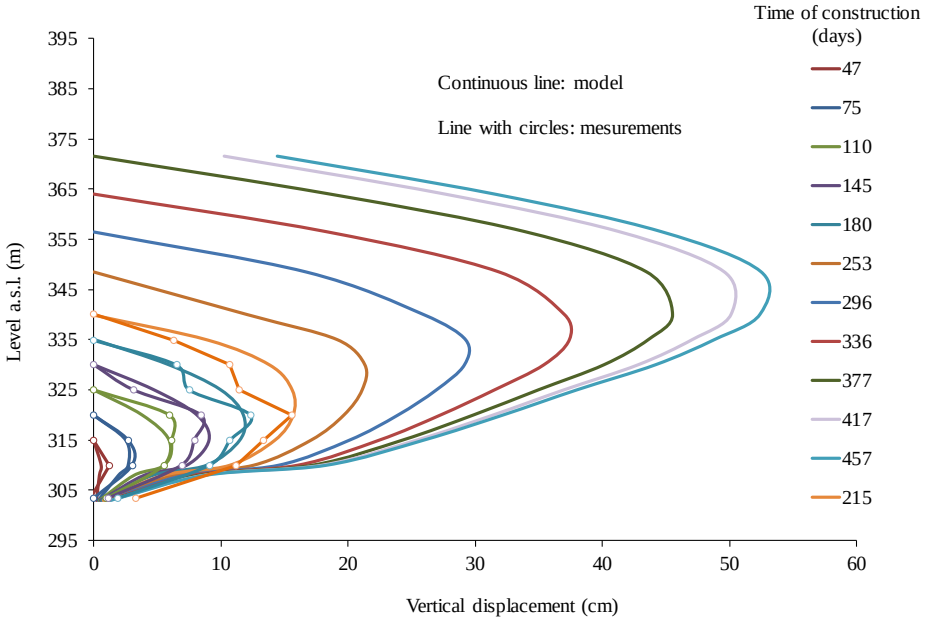

(b)

Figure 3: Computed (calibrated model) and measured vertical displacements along (a) a central profile and (b) a downstream profile.

4 CONCLUSIONS

The paper discusses some aspects of the modelling of Albagés dam, a zoned earth dam 90 m high currently under construction. Field and laboratory data on construction materials has accumulated in the period 2003-2017. Special attention is paid to the properties of the two main construction materials: the low plasticity silt core and the upstream and downstream shoulders made of a heterogeneous tertiary claystone. Model parameters based on laboratory tests allowed a “class A” prediction which exhibited significant discrepancies when compare with monitoring data. A better model calibration relied on actual density and water content determination in situ. The calibrated model led to a satisfactory prediction of field settlements records

REFERENCES

[i] Alonso EE, Olivella S, Pinyol NM. 2005.A review of Beliche Dam. Géotechnique. 55(4):267–85.

[ii] Alonso EE, Olivella S, Soriano A, Pinyol NM, Esteban F. 2011. Modelling the response of Lechago earth and rockfill dam. Géotechnique 61(5), 387-407.

[iii] Aguirre I. 2012. Modelling the SM-3 dam, Quebec, Canada. Barcelona, Spain.

[iv] Suriol J, Gens A, Alonso EE. 1998. Behaviour of compacted soils in suction controlled oedometer. In: 2nd Int Conf on Unsaturated Soils. p. 463–443.

[v] Alonso EE, Pinyol NM, Gens A. 2013. Compacted soil behaviour: initial state, structure and constitutive modelling. Géotechnique 63(6), 463-478

[vi] Proctor RR. 1933. Fundamental principles of soil compaction. Fundam Princ soil Compact. V11(9):148–56.

[vii] Romero E. 1999. Characterization and thermo-hydro-mechanical behaviour of unsaturated Boom clay: An experimental study. Universitat Politècnica de Catalunya, Barcelona, Spain.

[viii] Honda M, Seguchi H, Kim E, Hawai K, Iizuka A, Karube D. 2003. A study of the relation between volume change characteristics of compacted soil and the condition of compaction. In: 2nd Asian Conference on Unsaturated Soils. Osaka, Japan. p. 177–80.

[ix] Cuisinier O, Laloui L. 2004. Fabric evolution during hydromechanical loading of a compacted silt. Int J Numer Anal Methods Geomech. 28(6):483–99.

[x] Barrera M. 2002. Estudio experimental del comportamiento hidro-mecánico de suelos colapsables. Universitat Politècnica de Catalunya (UPC). Barcelona. España.

[xi] Alonso, E. E.; Gens, A.; Josa A. 1990. A constitutive model for partially saturated soils. Géotechnique. 40(3):405–30.

LONG-TERM DEFORMATION BEHAVIOUR OF CRUSHED SALT DUMP, SUBJECTED TO ATMOSPHERIC BOUNDARY CONDITIONS

M.T.Yubero[*], S. Olivella[*], A. Gens[*]

[*]Department of Civil and Environmental Engineering
Technical University of Catalonia (UPC)
Campus Nord UPC, 08034 Barcelona, Spain
e-mail: maria.teresa.yubero@upc.edu

Key words: Crushed salt dump, Long term, Coupled analysis

Abstract. *Porosity variations in saline media are induced by compaction process and atmospheric conditions. Input data include atmospheric temperature; atmospheric gas pressure, relative humidity and rain are imposed on a porous salt media. A coupled thermal multiphasic flow was developed to study mass and energy transfer in a crushed salt dump since it is placed in the tailing pile and it leads to significant variations of porosity and deformation over time.*

Based on recently published works, the main deformational mechanisms are also explained. The objective of this work is the study of the compaction process of waste salt materials due their self-weight since it is placed in the tailing pile. Dissolution and recrystallization phenomena are developed as a consequence of confining stresses and the water presence. It produces bonding between salt grains increasing the strength of the material and reductions of porosity. Intra-crystalline deformations also take place. This was investigated by means the modelling of a tailing deposit which includes the simulation of the construction and the long term response. In addition, a sensitivity analysis was performed.

An experimental program was carried out by Yubero (2008) on salt samples obtained from a tailing pile located at Súria (Spain) in order to establish the mechanical behaviour of the material.

The experimental research was divided in two stages. Firstly, the geotechnical profile could be characterized from a comprehensive laboratory testing. In a second stage, the behaviour of the salt aggregates was studied by means of oedometer tests on compacted samples. In the Figure 1a, we can see the odometer test cells used.

The material used was obtained from two different depths. One of the first group of samples (TP1) from 6 meters deep (Figure 1b) and the other sample is from 65 meters depth (Figure 1c).

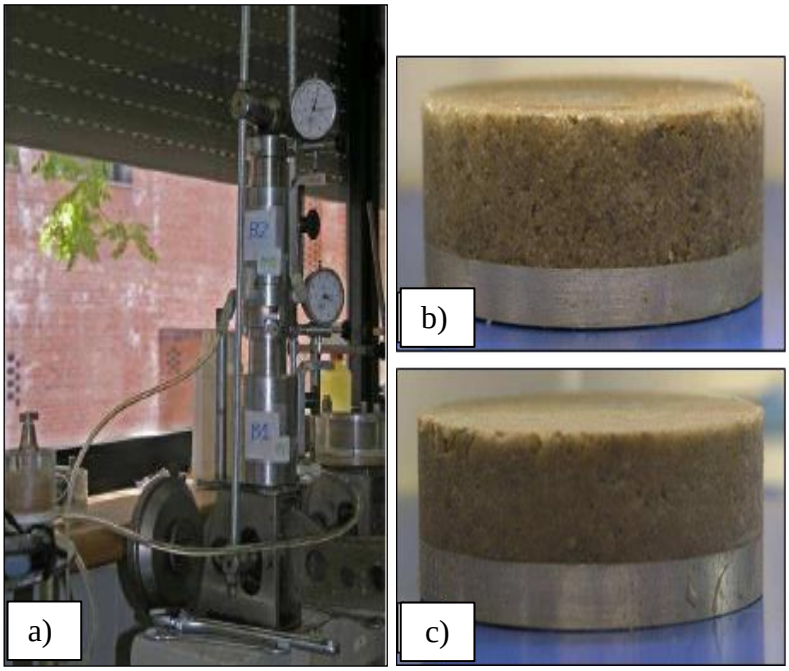

Figure 1. a) The odometer test cells and b) the salt samples tested

Samples were saturated during two months using a salt solution under isothermal conditions (23ºC). Vertical stresses applied varied from 0.05 to 1.5MPa. Permeability measurements were obtained from oedometer tests (initial and final measurements) where a relationship between permeability and void ratio was established.

The experimental results were validated using the model constructed by CODE_BRIGHT for studying the mechanical behaviour of salt aggregates. The stress paths applied to each sample were modelled and numerical and experimental results were compared. Using this model, the strain velocity of the salt aggregates subjected to compaction under constant stress could be obtained.

Moreover, the evolution of porosity and strength under variables as stress was modelled using the viscoelasticity and viscoplasticity constitutive laws for saline materials. The coupled water flow-deformation problem is solved under the study of conditions variable with time (rain, temperature, relative humidity) and numerical results of the strain velocity of

the salt aggregates subjected to compaction under variables as stress could be obtained. Once the model is calibrated, the maximum displacements the settlements of the tailing deposit are calculated.

The evolution of porosity is represented at 365 days and 3650 days in figures 2a and 2b, respectively. Porosity varies from 0.47 to 0.31 during the first year and is reduced to 0.15 during the following 9 years.

In the Figure 2, show the evolution of porosity at 365 days (Figure 2a) and 3650 days (Figure 2b) (at figure 2). Porosity varies from 0.47 to 0.31 during the first year and is reduced to 0.15 during the following 9 years (Figure 2b).

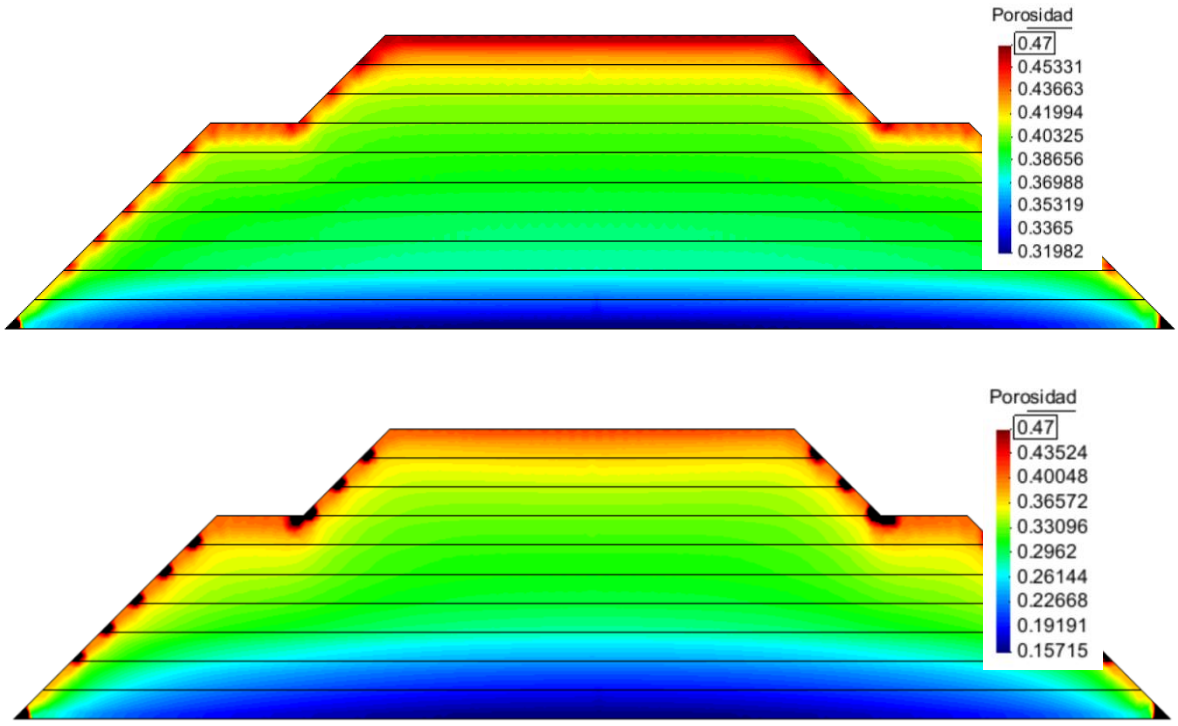

Figure 2. a) Evolution of porosity at 365 days b) evolution of porosity during 3650 days

The Suria materials have a low initial porosity and high compressibility whereof they become rigid material. So, we expect high compression, the porous material becomes more resistant and less permeable, and therefore the brine is retained. Large settlements were observed.

REFERENCES

Arnedo, D., Alonso, E., Olivella, S., 2005, Canales en Terraplén sobre suelo natural y compactado. Ingeniería Civil, Issue Number, 139, pp: 68-80.

Gerard, P., Léonard, A., Masekanya, J.P., Charlier, R., Collin, F., 2010, "Study of the soil-atmosphere moisture exchanges through convective drying test in non-isothermal conditions". International Journal for Numerical and Analytical Methods in Geomechanics, Vol 34, pp: 1297-1320.

Gran, M., Carrera, J., Olivella, S., Saaltink, W.M., 2011, "Modeling evaporation processes in a saline soil from saturation to oven dry conditions". Hydrology and Earth System Sciences, Vol 15, pp: 2077-2089.

Olivella, S., Castanga, S., Alonso, E., Lloret, A., 2011, "Porosity Variations in Saline Media Induced by Temperature Gradients: Experimental Evidences and Modelling". Transport in Porous Media, 90, 763-777.

Olivella, S., Gens, A., Carrera, J., Alonso, E., 1996, "Numerical Formulation for a Simulator (CODE_BRIGHT) for the Coupled Analysis of Saline Media". Engineering Computations, Vol 13, No 7, pp: 87-112.

Olivella, S., A. Gens, J. Carrera, E. E. Alonso, 1996, 'Numerical Formulation for a Simulator (CODE_BRIGHT) for the Coupled Analysis of Saline Media " Engineering Computations, Vol 13, No 7, pp: 87-112.

PARALLEL COMPUTING WITH CODE_BRIGHT

S. Olivella and A. Rodriguez-Dono

Department of Civil and Environmental Engineering
Universitat Politècnica de Catalunya – BarcelonaTech (UPC)
Campus Nord UPC, 08034 Barcelona, Spain
Email: sebastia.olivella@upc.edu

Key words:

Abstract. *A parallel version of code_bright for windows environment is presented. Parallelization in a shared memory environment makes sense in a workstation context taking into account that multicore personal computer architectures have become popular. The iterative solution of the linear system includes some algebra operations which can easily be parallelized using OpenMP directives. In addition, iterative solutions facilitate the fully optimized storage of the sparse Jacobian matrix. This reduced storage of the sparse permits to optimize the use of the computer Ram memory. A first step has been taken by including directives in the matrix vector multiplication included in the algorithm of conjugated squared method. Results for some applications are presented.*

1 STORAGE OF THE JACOBIAN MATRIX

A finite element Jacobian matrix is an empty matrix or sparse matrix. This means that the matrix contains a large number of zero values. The nonzero values are fixed for a given mesh. If the mesh nodes are adequately renumbered, a band structure is achieved and the matrix can be stored in a reduced space. However, there are still a relatively large number of zeros and a skyline system can be considered.

$$\text{N}\times\text{N matrix}: \text{A} = \begin{pmatrix} a_1 & & a_2 & a_3 \\ & a_4 & a_5 & \\ a_6 & a_7 & a_8 & \\ a_9 & & & a_{10} \end{pmatrix}$$

with NZ non - zero coefficients

$$\text{AN}: (a_1 \quad a_2 \quad a_3 / a_4 \quad a_5 / a_6 \quad a_7 \quad a_8 / a_9 \quad a_{10})$$

$$\text{JA}: (1 \quad 3 \quad 4 / 2 \quad 3 / 1 \quad 2 \quad 3 / 1 \quad 4)$$

$$\text{IA}: (1 \quad 4 \quad 6 \quad 9 \quad 11)$$

(this is for NDF=1)

AN (dimension NZ): a real array that contains the non-zero values of the Jacobian matrix
JA (dimension NZ) is an integer array that contains the column indices of the non-zero coefficients
IA (dimension N) contains the positions in AN where every row begins

N: number of nodes
NZ: number of non-zero coefficients

NDF: number of degrees of freedom
NDF>1, then AN is a (NDF, NZ*NDF) array

Figure 1. Compressed sparse row (CSR) format used in CODE_BRIGHT to store the system matrix when CGS solution method is used.

A fully optimized storage can be obtained simply by storing the non-zero values of the matrix in the so called CSR: Compressed Sparse Row Format.

2 ITERATIVE SOLUTION

The conjugate gradients squared method (CGS) is used to solve the linear system for large meshes (Sonneveld, 1989, van der Vorst, 1990). CGS is a modification of the conjugate gradients method for non-symmetric matrices. The method requires a preconditioner matrix for which the diagonal scaling or block diagonal scaling is used. This is the simplest alternative. Pini and Gambolatti (1990) have shown that in vectorial machines, diagonal scaling was the most efficient pre-conditioner in the majority of the applications they compared.

$\mathbf{x} := \mathbf{x}_0$ (intial guess);
$\mathbf{r} := \mathbf{b} - \mathbf{A}\mathbf{x}$;
$\tilde{\mathbf{r}}$ is an arbitrary vector such that $(\mathbf{r}, \tilde{\mathbf{r}}) \neq 0$ (e.g. $\tilde{\mathbf{r}} = \mathbf{r}$);
$\rho_0 = (\mathbf{r}, \tilde{\mathbf{r}})$; $\beta_0 = \rho_0$; $\mathbf{p} = \mathbf{q} = \mathbf{0}$;
$\mathbf{K}$ is a preconditioner matrix;
for i = 0,1,2,...
  $\mathbf{u} := \mathbf{r} + \beta_i \mathbf{q}$;
  $\mathbf{p} := \mathbf{u} + \beta_i (\mathbf{q} + \beta_i \mathbf{p})$;
  Solve $\mathbf{q}$ from $\mathbf{K}\mathbf{q} = \mathbf{p}$;
  $\mathbf{v} := \mathbf{A}\mathbf{q}$;
  $\alpha_i = \rho_i / (\tilde{\mathbf{r}}, \mathbf{v})$;
  $\mathbf{q} := \mathbf{u} - \alpha_i \mathbf{v}$;
  Solve $\mathbf{v}$ from $\mathbf{K}\mathbf{v} = \mathbf{u} + \mathbf{q}$;
  $\mathbf{u} := \mathbf{A}\mathbf{v}$;
  $\mathbf{x} := \mathbf{x} + \alpha_i \mathbf{v}$;
  $\mathbf{r} := \mathbf{r} - \alpha_i \mathbf{u}$;
  if $\mathbf{x}$ close enough to $\mathbf{A}^{-1}\mathbf{b}$ then quit;
  $\rho_{i+1} = (\mathbf{r}, \tilde{\mathbf{r}})$;
  $\beta_{i+1} = \rho_{i+1} / \rho_i$;
end i

BlockMatrix: Each element (a_i) of the matrix shown in Figure1 is an NDF×NDF submatrix

BlockVector: Each element is an NDF×NDF submatrix

Summary of operations:

- Two *BlockMatrix – BlockVector products*
- *Two BlockVector – BlockVector products (indicated by (,))*
- *Vector updates*
- *Inversion of the Block Diagonal Matrix (requires inversion NDF×NDF submatrices (N times) using direct solver)*

Figure 2. Algorithm for the CGS iterative solution and summary of operations.

Using CSR storage mode plus CGS iterative method plus block-diagonal scaling produces a quite simple structure of the solver. In fact, only vector-vector products, matrix-vector products and inversion of NDF×NDF matrices have to be performed. The requirements of extra space are only 8×N×NDF where N is the number of nodes and NDF the number of degrees of freedom per node. It should be mentioned that the matrix-vector products are easily performed with the CRS storage mode because the matrix is stored by rows.

3 PARALLELIZATION

OpenMP (Open Multi-Processing) is an application programming interface (API) that supports multi-platform shared memory multiprocessing programming in several languages including Fortran, and on most platforms, instruction set architectures and operating systems, including Windows. It consists of a set of compiler directives, library routines, and environment variables that influence run-time behavior (Wikipedia).

OpenMP is managed by the nonprofit technology consortium OpenMP Architecture Review Board (or OpenMP ARB), jointly defined by a group of major computer hardware and software vendors, including AMD, IBM, Intel, Cray, HP, Fujitsu, Nvidia, NEC, Red Hat, Texas Instruments, Oracle Corporation, and more (Wikipedia).

OpenMP uses a portable, scalable model that gives programmers a simple and flexible interface for developing parallel applications for platforms ranging from the standard desktop computer to the supercomputer (Wikipedia).

Figure 3 shows how the OpenMP directives are used before and after the loop that carries out the matrix-vector product.

```
      dimension a(ldanr,lcanr),  ! matrix, sparse storage mode
     .          x(numnu),        ! solution
     .          r(numnu)         ! auxiliary vector


!$omp PARALLEL DO NUM_THREADS(4) PRIVATE(irow)
      do irow=1,numnp                        ! rows for 'ndf=1'
         do l1=1,ndf                         ! rows in 'a' for each 'irow'
           r((irow-1)*ndf+l1) = 0.
          do j=ia(irow),ia(irow+1)-1          ! positions of row 'irow' in 'a'
             do l2=1,ndf
                r((irow-1)*ndf+l1) = r((irow-1)*ndf+l1)+
     .          x((ja(j)-1)*ndf+l2)*a(l1,(j-1)*ndf+l2)
             end do
          end do
         end do
      end do
!$omp END PARALLEL DO

      return
      end
```

Figure 3. Matrix vector product and OpenMP directives.

Once the directives are included, the Fortran compiler should be used with appropriate compiling options.

4 RESULTS

The results of the parallel computing are shown in terms of Speed Up and Efficiency. Speed Up is a ratio between the runtime with a single processor and the runtime with multiple processors. Efficiency is the ratio between the Speed Up and the number of processors or cores. An ideally perfect parallel calculation using N_c = 4 processors/cores should produce a speed up equal to: $SpeedUp = t_{1c}/t_{4c} = 1/0.25 = 4$ and an efficiency equal to $Efficiency = SpeedUp\ /N_c = 4 / 4 = 1$. If a calculations has a non-parallel fraction, the maximum speed up is limited by Amdahl's law: $s = 1 / (1–p)$ where p is the parallelizable portion.

Speed Up can be calculated either with the wall clock time or with the total cputime. The two must be equal in a system that does not have other processes running. The cputime given by the program can be decomposed into cputime_solver and (cputime – cputime_solver).

5. CONCLUSIONS AND FUTURE WORK

A parallel version of CODE_BRIGHT is available for windows environments. The results show good performance/efficiency for 2 cores (80%) but poor efficiency for 4, 6, 8 cores (50% and lower). A next step is to parallelize more operations of the solver (vector products and pre-conditioner inversion).

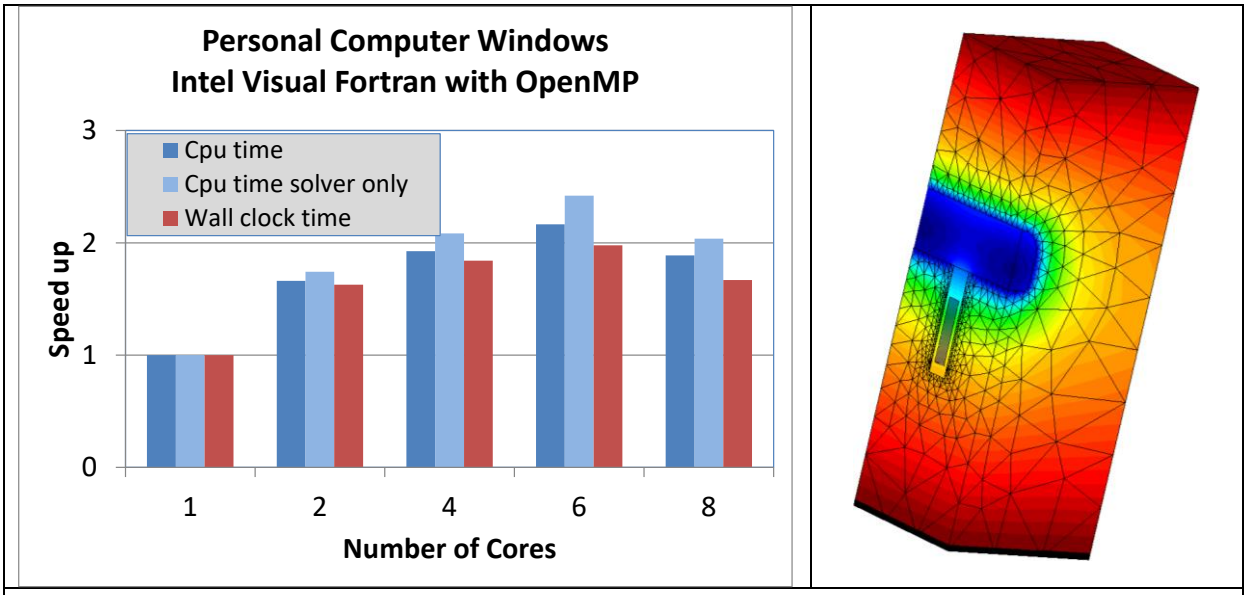

Figure 4. Speed up for parallel computing of a 3D THM model (3982 x 5dof = 19910 dof). (Solver cputime is 90% of the total cputime for this model).

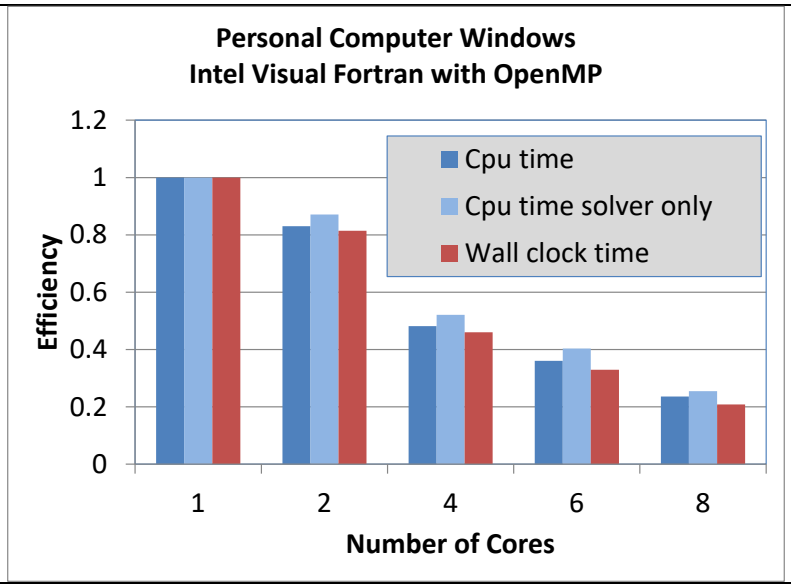

Figure 5. Efficiency for parallel computing of a 3D THM model (3982 x 5dof = 19910 dof)

REFERENCES

Pini, G. and Gambolatti, G. (1990), Is a simple diagonal scaling the best pre-conditioner for conjugate gradients on super-computers?, Advances in Water Resources.

Sonnelveld, P., (1989), CGS, A fast Lanczos-type solver for non-symmetric linear systems, SIAM J. Sci. Stat. Comput., 10, 36-52.